INFORMATION TO USERS

This manuscript has been reproduced from the microfilm master. UMI films the text directly from the original or copy submitted. Thus, some thesis and dissertation copies are in typewriter face, while others may be from any type of computer printer.

The quality of this reproduction is dependent upon the quality of the copy submitted. Broken or indistinct print, colored or poor quality illustrations and photographs, print bleedthrough, substandard margins, and improper alignment can adversely affect reproduction.

In the unlikely event that the author did not send UMI a complete manuscript and there are missing pages, these will be noted. Also, if unauthorized copyright material had to be removed, a note will indicate the deletion.

Oversize materials (e.g., maps, drawings, charts) are reproduced by sectioning the original, beginning at the upper left-hand corner and continuing from left to right in equal sections with small overlaps.

Photographs included in the original manuscript have been reproduced xerographically in this copy. Higher quality 6" x 9" black and white photographic prints are available for any photographs or illustrations appearing in this copy for an additional charge. Contact UMI directly to order.

ProQuest Information and Learning
300 North Zeeb Road, Ann Arbor, MI 48106-1346 USA
800-521-0600



Downloaded from SHAREOK. Persistent Handle URL: https://hdl.handle.net/11244/345

NOTE TO USERS

This reproduction is the best copy available.

UMI®

UNIVERSITY OF OKLAHOMA

GRADUATE COLLEGE

A GEOTECHNIQUES-BASED EXPLORATORY INVESTIGATION OF VOG IMPACTS TO THE ENVIRONMENTAL SYSTEM ON HAWAI'I ISLAND

A Dissertation

SUBMITTED TO THE GRADUATE FACULTY

in partial fulfillment of the requirements for the

degree of

Doctor of Philosophy

By

BARBARA A. GIBSON
Norman, Oklahoma
2001

UMI Number: 3014524



UMI Microform 3014524

Copyright 2001 by Bell & Howell Information and Learning Company.
All rights reserved. This microform edition is protected against unauthorized copying under Title 17, United States Code.

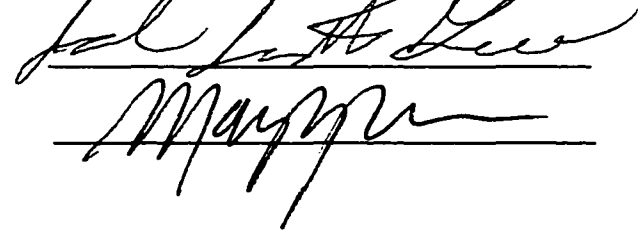
Bell & Howell Information and Learning Company
300 North Zeeb Road
P.O. Box 1346
Ann Arbor, MI 48106-1346

A GEOTECHNIQUES-BASED EXPLORATORY INVESTIGATION OF VOG IMPACTS TO THE ENVIRONMENTAL SYSTEM ON HAWAI'I ISLAND

A Dissertation APPROVED FOR THE GRADUATE COLLEGE

BY

Susan Postawko



©Copyright by BARBARA A. GIBSON 2001
All Rights Reserved.

ACKNOWLEDGMENTS

Whew! It is finally finished. The path that led me to this point in my life was a long one with a great many twists and turns; but hey, that's what makes it so much sweeter to be done. This dissertation was completed through the help of *many* people guiding me, and without which I would have been a lost soul indeed.

First, I would like to acknowledge Ms. Pam Neal - she started me on this grand adventure by suggesting I contact Dr. Susan Postawko to be my advisor those many years ago when I was still an undergrad. Nothing gets going without that all important first step, so I give you my wholehearted thanks! I would also like to acknowledge each member of my dissertation committee: Dr. May Yuan for her patience and insightful suggestions on methodology; Dr. Barry Weaver for inviting me to go with his class on that ever infamous field trip to Hawai`i, which allowed me meet the HVO personnel, which in turn solidified my dissertation topic. (And I must admit that I regret not going "bushwhacking" with Patrick and James just so I could fly through the sky on a rope hanging from a helicopter.....); Dr. Scott Greene for his patience, perceptive guidance, and willingness to listen to my silly crack-ups; Dr. Mark Morrissey for his sage advice and for *his* silly crack-ups; and Dr. Susan Postawko...what can I say??? Well I'll get back to that one in a bit....

I would also like to acknowledge the following people for their part in helping to complete this dissertation: Dr. Karen Humes for sharing her vast knowledge of remote sensing with me; Sandy Margriter at Hawai`i Volcanoes National Park for providing data and technical advice; the EVAC staff ("Karlar", Naïla, John, etc.) for their encouragement and support; Tamar Elias and Jeff Sutton of the USGS Hawaiian

Volcano Observatory for their suggestions and sharing of data from their many years of studying Kilauea's emissions; Martha Scholl and S. Ingebritsen of the USGS for also sharing data; and my many fellow graduate students who gave their support and confidence via backyard BBQs and partaking of adult beverage (that means you guys, Bill T., Marco, and Melany!!). I especially want to thank Melany for giving me the gift of her unconditional friendship. Through time and space you will always be my sis! I also want to thank Brad McGavock for listening to my many bitch sessions when I got frustrated, and giving me pep talks to keep me going.

This project was funded by grants and scholarships from many agencies, including the International Geographic Information Foundation, the University of Oklahoma Graduate College, the Environmental Verification and Analysis Center, and the Oklahoma NASA Space Grant Consortium. I thank you for your generosity in helping this project come to fruition.

Finally, I would like to acknowledge two woman with very special gifts who gave that little extra of themselves to help me finish this project. I want to thank Dr. Victoria Duca-Snowden for being a great friend and supporter. She is my Celestine sister who knows from where I came, and helps to guide me to where I need to be. I know that if I ever falter, you will be there to encourage me to go the next step. Thank you, Victoria, for listening and sharing the wisdom of an "old soul".

I also want to give a *mahalo nui loa* to Dr. Susan Postawko (told you I would get back to her). Susan, you are a very special person and I feel blessed that you are my mentor and friend. You have selflessly given your time and resources to many a student (including myself), and I wanted you to know that we all appreciate your gifts

more than simple words can express. If what they say about karma is true, in the next life you will certainly be the richest person in the world!

There are only two ways to live your life. One is as though nothing is a miracle. The other is as though everything is a miracle.

Albert Einstein (1879-1955)

Indeed, as the completion of this dissertation demonstrates, miracles do happen!

TABLE OF CONTENTS

ACKNOWLEDGMENTS iv

LIST OF TABLES ix

LIST OF FIGURES xi

ABSTRACT xv

CHAPTER 1: INTRODUCTION
- 1.1 Background 1
- 1.2 Recent History of Kilauea Eruptions 3
- 1.3 Importance of Meteorological Conditions 4
- 1.4 Impact of Volcanic Gases on Water Quality 7
- 1.5 Impact of Volcanic Gases on Vegetation and Agriculture 8
- 1.6 Research Objectives 11

CHAPTER 2: STUDY AREA
- 2.1 Geographic Information 13
- 2.2 Biogeography of Hawai'i Island 15
- 2.3 Weather and Climate of Hawai'i Island 20
- 2.4 Geology and Soils 26

CHAPTER 3: DATA AND METHODOLOGY
- 3.1 Description of Satellite Imagery 29
- 3.2 Image Preprocessing 35
- 3.3 Vegetation Change Detection Methodologies 38
  - *3.3a Multispectral classification* 38
  - *3.3b Normalized Difference Vegetation Index (NDVI)* 40
- 3.4 Derived NDVI for SPOT and Landsat MSS 43
- 3.5 NDVI Calculations and Differencing 44
- 3.6 Rainfall and Temperature Data Characteristics 46
  - *3.6a Precipitation data* 46
  - *3.6b Temperature data* 48
- 3.7 Exploratory Statistical Analysis of Monthly Rainfall and Temperature Data 48

CHAPTER 4: RESULTS AND DISCUSSION
- 4.1 Analysis of NDVI Scenes Prior to Differencing 59
- 4.2 Analysis of NDVI Scenes: Post-differencing 62
  - 4.2a NDVI differencing between MSS 77 and SPOT 89 scene . 66
  - 4.2b *NDVI differencing between MSS 77 and SPOT 95 scene* . 72
  - 4.2c NDVI differencing between SPOT 89 and SPOT 95 scene . 78

4.3 Results of Exploratory Analysis of Rainfall Data 83
4.3a Rainfall trends for the complete time series 85
4.3b Rainfall trends for pre-eruption vs. post-eruption time series 91
4.4 Results of Exploratory Analysis of Surface Temperature Data 94
4.4a Temperature trends for the complete time series 95
4.4b Temperature trends for pre-eruption vs. post-eruption time series 99
4.5 Autocorrelation Results for Rainfall and Temperature Data 110

CHAPTER 5: CONCLUSIONS AND SUGGESTED FUTURE RESEARCH
5.1 Vegetation Impacts 113
5.2 Rainfall Impacts 115
5.3 Temperature Impacts 116

REFERENCES 118

LIST OF TABLES

Table 1.1: Summary of Kilauea's eruptions, 1969-present 6
Table 3.1: Specifications of satellite data used in study 33
Table 3.2: List of precipitation sites along with each station's corresponding regression equation, r^2 value, S_b value, and calculated *t* value for the complete 31 year time series. Those that are significant are indicated by * 51
Table 3.3: List of precipitation sites along with each station's corresponding regression equation, r^2 value, S_b value, and calculated *t* value for the 14 years prior to current eruption. Those that are significant are indicated by * 52
Table 3.4: List of precipitation sites along with each station's corresponding regression equation, r^2 value, S_b value, and calculated *t* value for the 17 years since Kilauea began erupting in 1983. Those that are significant are indicated by * 53
Table 3.5: Station's corresponding regression equation, r^2 value, S_b value, and calculated *t* value for the complete 31 year time series (lt), for the 14 years prior to the eruption (be), and the 17 years since eruption began (ae) calculated from monthly temperature data. Those that are significant are indicated by * 54
Table 3.6: Table 3.6: Station's corresponding regression equation, r^2 value, S_b value, and calculated *t* value for the complete 31 year time series (lt), for the 14 years prior to the eruption (be), and the 17 years since eruption began (ae) calculated from monthly temperature data. Those that are significant are indicated by * 55

Table 3.7: Table 3.7: Station's corresponding regression equation, r^2 value, S_b value, and calculated *t* value for the complete 31 year time series (lt), for the 14 years prior to the eruption (be), and the 17 years since eruption began (ae) calculated from monthly temperature data. Those that are significant are indicated by * 56

LIST OF FIGURES

Figure 1.1: Map showing area covered by lava flows created during the Pu'u O'o - Kupaianaha eruption between 1983 and July 1999 5
Figure 2.1: The eight main Hawai'ian Islands 14
Figure 2.2: The location of HAVO in relation to the Big Island 19
Figure 2.3: Map of average annual rainfall for Hawai'i Island 21
Figure 2.4: Graphic showing the predominate NE trade wind pattern in relation to the physiography of the Big Island. The direction of the kona winds is also shown 22
Figure 2.5: An enhanced satellite image showing the path of the vog plume around Hawai'i Island 24
Figure 2.6: The Koppen climate classification of Hawai'i Island 25
Figure 2.7: Map of major soil orders present on Hawai'i Island 27
Figure 3.1: Landsat MSS scene acquired 27 October 1977 30
Figure 3.2: SPOT HRV scene acquired 12 December 1989 31
Figure 3.3: SPOT HRV scene acquired 28 January 1995 32
Figure 3.4: Spectral reflectance characteristics for healthy green grass, dead or senescing grass, and bare dry soil. Though this graph specifically shows general grass spectral reflectance, the spectral characteristics for other vegetation types would only vary slightly from the above 41
Figure 3.5: Location of precipitation stations used in trend analysis 47
Figure 3.6: Location of temperature sites used in trend analysis 49
Figure 4.1: Frequency histogram of NDVI values computed from 1977 Landsat MSS sub-scene using band 7 (NIR) and band 5 (red) 60
Figure 4.2: Frequency histogram of NDVI values computed from 1977 Landsat MSS sub-scene using band 6 (NIR) and band 5 (red) 61
Figure 4.3: Frequency histogram of NDVI values computed from 1989 SPOT HRV sub-scene using band 3 (NIR) and band 2 (red) 63

Figure 4.4: Frequency histogram of NDVI values computed from 1995 SPOT HRV sub-scene using band 3 (NIR) and band 2 (red) 64
Figure 4.5: Computed difference NDVI layer between MSS 1977 (band 7) NDVI and SPOT HRV 1989 NDVI 67
Figure 4.6: Computed difference NDVI layer between MSS 1977 (band 6) NDVI and SPOT HRV 1989 NDVI 68
Figure 4.7: Frequency histogram of differenced NDVI layer between MSS 1977 (band 7) and 1989 SPOT HRV 70
Figure 4.8: Frequency histogram of differenced NDVI layer between MSS 1977 (band 6) and 1989 SPOT HRV 71
Figure 4.9: Computed difference NDVI layer between MSS 1977 (band 7) NDVI and SPOT HRV 1995 NDVI 73
Figure 4.10: Computed difference NDVI layer between MSS 1977 (band 6) NDVI and SPOT HRV 1995 NDVI 74
Figure 4.11: Frequency histogram of differenced NDVI layer between MSS 1977 (band 7) and 1995 SPOT HRV 75
Figure 4.12: Frequency histogram of differenced NDVI layer between MSS 1977 (band 6) and 1995 SPOT HRV 77
Figure 4.13: Computed difference NDVI layer between SPOT HRV 1989 NDVI and SPOT HRV 1995 NDVI 80
Figure 4.14: Frequency histogram of differenced NDVI layer between 1989 SPOT HRV and 1995 SPOT HRV 82
Figure 4.15: Graphic showing ENSO events 84
Figure 4.16: Graph of mean annual rainfall for Lanihau site 86
Figure 4.17: Graph of mean annual rainfall for Kainaliu site 87
Figure 4.18: Graph of mean annual rainfall for Middle Pen site 88
Figure 4.19: Graph of mean annual rainfall for Opihihale site 89
Figure 4.20: Map of rainfall stations with significant changes in precipitation trends between 1969 and 1999. Also shows the relative geographic location of stations with negative trends vs. positive trends (regardless

of significance 90
Figure 4.21: Map of rainfall stations with significant changes in precipitation trends between 1969 and 1982. Also shows the relative geographic location of stations with negative trends vs. positive trends (regardless of significance 92
Figure 4.22: Map of rainfall stations with significant changes in precipitation trends between 1983 and 1999. Also shows the relative geographic location of stations with negative trends vs. positive trends (regardless of significance 93
Figure 4.23: Graphs of yearly mean monthly temperature, yearly mean monthly minimum temperature, and yearly mean monthly maximum temperature (1969 to 1999) for the Hawaii Volcanoes NP station. 96
Figure 4.24: Graphs of yearly mean monthly temperature, yearly mean monthly minimum temperature, and yearly mean monthly maximum temperature (1969 to 1999) for the Opihihale station 97
Figure 4.25: Graphs of yearly mean monthly temperature, yearly mean monthly minimum temperature, and yearly mean monthly maximum temperature (1969 to 1999) for the Hilo International AP station 98
Figure 4.26: Graphs of yearly mean monthly temperature for the Hilo International AP station for pre-eruption (1969 to 1982) and post-eruption (1983 to 1999) time periods 100
Figure 4.27: Graphs of yearly mean monthly temperature for the Opihihale station for pre-eruption (1969 to 1982) and post-eruption (1983 to 1999) time periods 101
Figure 4.28: Graphs of yearly mean monthly temperature for the Hawaii Volcanoes NP station for pre-eruption (1969 to 1982) and post-eruption (1983 to 1999) time periods 102
Figure 4.29: Graphs of yearly mean monthly minimum temperature for the Hilo International AP station for pre-eruption (1969 to 1982) and post-eruption (1983 to 1999) time periods 103

Figure 4.30: Graphs of yearly mean monthly minimum temperature for the Hawaii Volcanoes NP station for pre-eruption (1969 to 1982) and post-eruption (1983 to 1999) time periods 104
Figure 4.31: Graphs of yearly mean monthly minimum temperature for the Opihihale station for pre-eruption (1969 to 1982) and post-eruption (1983 to 1999) time periods 105
Figure 4.32: Graphs of yearly mean monthly maximum temperature for the Hawaii Volcanoes NP station for pre-eruption (1969 to 1982) and post-eruption (1983 to 1999) time periods 106
Figure 4.33: Graphs of yearly mean monthly maximum temperature for the Opihihale station for pre-eruption (1969 to 1982) and post-eruption (1983 to 1999) time periods 107
Figure 4.34: Graphs of yearly mean monthly maximum temperature for the Hilo International AP station for pre-eruption (1969 to 1982) and post-eruption (1983 to 1999) time periods 108
Figure 4.35: Sample graphs showing the results of the autocorrelation test for yearly mean rainfall time series 111
Figure 4.36: Sample graphs showing the results of the autocorrelation test for yearly mean temperature time series 112

ABSTRACT

The purpose of this research is to analyze the direct and indirect impacts of gases produced by basaltic volcanism on interactions between environmental systems. Related studies of natural hazards have been performed involving explosive, composite volcanic eruptions, including the Mt. St. Helens, El Chichón, and Mt. Pinatubo eruptions to determine if they contributed to global cooling among other environmental impacts. Unlike these previous studies that emphasized impacts of volcanic gases in the stratosphere, this research will examine the possible long-term effects on Hawai`i Island's environmental system due to sulfur gases (and resulting sulfate aerosols) released by a non-explosive eruption into the troposphere. Although basaltic events may not be as dynamic as composite eruptions, they can eject significantly greater amounts of sulfur into the atmosphere than a more silicic magma of the same volume. This is important because changes in environmental factors have been attributed to a larger than normal presence of sulfur compounds in the atmosphere.

Hawai`i Volcanoes National Park and surrounding regions on Hawai`i Island were chosen for the research site because the basaltic volcanism taking place is significant, and relevant data concerning many environmental variables are readily available. Specifically, changes to spatial and temporal trends in precipitation and surface temperature as well as negative impacts to vegetation health due to volcanic emissions (*vog*) from Kilauea Volcano are investigated using exploratory statistics, a geographical information system (GIS), and remote sensing techniques. Results were inconclusive concerning possible *vog* impacts to vegetation health; but the study's

findings do support the hypothesis that the *vog* is influencing both rainfall and temperature trends and patterns for Hawai'i Island.

CHAPTER ONE

INTRODUCTION

1.1 Background

Changes in the variables that comprise the Earth system are critical concerns at regional and global scales. Within the last 10 years, the United States Global Change Research Program called for scientific investigations "to describe and understand the interactive physical, chemical, and biological processes that regulate the total Earth system" (Wickland 1991). One such process is the effect of volcanic activity on global climate and environmental systems. Besides the immediate devastation to landcover and ecosystems, results from previous investigations suggest that explosive volcanic activity contributes to global cooling (Dutton and Christy 1992). The degree to which volcanic activity promotes cooling greatly varies. This is supported by studies that have indicated that the environmental impact of volcanic eruptions is not only related to the eruption's magnitude, explosivity, and volume, but is also correlated to the concentration of the volatile species sulfur dioxide (SO_2), hydrogen sulfide (H_2S), and to a smaller degree chlorine (Cl) and fluorine (F) (Schnetzler et al. 1992). The solubility of sulfur and the volume of magma erupted are particularly related to possible effects on the climate and environment, and basaltic volcanic eruptions are more sulfur-rich than explosive eruptions (Sigurdsson 1982; Rampino et al. 1985). Most basaltic eruptions do not affect the global environment since they do not eject large amounts of ash and dust, and the aerosols and gases that they release do not reach the stratosphere. However, as the 1783 Laki (Iceland)

fissure eruption shows, there are exceptions to the rule (Sigurdsson 1982).

The Laki eruption provides an example of how basaltic eruptions can affect climate and environmental conditions. It is now known that the Laki magma was unusually sulfur-rich. Since sulfur is a very volatile element in magma, it is mostly partitioned into the gas phase when the magma is erupted at the surface (Sigurdsson 1982). The eruption produced only 12.3 km^3 of lava over a period of eight months, but injected 10^7 to 10^8 tons of H_2SO_4 into the atmosphere spawning a *vog* (volcanically induced fog) rich in sulfur and fluorine compounds. The eruption ejected approximately 0.3 km^3 of tephra into the air; the same amount of airfall ash that Mt. St. Helens produced when it erupted in 1980. The Laki eruption also produced a 5°C drop in temperature during the following winter in the northern hemisphere, and continued to affect regional weather over the next two years. The *vog* caused most of the damage generated by the volcano and was responsible for the death of 24% of Icelanders and the loss of 75% of all livestock (Sigurdsson 1982; Thordarson and Self 1993; Asrar and Dozier 1994).

Large amounts of fine ash and dust erupted into the upper atmosphere can significantly alter the amount of solar radiation reaching the Earth's surface, and eruptions with high sulfur dioxide content particularly can affect climate (Decker and Decker 1989). Basaltic volcanic eruptions typically eject large volumes of sulfur compounds into the troposphere, where the residence time of sulfate aerosols is much shorter (only a week or so) in contrast to a lifetime of several years in the stratosphere (Watson et al. 1992). But in the case of Kilauea's current long-term eruption event, a steady supply of SO_2 and H_2SO_4 is being introduced into the troposphere. The

impacts on vegetation, surface temperature, and rainfall need to be surveyed since perturbations in those environmental controls could produce severe impacts to human life as well as ecologic and economic stability in the region.

1.2 Recent History of Kilauea Eruptions

Since Kilauea volcano began erupting almost continuously in 1983, it has outpoured the most voluminous amount of lava on the volcano's east rift zone in the last 200 years (USGS 1999). A recent report from the U.S. Geological Survey (USGS) (1999) estimates that in January 1999 an additional 206 hectares were added to the island's southern shore. Moreover, in the process of land-building, the volcano has destroyed 181 houses and destroyed 13 km of highway (USGS 1999).

This outflow of lava is also responsible for emitting a steady supply of sulfur compounds into Hawai`i's local atmosphere. The amount of SO_2 emissions from Kilauea Volcano varies from 350 tons/day during eruptive pauses to over 2,000 tons/day when the volcano is actively erupting (Sutton et al. 1994). This is significantly greater than the Environmental Protection Agency's (EPA) guideline of 0.25 tons/day for major sources of industrial pollution (Sutton and Elias 1993). The concentration of sulfur compounds emitted by the volcano has varied during the current eruption's duration due to factors such as changes in eruption rates and location of lava outbreaks. Eruption rates are important since it is the ejected basaltic lava (known to have a relatively high sulfur concentration) that degasses the sulfur compounds into the air; the more magma ejected, the larger the amount of sulfur released. The location of the magma outbreak is important because the trade winds (or lack thereof) across the

Island are important in dispersing the volcanic gases, and greatly affect the gas concentrations. Furthermore, magma which is erupted into the ocean (via the lava-tubes which run to the Island's southeast coast) induce thermo-chemical reactions which produce harmful compounds such as hydrogen chloride (HCl) (Sutton et al. 1994).

The first three years of Kilauea Volcano's most recent continuous eruption was localized to the Pu`u O`o vent and was predominantly episodic fountaining. From 1986 to 1992, the volcano began continuously effusing lava and the Kupaianaha lava pond was formed approximately 3 km downrift of Pu`u O`o (Sutton et al. 1994) (Fig. 1.1). Kupaianaha vent ceased erupting in February 1992, but the eruption continues (except for brief pauses) near the Pu`u O`o vent (Kauahikau et al. 1992; Mattox et al. 1992). It was decided by the USGS to narrow collection of sulfur emission rates to the area of the Eastern Rift Zone (ERZ) (near Pu`u O`o eruption) and the Kilauea caldera since this was (and continues to be) where the most notable discharge takes place. Table 1.1 shows Kilauea's eruption history since 1969.

1.3 Importance of Meteorological Conditions

Sutton et al. (1994) showed the importance of meteorological conditions, specifically wind speed and direction, and site location in determining the potential impacts of sulfur emissions from Kilauea. For example, grab-sample measurements near Pu`u O`o show that during kona winds (low speed variable wind conditions) measured ambient SO_2 and H_2S concentrations are highest. Furthermore, the precipitation samples taken near the shore at coastal entries display a lower pH and

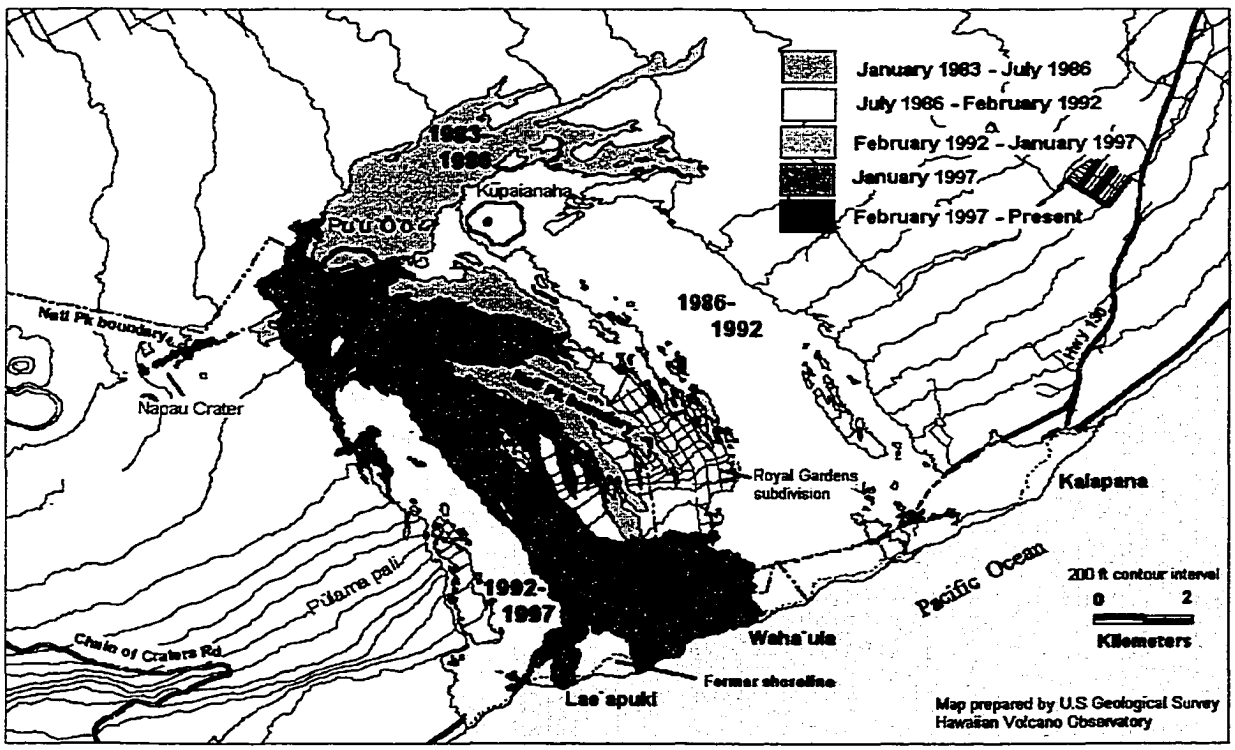


Figure 1.1: Map showing area covered by lava flows created during the Pu'u O'o - Kupaianaha eruption between 1983 and July 1999. Taken from Hawai'i Volcanoes Observatory (USGS) Web site.

YEAR	START (mm/dd)	Duration (days)	Eruptive Subdivision	Area Covered (km^2)	Volume (km^3)
1983	01/03	>6,200 *,**	ER	102	1.9
1982	09/25	<1	C	0.8	0.003
1982	04/30	<1	C	0.3	0.0005
1979	11/16	1	ER	0.3	0.00058
1977	09/13	18	ER	7.8	0.0329
1975	11/29	<1	C	0.3	0.00022
1974	12/31	<1	SWR	7.5	0.0143
1974	09/19	<1	C	1.0	0.0102
1974	07/19	3	C, ER	3.1	0.0066
1973	11/10	30	ER	1.0	0.0027
1973	05/05	<1	ER	0.3	0.0012
1972	02/03	900*	ER	46	0.162
1971	09/24	5	C, SWR	3.9	0.0077
1971	08/14	<1	C	3.1	0.0091
1969	05/24	874*	ER	50	0.185
1969	02/22	6	ER	6.0	0.0161

Table 1.1: Summary of Kilauea's eruptions, 1969 - present (USGS 2000; after Macdonald et al. 1986) C=caldera; ER=east rift; SWR=southwest rift.

** The very long duration of activity is more comparable with the long-continued lava-lake activity in Halemaumau previous to 1924 than with the other eruptions listed in the above table.*

*** Activity at Pu'u O'o is still continuing.*

higher sulfate concentration because of on-shore and along-shore wind effects.

1.4 Impact of Volcanic Gases on Water Quality

The impacts on water quality are a major concern to Island residents. One study in the early 1980s suggested that low rainfall pH levels were not the result of volcanic emissions, but rather the consequence of anthropogenic pollutants being transported over great distances in the upper atmosphere (Miller and Yoshinaga 1981). But Miller and Yoshinaga appear to contradict their argument by mentioning that during a two-week eruption, the sample site closest to the eruption showed lower than normal pH values (3.5-4.0), and these values later returned to the all-island average (4.5) (Miller and Yoshinaga 1981). Harding and Miller (1982) came to a similar conclusion; they found that during a non-eruptive phase of Kilauea and Mauna Loa, the influence of the volcanoes on rainfall chemistry greatly decreased. They also reported that sulfate was the major anion present in the rainwater they sampled. It should be noted that these studies were not done during a long-term continuous eruption. Thus there still appear to be several unknown factors concerning the influence of volcanic emissions on rainfall chemistry and pH. Furthermore, the influence of the possible low rainfall pH on soil chemistry is another key factor influencing vegetation condition and patterns on the island.

A study concerning total and non-seasalt (nss) sulfate measured in bulk precipitation samples from the Kilauea area done by Scholl and Ingebritsen (1995) indicated that "patterns of total and nss sulfate deposition show a definite relation to sources of volcanic SO_2." The study was done to help address concerns of possible

effects of volcanic gas emissions on crops and drinking water. Additionally, many Hawai'i Island residents use rooftop catchment systems for drinking water. The contamination of rainwater occurs when sulfur dioxide combines with water vapor in the atmosphere to form acid rain (H_2SO_4), which leaches lead from the roofing nails and paint in Hawai`i residents' catchments. The lead then contaminates the residents' drinking water which poses an obvious serious health hazard (Sutton and Elias 1993). Acid rain "is a broad term used to describe several ways that acids fall out of the atmosphere. A more precise term is acid deposition, which has two parts: wet and dry. Wet deposition refers to acidic rain, fog, and snow."(EPA 2000). There are many sources of acid rainfall, including carbon dioxide and sulfur dioxide in the atmosphere. In Hawai`i Island's case, sulfur dioxide is the primary producer of acid rain. The reaction that creates the acidic rainfall from volcanic SO_2 gas is triggered by the presence of water vapor and light in the atmosphere (NASA 1994).

1.5 Impact of Volcanic Gases on Vegetation and Agriculture

Potentially one of the most devastating impacts of gases and aerosols released by Kilauea is on the vegetation. Sutton et al. (1994) point out that "although rainfall to the southwest of Kilauea Caldera is roughly equivalent to that of Portland, Oregon (100-130 cm/yr) the SO_2 and H_2SO_4 help to sustain the sparsely vegetated landscape of the Ka`u Desert." The toxic gases emitted by Kilauea can migrate to the Ka`u Desert, where few plants are able to sustain growth. The plants that do survive include the ohia lehua (*Metrosideros polymorpha*) which partially is able to avoid the poisonous effects of SO_2 by closing its stomates (Mohlenbrock 1996).

There have been several related studies concerning the impacts of SO_2 and sulfate aerosols on vegetation, but few concerning the effects of long-term natural sources of the pollutants. Winner and Mooney (1980 and 1985) demonstrated the importance of stomatal conductance in individual species in determining the amount of impact that volcanic SO_2 had on native and exotic plant species present on Hawai'i Island. They deduced that there was no correlation between leaf injury due to volcanic SO_2 on exotic and native species. It was previously thought that perhaps native species would have been better adapted to the environment produced by the volcanic eruptions, but their research proved this otherwise (Winner and Mooney 1985). It was also found that younger leaves in all species were the most susceptible to the effects of SO_2; a reduction or removal of the younger leaves on a plant has obvious implications for preventing a plant from prolonging itself (Winner and Mooney 1980; Winner and Mooney 1985).

There have been numerous studies relating anthropogenic SO_2 pollution to changes in plant communities. It has been ascertained that the stability, structure, and interactions of a plant community can be impacted by the presence of SO_2 pollution, but the amount of change is greatly dependant on both the species' response to the pollutant and the amount of SO_2 present (Kozlowski 1985; Lauenroth and Milchunas 1985). Just as important as the actual damage caused by SO_2 is the recovery of the plant. Likens et al. (1996) performed a study using the Hubbard Brook Experimental Forest (HBEF) to investigate if ecosystems would recover from long-term effects of acid rain (caused by anthropogenic sources of SO_2) and if so at what rate. They discovered that the acidification of the ecosystem was reversible, but the rate at which

the ecosystem was returning to normal was exhibiting a hysteresis pattern. This implies that the recovery rate is very slow, and that present reductions in anthropogenic outputs of SO_2 may not be adequate over the long-term (Likens et al. 1996).

The *vog* has been blamed for several adverse effects on Hawai`i Island's agriculture industry. While the yield per acre of many crops on the Big Island have declined since Kilauea began erupting in 1983, most of the blame is due to speculation and not confirmed by studies directly linking the impacts to the *vog* (Personal Communication James Yamaki, Hawaii Agricultural Statistics Service 1997). These impacts include decreased production in tomato, coffee, anthuriums, aquaculture and cattle (Hawaii County Vog Authority 1990). The vog has especially been blamed in the death and illness of newborn calves. It is believed by some that the vog is responsible for selenium deficiency in the animals due to leaching elements out of the region's soil (Bergin 1990; Clark 1990). Again, most of this is theory and conjecture as no known quantitative studies have been conducted to directly link vog to impacts in agriculture.

1.6 Research Objectives

Sulfate aerosols and gases released by less explosive-type of volcanism usually only reach the troposphere and only have a residence time of a few weeks. But Kilauea Volcano has been erupting almost continuously since 1983, and thus has been a steady source for the production of sulfur gases and sulfate aerosols. There appears to be little research concerning the long-term effects of gases and aerosols released by basaltic volcanism on environmental processes. Most related studies have dealt with the effects of explosive volcanism on atmospheric processes or with the short-term effects of a basaltic eruption. The primary goal of this research is to investigate the effects of gases and aerosols released by relatively long-term basaltic volcanism on physical and biological systems using exploratory statistics, remote sensing, and GIS techniques. It is hoped that the results of this study will enable one to determine how influential the less studied basaltic volcanic eruptions are to Earth-environmental systems. The hypotheses of this proposal are that sulfate aerosols and SO_2 gases released by basaltic volcanism existing on Hawai'i Island have affected:

(1) Hawai`i Island's rainfall trends;

(2) Hawai`i Island's surface temperatures; and

(3) vegetation vigor and health on the island, specifically the immediate region of Hawaii Volcanoes National Park.

This project will also address how well the geotechniques used are able to detect any changes, and whether the available data are spatially and spectrally adequate to determine trends in the data. It is hoped this study will be used by other

scientists as a base for further research, especially studies related to human-health and economic impacts. Moreover, this study will also help to lay a foundation for future studies relating to key objectives of the NASA EOS program, specifically the "analysis of atmospheric chemistry and the role of volcanism in modifying local and hemispheric climate over periods of a few months to several years" (Mouginis-Mark et al. 1991).

CHAPTER 2

STUDY AREA

This section describes the unique physical and biological features of Hawai'i Island. It is important to be aware of these characteristics as they may act as a buffer or intensifier to the "signals" this study is attempting to detect. For example, the type of vegetation is important as some species may be more resistant to the volcanic emissions (*vog*) than others. Moreover, knowledge of rainfall and temperature patterns are crucial to determine if the *vog* had somehow influenced a period of drought in an already dry portion of the Island. Finally, the geology, specifically soils, are important to consider as they also may hinder the effects of acid rainfall due to the vog by acting as a buffer.

2.1 Geographic Information

Hawai`i Island has an area of 10,458 km^2 and is approximately located between 19°N - 20.5°N and 156°W - 155°W (Morgan 1983) (Fig. 2.1). The Island is volcanic in origin and is composed of five large shield volcanoes: Kohala (oldest), Mauna Kea, Hualalai, Mauna Loa, and Kilauea (youngest). Basaltic volcanism has been a very important component in the evolution of vegetation species on the Island. It is assumed by some, such as the USGS personal stationed at Hawaiian Volcano Observatory (HVO), that most native species have adapted to their environment and thus would not be affected by Kilauea`s current long-term SO_2 emissions. As

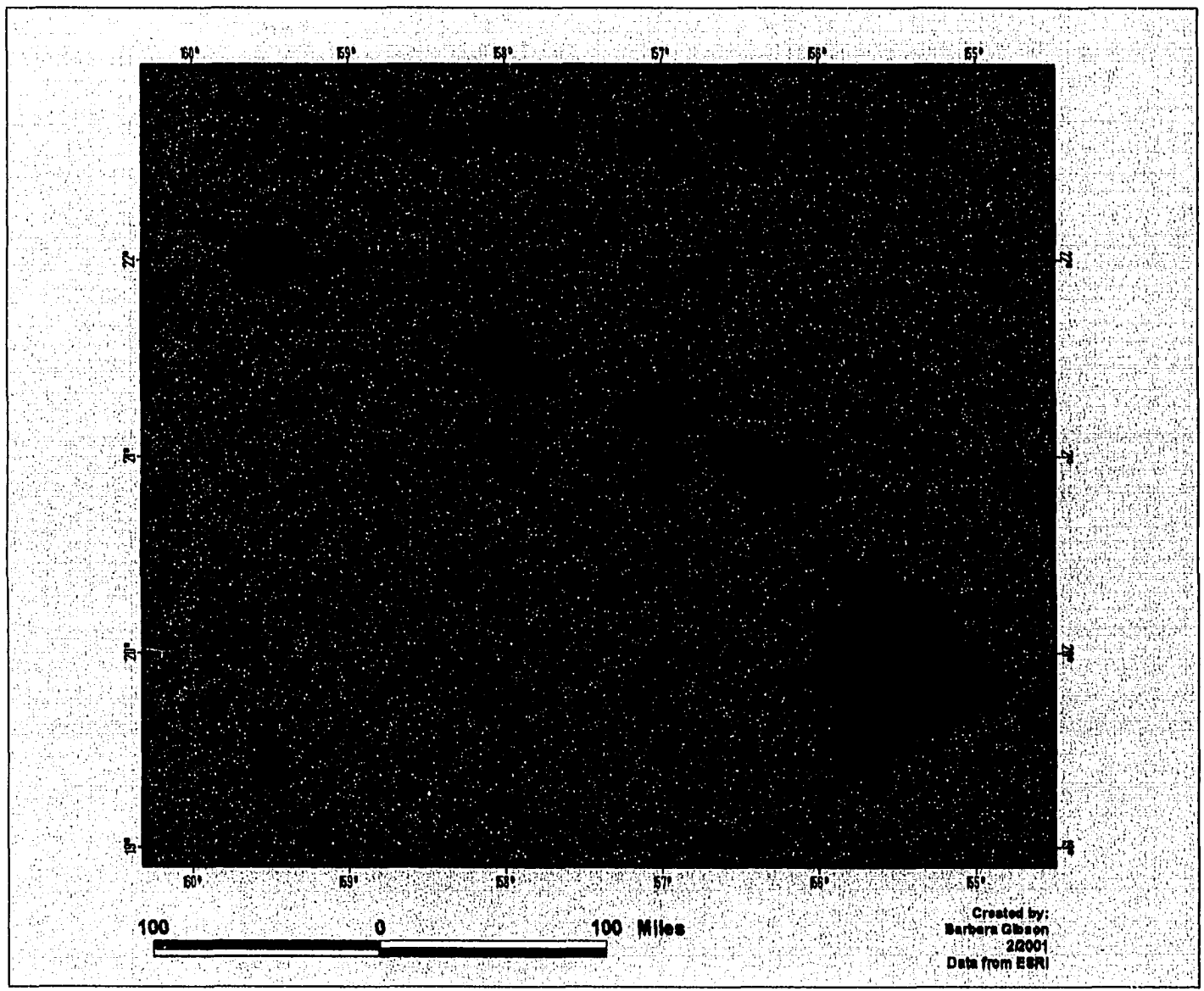


Figure 2.1: The eight main Hawai`ian Islands

demonstrated by the study done by Winner and Mooney (1985), this is not necessarily the case. Moreover, there are considerations for non-indigenous agricultural plants on the Big Island that need to be addressed and studied. It is expected that results from this study may be used as an archetype that can be applied to different, but similar ecological regions.

The Big Island of Hawai'i, specifically Hawai'i Volcanoes National Park (HAVO) and the region to the North of the park, was chosen for distinct reasons to study the impact on certain environmental variables due to gases and aerosols produced by basaltic volcanism. First and foremost, the basaltic volcanism taking place is significant. The Island also supports a wide variety of climate and vegetation types which would allow one to study how the gases may affect different environments. Since much of the region is also protected as either a Federal or State reserve, it is assumed that the impact to land cover and vegetation due to man would be less than other areas on the Island (such as the Kona coast). Finally, relevant data concerning pertinent environmental variables, such as rainfall and temperature data, are readily available.

2.2 Biogeography of Hawai'i Island

Even though Hawai'i is much smaller spatially when compared to many mainland states, it has a surprisingly diverse biogeography. Biogeographers often differentiate between "oceanic" and "continental" islands. Several Pacific islands are considered continental due to their geology suggesting they were once connected to a larger nearby landmass. Moreover, the biota present on an island can indicate a past connection to a larger landmass (Tivy 1993; Juvik 1998). Examples of

continental islands in the Pacific are New Zealand and Fiji.

Oceanic islands are islands that have formed from volcanic eruptions on the seafloor and thus have never been connected to a continent (Tivy 1993; Juvik 1998). The flora and fauna that exist on oceanic islands are present due to long-distance dispersal. This method of introduction gives rise to biota that are typically "disharmonic", or lacking representation of animals and plants present on surrounding continental landmasses (Juvik 1998). Hawai`i is extremely isolated geographically (more that 2,000 miles from the nearest continent), therefore most of its biota have evolved from groups that have the best dispersal capabilities. The methods of long-distance dispersal used by possible colonizers are: direct dispersal, windborne dispersal, waterbome dispersal, and dispersal by birds. These modes can be very limiting to possible colonizers, and these constraints are the primary reason for the lack of mammals and amphibians being native or endemic to Hawai`i Island. In fact, it is thought that today's 1000 native flowering plant species in Hawai`i have evolved from approximately 275 immigrants. If the age of the oldest Main Hawaiian Island is assumed to be 5.6 million years, then is it estimated that the rate of colonization for plants was one every 14,000 years (Lamoureux 1983; Morgan 1996; Juvik 1998).

Hawai`i's plants are usually described as one of the following: endemic; native or indigenous; Polynesian; exotic or alien; or cultivated (Stone and Pratt 1994; Pratt 1998). Endemic plants are those which have evolved in the Hawai`ian Islands and are found only in Hawai`i (including some species only on certain islands within the state). Native or indigenous plants have been present on Hawai`i before colonization by Polynesians, but also are found elsewhere in the world. Exotic or alien plants are those

that have populated the Hawai'ian Islands since the late 1700s when the Europeans arrived. Some of these were introduced to the islands intentionally, but most were accidental introductions and are considered weeds. Polynesian plants are those introduced by the ancient Polynesian settlers of Hawai'i. The number of plant species brought by the Polynesians is estimated to be about twenty five, with most being introduced in the coastal and lowland areas of the islands (Lamoureux 1976; Stone and Pratt 1994; Pratt 1998). Finally, cultivated plants are those that exist on the island as agricultural or garden plants. Ironically, many of these are thought to be "Hawai`ian" to the public, and examples include pineapple and some species of plumeria and ginger (Pratt 1998).

Due to its biota, history, and location, Hawai`i is an excellent laboratory to study the evolutionary process and biological invasion to an ecosystem (Stone and Pratt 1994). Unfortunately, the extinction process has reached a crisis level in Hawai`i due to alien species invading the islands and resulting in a loss of biological diversity. To put it in perspective, Hawai`i comprises only about 0.2 percent of land area in the U.S., but contains roughly one-third of the species listed on the Federal Endangered Species list are located in Hawai`i. Moreover, the "crisis" is reflected by the fact that over two-thirds of the plants and birds known to be extinct in the U.S. are from Hawai`i (Stone and Pratt 1994; Pratt 1998). The change in Hawai`i's ecosystem began with the discovery of the islands by the Polynesians, but was accelerated at an exponential rate with European contact (Lamoureux 1983; Stone and Pratt 1994). Hawai`i's endemic plants do not have any of the natural defenses, such as thorns or poison, that most Mainland plants have due to evolutionary processes. The lack of grazing

mammals allowed for these defense mechanisms to be absent from endemic species (Carson 1998). Thus with the introduction of feral animals like the pig, goat, and deer, many endemic species have become decimated. Moreover, the admission of alien plant species has caused significant habitat loss for native and endemic species (Stone and Pratt 1994; Pratt 1998). Today researchers, state officials, and managers are attempting to reduce the impact of alien plant species on the native habitat. A considerable amount of money and effort is going into building barriers such as fences to protect native species-dominated areas and educating the public of the hazards threatening Hawai`i's biological heritage (Stone and Pratt 1994).

Hawai`i Volcanoes National Park is the most extensive area in Hawai`i where primarily native ecosystems are protected and managed. It was established in 1916 and currently encompasses 209,695 acres (207,643 acres federal; 2,052 acres non-federal). It is also one of the few protected areas that includes continuous terrains from sea coast to mountaintop (Fig. 2.2). The park protects seven ecological zones including: seacoast; lowland; mid-elevation woodland; rainforest; upland forest and woodland; subalpine; and alpine/aeolian (Stone and Pratt 1994). The impact of Kilauea's eruption on the regional endemic and native ecosystems is not fully understood, and the diversity and presence of native ecosystems in HAVO make it an ideal study area for determining potential impacts of *vog* on vegetation. It is the purpose of this research to investigate these possible impacts.

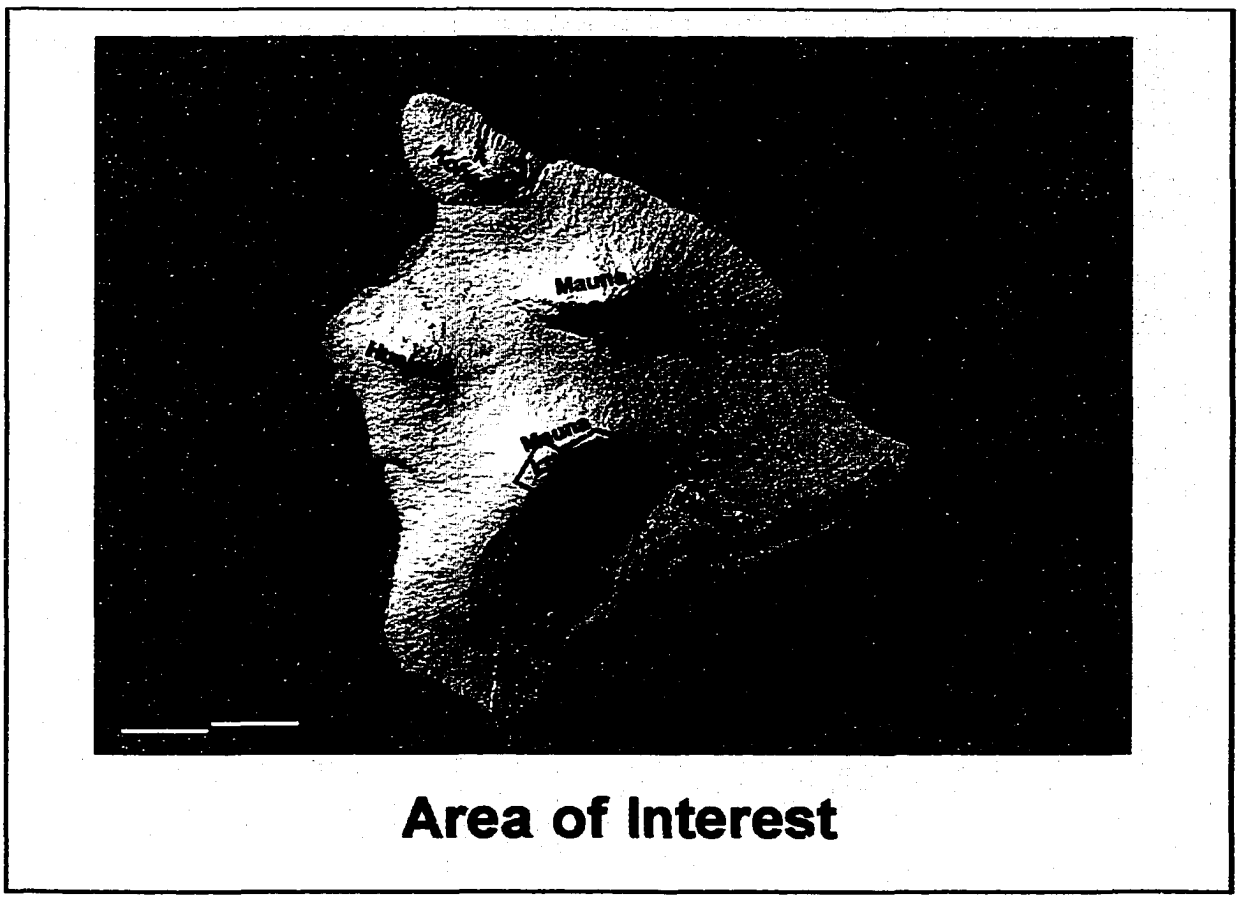


Figure 2.2: The location of HAVO in relation to the Big Island.

2.3 Weather and Climate of Hawai'i Island

The weather and climate of Hawai'i is one of the main reasons why the state appeals to so many visitors, and thus is considered one of its most important natural resources. Primary factors that influence Hawai`i Island's climate include island topography, island location, and the trade winds (Schroeder 1993). A map of Hawai`i Island's median annual precipitation is shown in Figure 2.3. By comparing rainfall amounts on the windward (east) side of Hawai`i verses the leeward (west) side of the island, the influence of orographic effect on the island's rainfall patterns can be seen.

Due to the influence of the Hadley Cell, the northeasterly trade winds govern the weather in Hawai`i (Figure 2.4). These breezes keep the temperatures and humidity in Hawai`i comfortable year round. A product of the Hadley Cell and trade winds is a trade wind inversion. This inversion can seen by the nearly flat cloud tops when clouds are viewed from above. The average inversion height over Hawai`i is about 2 km (6560 ft.) (Schroeder 1993; Giambelluca and Schroder 1998). This may be an important consideration as the presence of an inversion layer would help to keep the presence of the *vog* below the inversion height.

During the winter months there is a slight shift in wind patterns as the Kona winds begin to dominate the weather. The Kona winds are brought about by a Kona low positioned west of the Islands; this causes the winds to become light and variable, and predominately flowing from the southwest (Schroeder 1993; Giambelluca and Schroder 1998).

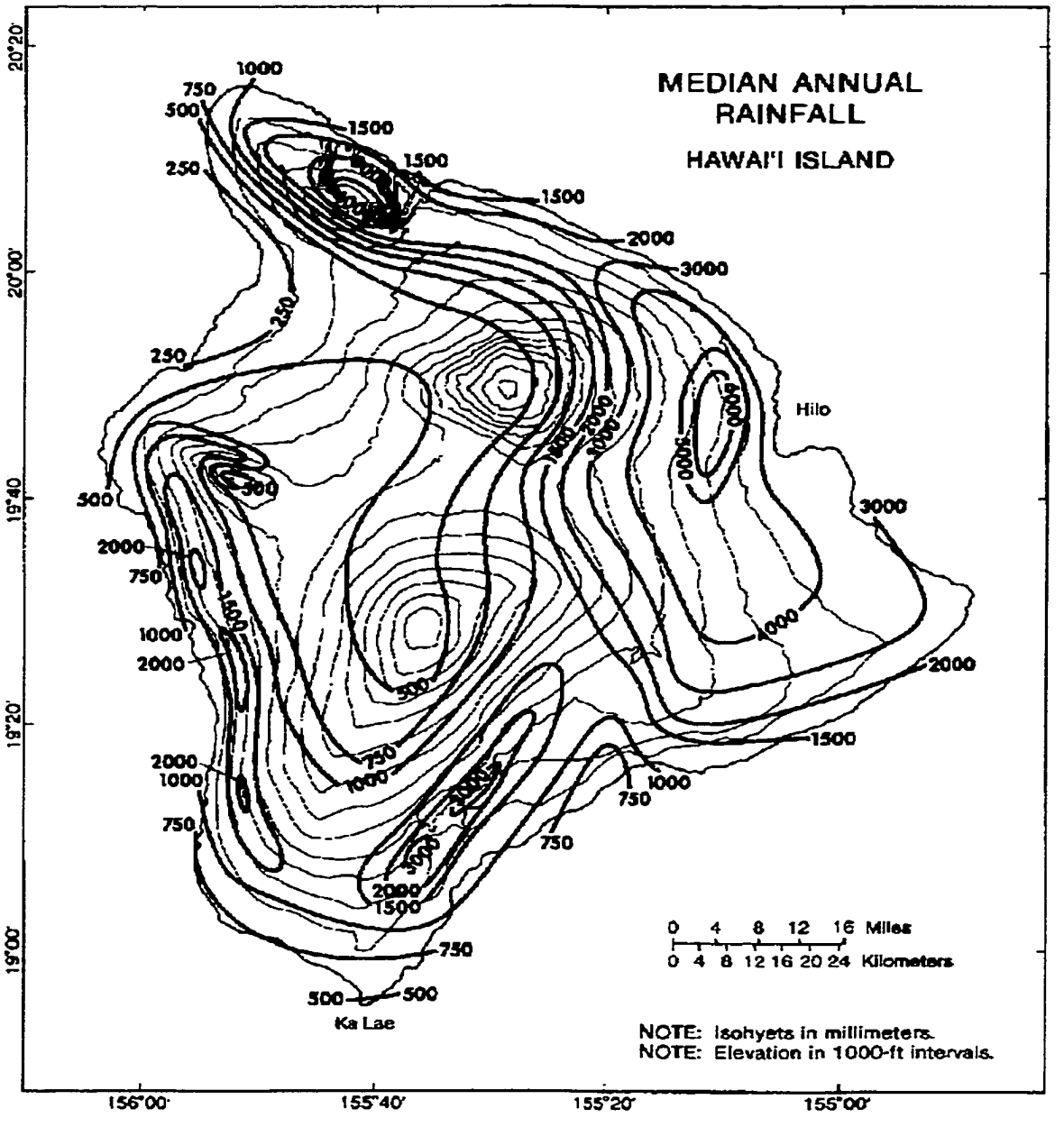


Figure 2.3: Map of median annual rainfall for Hawai`i Island. (Taken from Giambelluca et al. 1986).

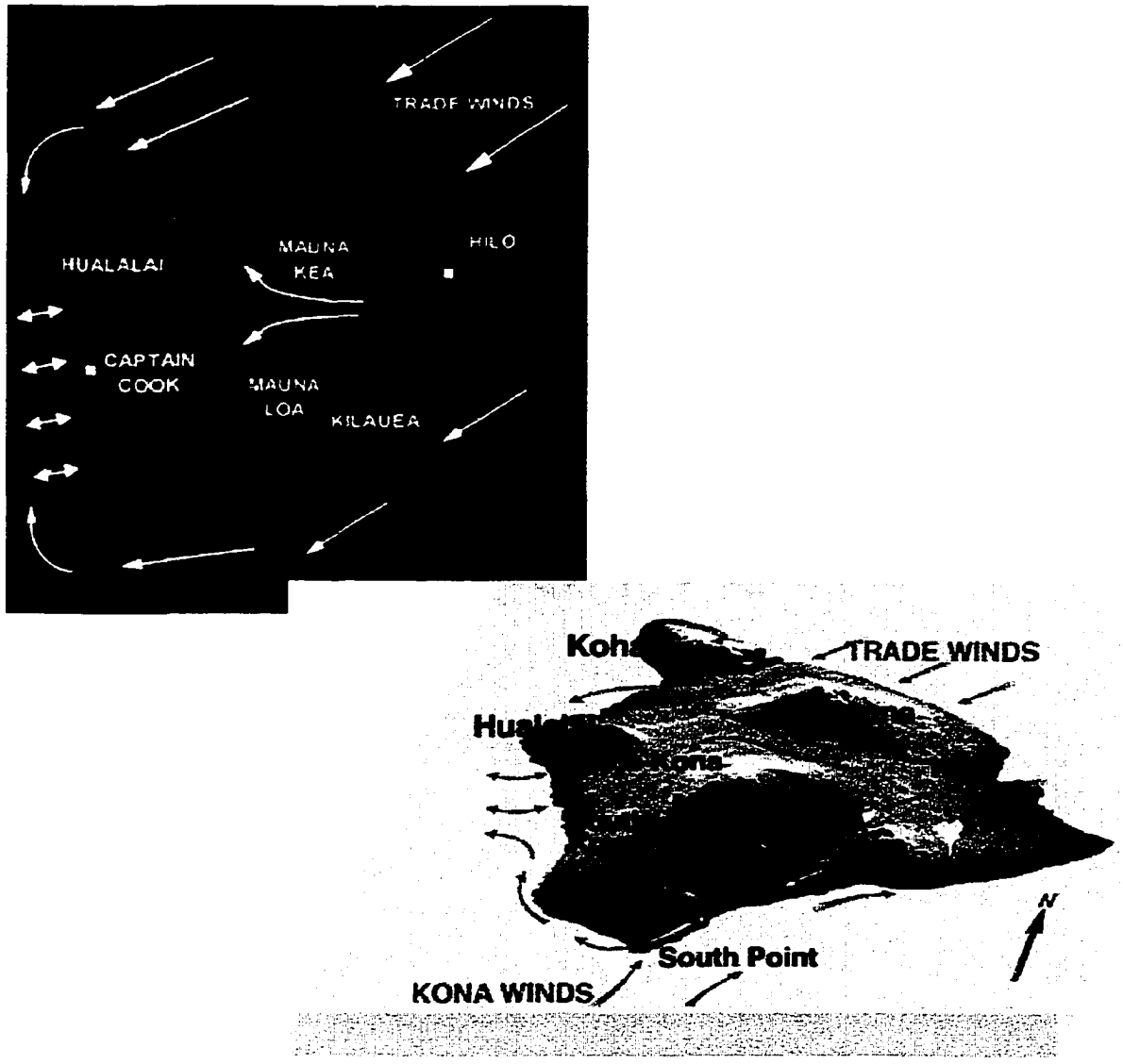


Figure 2.4: Graphic showing the predominate NE trade wind pattern in relation to the physiography of the Big Island. The direction of the kona winds is also shown. (Taken from Sutton et al. 1997 and USGS 2000)

Since the trade winds dominate the weather in Hawai'i for much of the year, the *vog* is mostly transported from the HAVO area to the Kona coast of the Big Island (Figure 2.5). The *vog* also begins to permeate the Saddle region of the Island (area between Mauna Kea and Mauna Loa) and tends to hover in the altitudes below the inversion layer. But during the winter months when the winds become variable, the dispersion of the *vog* to the Kona side abates and the vog can hover in the HAVO area and can begin to drift towards the windward side of the Island (Sutton et. al 1997).

Considering the size of Hawai'i Island, the climate regimes present are quite varied. As mentioned earlier, topography and wind patterns have a significant impact on the distribution and type of climate found on Hawai'i Island. Of the five major climate classes developed by Wladimir Köppen, all except Type D (Humid Middle-latitude with Severe Winters) are present on Hawai`i. From looking at Figure 2.6, one can see again how Mauna Loa and Mauna Kea induce orographic effects. Because the trade winds are northeasterly, the eastern (or windward) side of the island has the largest amount of rainfall while the western (or leeward) side has the least. Moreover, the shear height of Mauna Loa and Mauna Kea allow for a polar or Type E climate to be found in the tropics (Juvik et. al 1973).

It is has been accepted for some time that the sulfate aerosols in the stratosphere have a cooling affect on regional surface temperatures by scattering incoming radiation, while at the same time increasing the temperatures in the stratosphere through absorption (Rampino and Self 1984; Jakosky 1986). It is also now known that an increase in sulfates in the troposphere can instigate a cooling

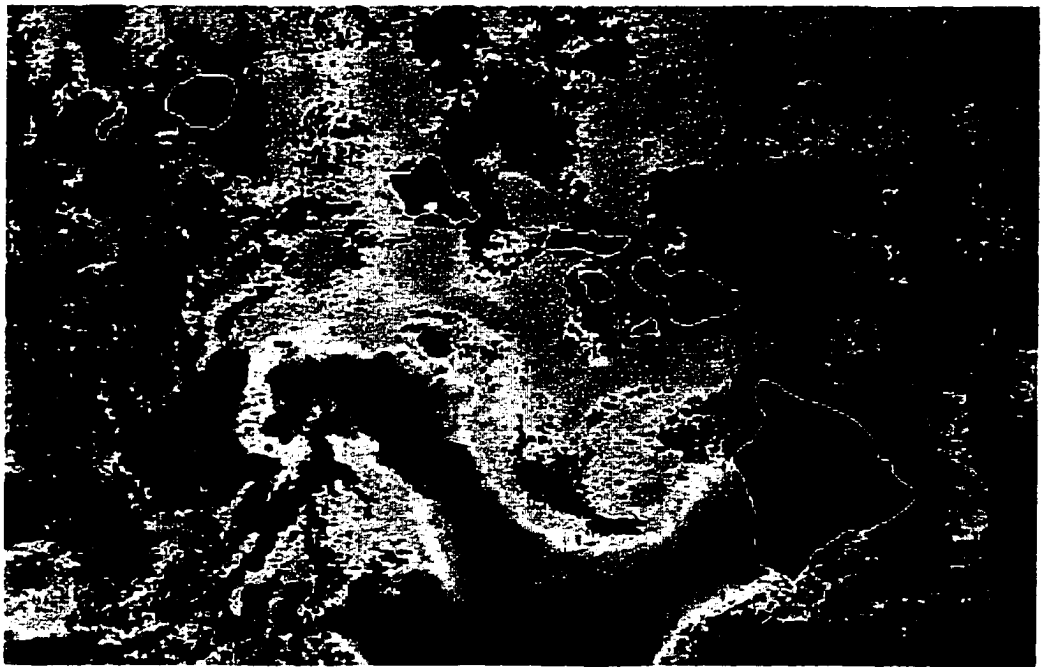


Figure 2.5: An enhanced satellite image showing the path of the vog plume around Hawai`i Island. (Taken from Sutton et al. 1997)

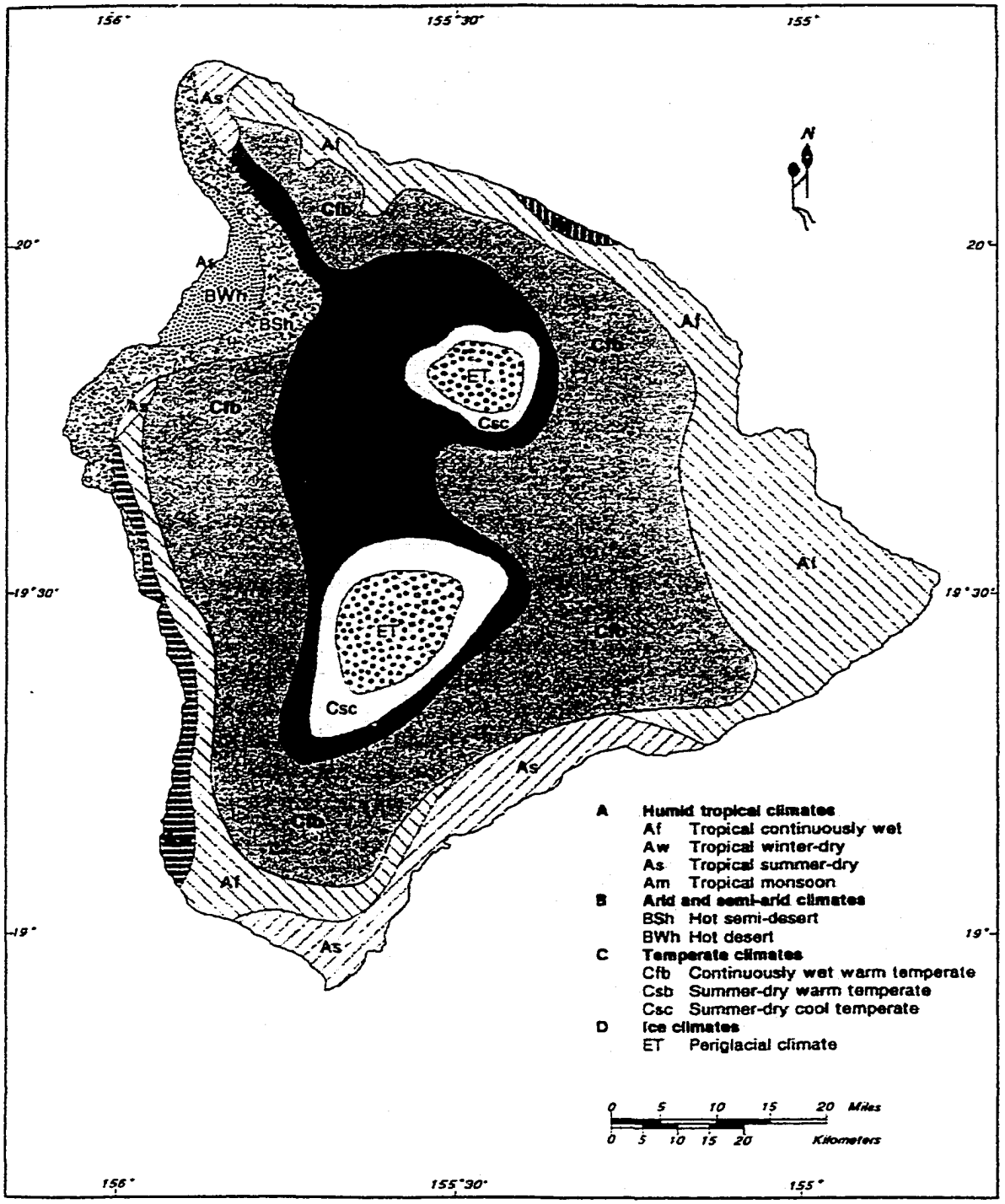


Figure 2.6: The Köppen climate classification of Hawai`i Island. After Juvik et al. 1978; taken from Morgan 1996.

trend in regional climate by acting as cloud condensation nuclei (CCN) in the formation of cirrus clouds (Charlson and Wigley 1984; McGee and Gerlach 1995; Chuang et al. 1997). The increase in cirrus clouds affect the Earth's radiation balance by reflecting incoming radiation back into the upper atmosphere or space (McGee and Gerlach 1995). Furthermore, the role of sulfate aerosols serving as CCN could also influence the precipitation process (Wallace and Hobbs 1977; Peixoto and Oort 1992) This research aims to detect patterns and trends in surface rainfall and temperatures on Hawai`i Island which would support the above conjectures.

2.4 Geology and Soils

Since Hawai`i Island is volcanic in origin, basalt is the dominate rock type. There are relatively few minerals present in the lava produced by Hawai`i's volcanoes. The most common are olivine, pyroxene, and plagioclase. These minerals are not present in the same amounts for all of Hawai`i's lavas and usually vary from location to location (Clague 1998). Finally, there are two types of lava flows present in Hawai`i: pāhoehoe and `a`ā. Pāhoehoe flows are usually the result of long-sustained eruptions and `a`ā flows are usually produced from short, high volume eruptions.

The basaltic base, presence of volcanic ash, and long-term weathering have produced very fertile soils on Hawai`i. Soil types present on the Island vary due to factors as local climate, hydrology, and parent material. Eight soil orders are identified on Hawai`i Island, with Histosols-lava-Andisols, Histosols-lava, and Andisols being located within the study area (HAVO region) (Uehara 1983; Gavenda et. al 1998). The spatial distribution of the soil orders is shown in Figure 2.7.

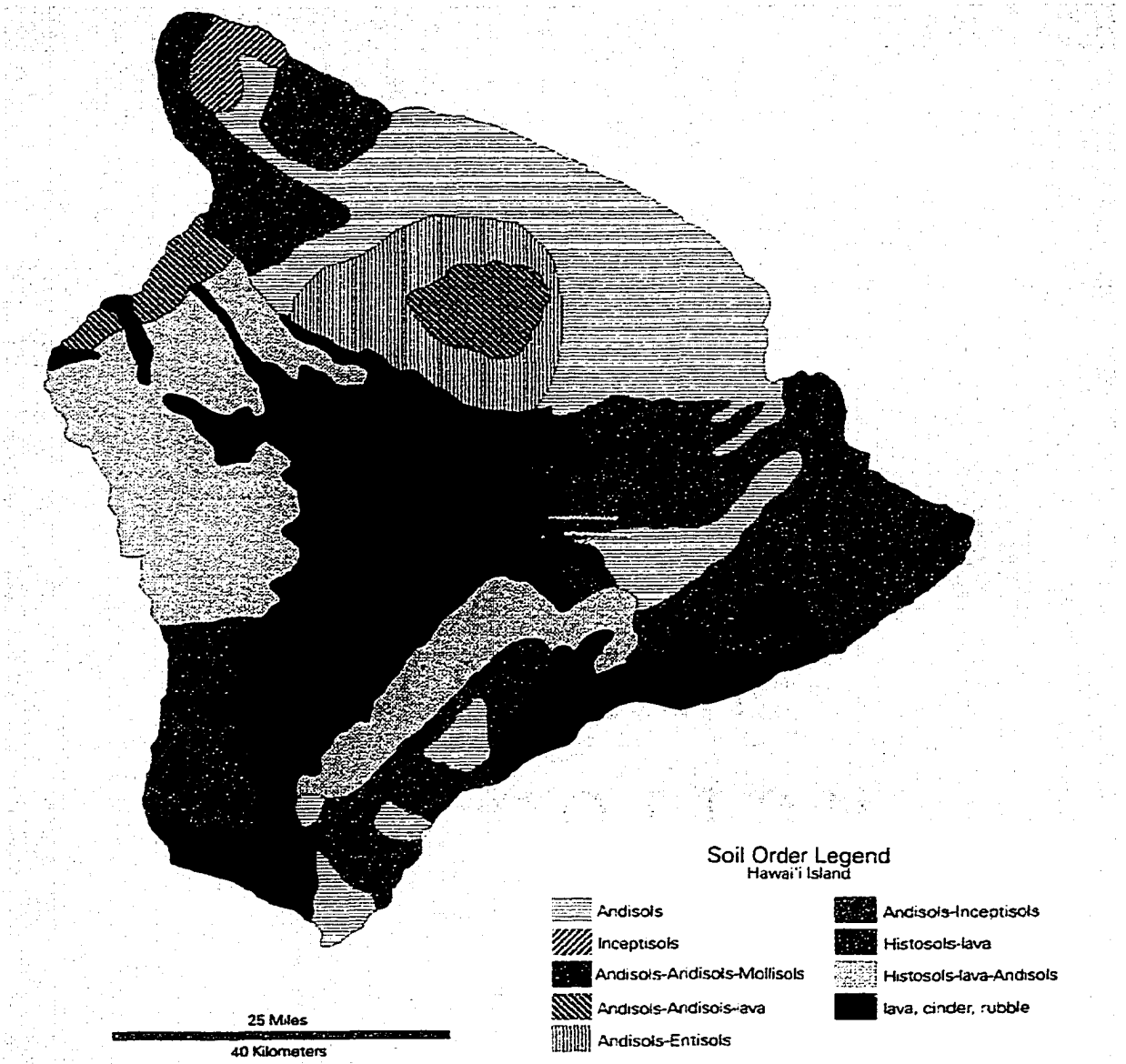


Figure 2.7: Map of major soil orders present on Hawai`i Island. (Taken from Gavenda et al. 1998).

The location of different soils is important when considering possible long-term impacts on vegetation as some have a higher buffering effect on acid rain than others (Winegardner 1996). When soil acts as a buffering system, it is resistant to changes in the amount of H+ present, thus resisting short-term changes in pH. Agents in soils that aid in the buffering process include carbonate materials and organic matter (Winegardner 1996). The soils present in the study area have a pH ranging from 4.5 to 8.0, with the variability partly dependant on high rainfall and temperatures, which increase soil weathering and conversion to acidic soil (Hue and Ikawa 1997; Uehara et al. 1997).

CHAPTER 3

DATA AND METHODOLOGY

This chapter includes a description of the satellite data and the temperature and rainfall data used in this study. Moreover, the methods used for data analysis are introduced and discussed.

3.1 Description of Satellite Imagery

In order to complete the objectives of this research concerning *vog* impacts on vegetation, pre- and post-eruption satellite scenes were needed. Considerations such as instrument spectral and spatial resolution as well as cloud cover severely limited data options. Moreover, it was discovered that there is a data gap for Landsat imagery over the Hawai'ian Islands from approximately 1979 to 1989 due to the lack of a ground station at the time to download the data for that part of the world (Personal Communication, EROS Data Center 1997).

Taking the above into consideration, a 1977 Landsat Multispectral Scanner (MSS) image (Figure 3.1) was selected to be used to represent pre-eruption vegetation. Landsat MSS has a relatively coarse resolution (79 m) especially when it is used to look at a small area such as Hawai'i Island; but finer multispectral imagery such as Landsat Thematic Mapper (TM) and SPOT did not exist until after the current long-term eruption began. It was decided to use System Pour l'Observation de la Terre (SPOT) Haute Resolution Visible (HRV) imagery (Figures 3.2 and 3.3) over Landsat TM to represent post-eruption vegetation due to its fine scale and the

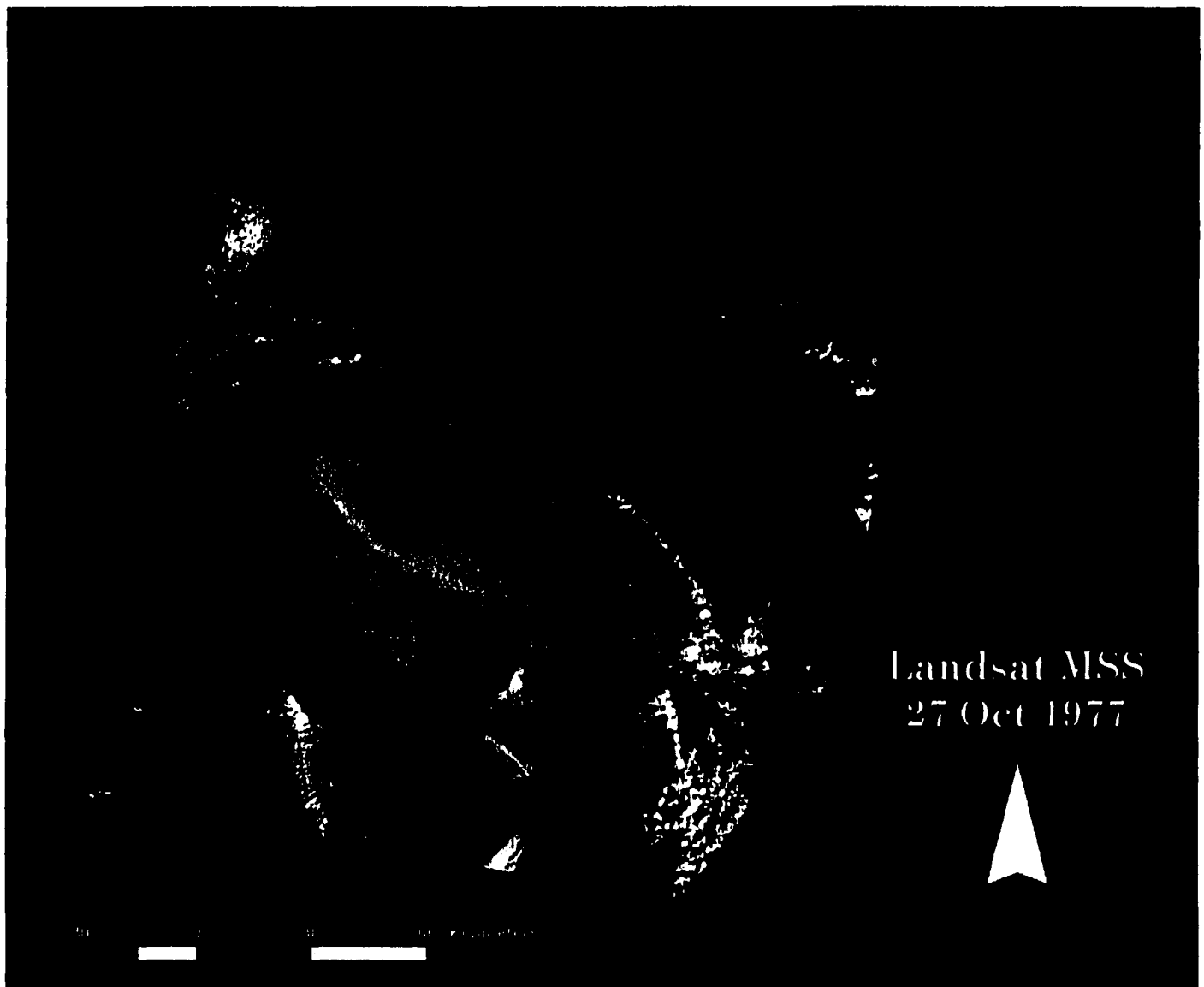


Figure 3.1: Landsat MSS scene acquired 27 October 1977.

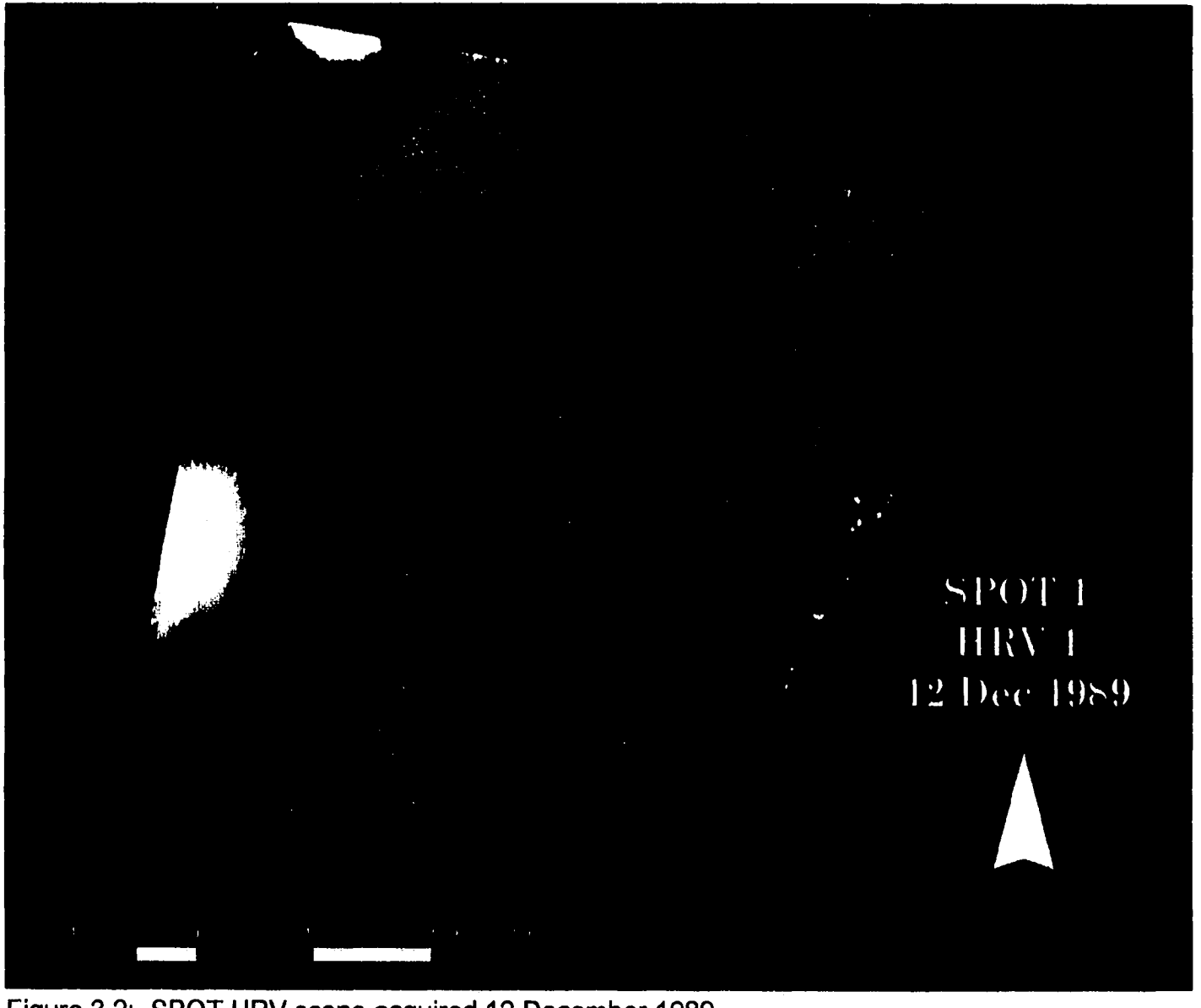


Figure 3.2: SPOT HRV scene acquired 12 December 1989.

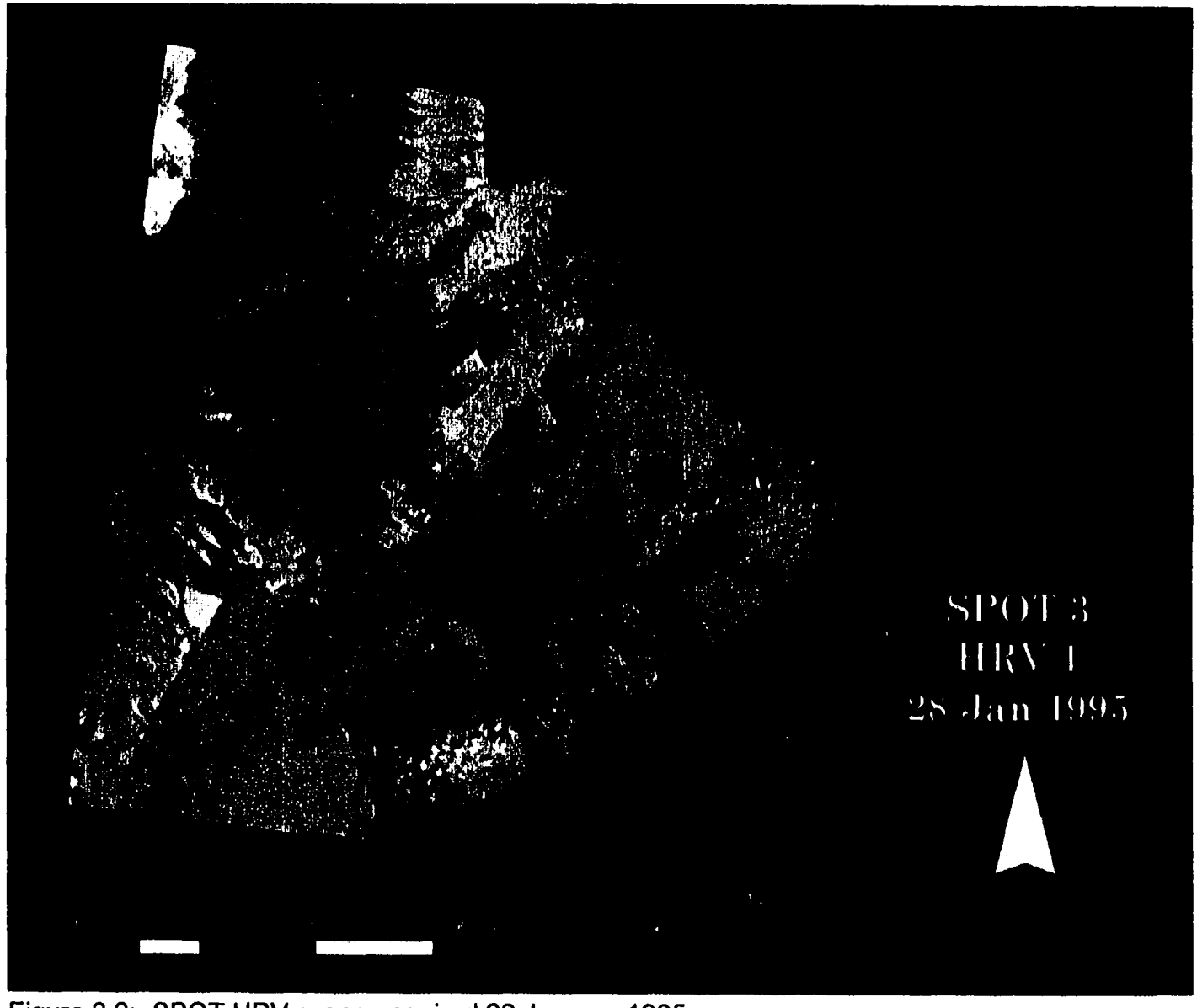


Figure 3.3: SPOT HRV scene acquired 28 January 1995.

availability of relatively cloud free scenes over the study area. These restrictions resulted in only two SPOT images satisfying the relatively cloud free requirement; the selected SPOT scenes were from 1989 and 1995. To account for possible seasonal variation that might affect the reflectance of vegetation, the months selected are within 90 days of each other. Table 3.1 describes the specific details of the data's characteristics.

	Landsat MSS	SPOT HRV	SPOT HRV
Acquisition Date	10/27/77	12/12/89	1/28/95
Spatial Resolution (m)	79	20	20
Spectral Resolution (μm)	Band 4: 0.5 - 0.6 Band 5: 0.6 - 0.7 Band 6: 0.7 - 0.8 Band 7: 0.8 - 1.1	Band 1: 0.5 - 0.59 Band 2: 0.61 - 0.68 Band 3: 0.79 - 0.89	Band 1: 0.5 - 0.59 Band 2: 0.61 - 0.68 Band 3: 0.79 - 0.89

Table 3.1: Specifications of satellite data used in study (NASA 1976; SPOT 1999)

Since the orbit path for each of the three satellites do not exactly match, the sensors acquire data over different portions of the study area with overlap in the region between HAVO and the town of Hilo. The region common to all three satellite scenes was subset from each, and the subsets were used in this study's analysis. (The common area of all three scenes is shown in Figures 4.5 and 4.9).

There are several concerns that need to be addressed when comparing imagery of different spectral and spatial resolutions. The difference in spatial resolution had to be accommodated. Initially, this was going to be done by converting the raster cells to polygons after each scene's NDVI was computed. This would create

thousands of polygons which would be difficult to manage. Thus after the conversion to polygons, the new coverages would have had another field added to their polygon attribute table (PAT) which would include a rescaled value for the NDVI. The "simplified" polygon coverages would then be "differenced" to determine what areas had changed. This method would have preserved the 20 m SPOT data the SPOT data, i.e. the scene would not have had to been resampled to the MSS spatial resolution of 79 m. Unfortunately, ArcInfo was not about to successfully convert the cells into polygons. Therefore to accommodate the spatial differences between the SPOT and Landsat MSS imagery, the SPOT scenes were resampled to the 79 m resolution of the Landsat MSS data after all pre- and post-processing was completed. The Landsat MSS data were not resampled to the SPOT's 20 m resolution as that would have resulted in the creation of spatial data where there was none. There is no way to "resample" the different spectral resolutions of the sensors, but the differences are noted when the final results are interpreted.

One final concern that should be noted is that the SPOT scenes were acquired off nadir; that is with the sensor not looking directly down at the Earth's surface. The view angle for the 1989 SPOT image was approximately 2 degrees while the 1995 SPOT image's view angle was 22 degrees. Since the images were acquired off nadir, this could produce some noticeable distortion towards the edges of the scenes.

3.2 Image Preprocessing

The Landsat MSS and two SPOT scenes were purchased without georectification. The pre-processing and image analysis was primarily done using ERDAS Imagine (ERDAS, Atlanta, Georgia) and ArcInfo (ESRI, Redlands, California)software. Pre-processing of imagery included performing image-to-image georectification to correct unsystematic errors, which make the images nonplanimetric (Jensen 1996). Ground control points (GCPs) were selected according to ease of identification between images. Accept features used for GCPs included road intersections, airport runways, and lava flows. The spatial resolution of each image along with the amount of cloud cover present influenced the number and type of GCPs used in the georectification process. The root-mean-square (RMS) error for each control point was calculated in Imagine using Equation 3.1, with the largest acceptable RMS error value being 0.5, or half a pixel.

$$RMS_{error} = \sqrt{(x'-x)^2 + (y'-y)^2} \qquad (3.1)$$

Where x' is longitude location for scene A ; x is longitude location for scene B; y' is latitude location for scene A, and y is latitude location for scene B.

The 1977 Landsat MSS scene was georectified first using a 1989 Landsat TM image that was referenced in Universal Transverse Mercator (UTM) coordinates. A total of 15 GCPs were coupled with a second-order transformation using nearest neighbor resampling with a total RMS error of 0.49. The spatial resolution of the 1977 Landsat MSS scene was kept at 79 meters. The 1989 and 1995 SPOT scenes were subsequently georectified using the 1977 Landsat MSS image. Ten GCPs were used

for the 1989 SPOT image with a second-order transformation resulting in a total RMS of 0.35. For the 1995 SPOT scene, fifteen (15) GCPs were utilized with a second-order transformation that resulted in a total RMS error of 0.47. During the georectification process, the two SPOT scenes were resampled to 20m using the nearest neighbor sampling scheme. In nearest neighbor interpolation, the value closest to designated input coordinate is assigned to the output coordinate (Jensen 1996). Thus, the nearest neighbor sampling regime is often favored by earth scientists because it does not change the pixel values during the resampling process (Duggin and Robinove 1990). Other interpolation techniques such as bilinear and cubic convolution resampling use averages to calculate output cell values (Jensen 1996).

The next step of image preprocessing involved transforming the raw digital numbers (DNs) of each scene to absolute radiance values. The conversion of DNs to absolute radiance and then to exoatmospheric reflectance values is required for analysis that involves multiple images taken by different sensors (Lillesand and Kiefer 1987; Goward et al. 1991; Song et al. 2001). This conversion process helps to reduce deviations in DN values due to instrument calibration, viewing geometry, and atmospheric attenuation (Goward et al. 1991; Song et al. 2001). Radiometric calibration of a sensor's raw digital data is derived from prelaunch calibration and is continually calibrated onboard the sensor by comparing known radiance values with the consequent DNs (Markham and Barker 1986; Lillesand and Kiefer 1987). For Landsat MSS data that was acquired prior to February 1, 1979, the conversion to spectral radiance is described by Equation 3.2 (EOSAT Landsat Technical Notes 1986):

$$L_\lambda = Lmin_\lambda + ((Lmax_\lambda - Lmin_\lambda) / QCALMAX)QCAL \qquad (3.2)$$

where L_λ represents spectral radiance in mW • cm^{-2} •$ster^{-1}$; $Lmin_\lambda$ is the spectral radiance at QCAL = 0; $Lmax_\lambda$ describes spectral radiance at (QCAL - QCALMAX); QCALMAX is the range of spectral radiance in DN; and QCAL is the calibrated and quantized scaled radiance in units of DN. $Lmin_\lambda$ and $Lmax_\lambda$ calibration parameters can be obtained from EOSAT Landsat Technical Notes No. 1 (August 1986). Since the MSS scene used in this study was acquired prior to February 1, 1979, QCALMAX is 63 DN.

The translation of SPOT DNs to radiance values uses a different conversion process and is described in Equation 3.3 (Messina 1996):

$$L(k) = DN / A(k) \qquad (3.3)$$

where L(k) is the equivalent radiance in W • m^{-2}• $srad^{-1}$; DN is the digital number value of the cell; and A(k) is the absolute calibration coefficient provided by SPOT.

The final step of preprocessing for all three images is to reduce the between-scene variability by normalizing for solar irradiance. This is accomplished by converting the spectral radiances to effective at-satellite reflectance. The combined atmospheric and surface reflectance of the Earth is described by Equation 3.4 (EOSAT Landsat Technical Notes 1986):

$$\rho_p = (\pi \bullet L_\lambda \bullet d^2) / (ESUN_\lambda \cdot \cos\Theta_s) \qquad (3.4)$$

where ρ_p is the unitless effective at-satellite planetary reflectance; L_λ is the spectral radiance at sensor aperture; d is the Earth-Sun distance in astronomical units from

nautical handbook; $ESUN_\lambda$ is the mean solar exoatmospheric irradiances; and Θ_s is the solar zenith angle in degrees.

3.3 Vegetation Change Detection Methodologies

Two strategies were identified as possible methods to detect changes in vegetation within the study area. Option one was to perform a multispectral unsupervised classification on the area using the Iterative Search of Data (ISODATA) classification algorithm in ERDAS Imagine. The second option was to utilize the Normalized-Difference Vegetation Index (NDVI) which is commonly used for vegetation monitoring.

3.3a Multispectral Classification

The purpose of image classification algorithms is to automatically catagorize all pixels in a remotely-sensed image into separate classes or themes, with the resultant thematic file depicting categories such as vegetation or land cover types (Lillesand and Kiefer 1987; Jenson 1996; ERDAS 1999). Multispectral classifications include a supervised or unsupervised approach.

In a supervised classification, the image analyst controls the classification process by defining training sites that are used to determine how the classification algorithm categorizes the pixels in the image (Lillesand and Kiefer 1987; Jenson 1996). This requires the analyst to have *a priori* knowledge of the area from fieldwork, maps, and personal experience.

An unsupervised classification is based on the inherent groupings of pixel

values plotted in spectral space; it does not depend on training sites as the premise for classification (Lillesand and Kiefer 1987; Jenson 1996; ERDAS 1999). It relies on the assumption that similar land cover types will be located close together in spectral space (Lillesand and Kiefer 1987; ERDAS 1999). The ISODATA Classification algorithm is an example of a classification program used for unsupervised classification. Specifically, the ISODATA program utilized by Imagine uses minimum spectral distance to allocate an accumulate for each candidate pixel. The ISODATA method starts with a number of indiscriminate cluster means that are specified by the user, then repeatedly classifies the scene and recalculates statistics until the user specified convergence threshold is obtained (ERDAS 1994). This creates a single thematic layer. After the data are classified, an *a posteriori* assignment of the spectral clusters to thematic classes is performed by the image analyst.

Selecting a classification process is not the only decision that an analyst needs to make when performing an image classification. A classification scheme outlines the taxonomy of the class definitions (Jensen 1996). Moreover, the classification scheme used must suit the needs of the user. Not all users share the same objectives when performing a land cover classification. For example, some may wish to emphasize land cover verses land use, such as the USGS's Land Use Land Cover Classification System, which stresses the land areas that are not built up or urbanized (Anderson et al. 1976). Other agencies, such as the U.S. Fish and Wildlife and N.O.A.A, have developed their own classification systems to suite their needs (Jensen 1996). Trial classifications using generalized classification categories have been done on portions of Oahu and Hawai`i using both Landsat MSS and TM imagery, but

the results were mixed due to problems with collecting data over the islands (DPED 1981; DPED 1998). For example, cloud cover is known to cover large portions of land area and the useable data ended up being collected over different years and months (DPED 1998).

3.3b Normalized Difference Vegetation Index (NDVI)

It is well established that vegetation canopy characteristics such as productivity, leaf area index (LAI), and absorbed photosynthetically active radiation (APAR) can be inferred from remotely sensed data (Jensen 1996; Chen et al. 1998). Figure 3.4 shows generalized spectral reflectance characteristics for healthy vegetation, dead or senescing vegetation, and dry soil. It also exhibits how healthy vegetation typically has high reflectance in the near infrared (NIR) portion of the spectrum, while also having low reflectance in the red portion of the EMR spectrum. If a plant is subjected to stress that reduces its productivity, the amount of chlorophyll produced may decrease or cease all together. This causes a decrease in the amount of reflected infrared light (Chen et al. 1998). Several vegetation indices have been developed which use this relationship between the red and NIR bands in order to model vegetation health, including the Normalized Difference Vegetation Index (NDVI), Ratio Vegetation Index (RVI), and Soil Adjusted Vegetation Index (SAVI). (Jordan 1969; Rouse et al. 1973; Huete 1988; Goward et al. 1991; Jensen 1996; Chen et al. 1998). Perhaps the most utilized is the NDVI as it is recognized as one of the first effective vegetation indices based on ratioing (Rouse et al. 1973; Mather 1987). Specifically, the NDVI uses red and NIR bands and is generally characterized by Equation 3.5.

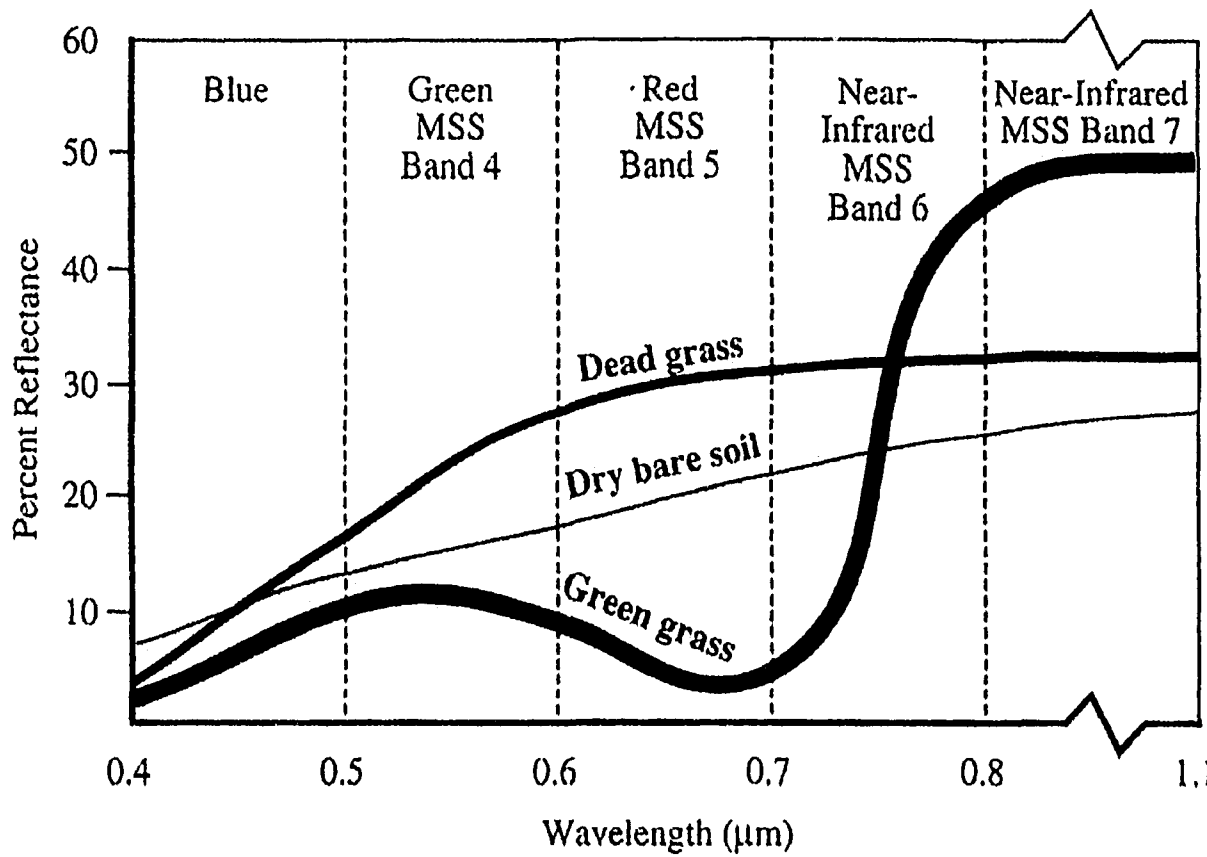


Figure 3.4: Spectral reflectance characteristics for healthy green grass, dead or senescing grass, and bare dry soil. Though this graph specifically shows general grass spectral reflectance, the spectral reflectance for other vegetation types would only vary slightly from the above. (Taken from Jensen 1996)

$$NDVI = (NIR - Red) / (NIR + Red) \quad (3.5)$$

Taking the characteristics of each method into consideration, it was decided that the best program for determining changes in the vegetation located in the study was to use the NDVI. This decision was based on several factors. First, performing a land cover classification over the area would be extremely time and labor intensive due to Hawai`i's rugged terrain and trespass restrictions. Moreover, the size of the vegetation patches that represent specific ecosystem or forest clusters are relatively small, and thus may not be discernable at the spatial resolutions provided by SPOT and certainly not Landsat MSS imagery. Due to the above reasons, there currently is no detailed land cover map existing for Hawai`i. The state is also one of the last to participate in the National GAP Analysis Program's land cover mapping project, whose goal is "to provide regional assessments of the conservation status of native vertebrate species and natural land cover types and to facilitate the application of this information to land management activities" through sponsoring mapping carried out through the use of satellite data and groundtruthing (GAP 2001). Finally, groundtruthing a land cover classification done on historic imagery would require the assumption that the land had not changed much since the imagery was acquired. For many regions of Hawai`i, this assumption would not be valid due to the severe problem of alien species invasion and the rapidly expanding commercial and residential housing developments.

For the objectives of this study, the NDVI is a sufficient measure of the "health" of the vegetation present, and any change over time can be discerned by subtracting NDVI thematic layers from one another (Coppin and Bauer 1996). No classification

or specific species identification is necessary; though this could also be considered a negative if a change is detected; specifically, the index does not distinguish whether the change is in the health of the vegetation or if the species of vegetation occupying the study area has changed. One final incentive for using the NDVI is that the index can also be applied to future studies for estimating percent vegetation cover (Purevdor et al. 1998).

3.4 Derived NDVI for SPOT and Landsat MSS

Since this study used Landsat MSS and SPOT HRV multispectral imagery, the NDVI computation was expanded to Equations 3.6 and 3.7 respectively. For Landsat MSS, band 7 (NIR) and band 5 (red) are usually used in the NDVI analysis (as shown in Equation 3.6). The MSS band 7 spectral bandwidth is closer to the SPOT HRV band 3 (NIR), but for exploratory analysis, a NDVI was also computed using the MSS band 6 (NIR). The NDVI for MSS band 6 is shown in Equation 3.8.

$$NDVI_{mss} = (b7 - b5) / (b7 + b5) \quad (3.6)$$

$$NDVI_{spot} = (b3 - b2) / (b3 + b2) \quad (3.7)$$

$$NDVI_{mssb6} = (b\,6 - b\,5) / (b\,6 + b\,5) \quad (3.8)$$

Computed NDVI values can range between -1.0 and 1.0, with lower values indicating an area that is not very green (including urban areas) and higher values representative of very green areas (healthy vegetation). Typical NDVI values range from -0.1 to 0.6 (NOAA 1998). This range does not correspond with the byte data

range for 8-bit satellite data (256 bytes) and is usually rescaled such that -1.0 equals 0, 0 equals 100, and a NDVI of 1.0 equals 200. Once the original NDVI are rescaled, values less than 100 represent clouds, water, snow and other non-vegetated areas, while NDVI values greater than 100 represent vegetated surface areas (Kidwell 1990).

3.5 NDVI Calculations and Differencing

The Model Maker module in ERDAS Imagine was used to build and compute the NDVI values for each of the three satellite scenes, including the NDVI values for both MSS band 7 and MSS band 6. The raw NDVI values for each satellite image were rescaled from 0.0 to 200 using the method described by Equation 3.9. Histogram plots for the four resulting single-layer thematic images are shown and discussed in Chapter 4.

$$NDVI_{rescaled} = [(NIR - Red / NIR + Red) \bullet 100] + 100 \qquad (3.9)$$

The next step was to subtract the SPOT NDVI layers from the 1977 NDVI layers to determine differences or changes in the NDVI values over time. Before this could be done however, the SPOT NDVI layers had to be resampled to the same sample scale or pixel size as the Landsat MSS NDVI layers. This was done using the RESAMPLE function in the GRID module within ArcInfo. The RESAMPLE function allows the user to change the input grid's cell size to the dimensions of a specified output (ESRI 1999). The specific number of rows and columns in the output grid is regulated by the following guidelines (ESRI 1999):

$$\textbf{\# columns} = \textbf{(xmax - xmin) / cell size} \qquad (3.10)$$

#rows = (ymax - ymin) / cell size (3.11)

"If there is any remainder from the above equations, then rounding of the number of columns and/or rows is performed" (ESRI 1999). Within the RESAMPLE function, the NEAREST option was utilized as it performs a nearest-neighbor assignment. Again, this type of computation does not change the value of the cells at the user-specified locations; in other words, if at the new cell's location the current NDVI value was 100, then that cell keeps the value of 100, but the 100 NDVI value also is extended out spatially to the new cell size. Prior cell values next to the new location cell would be dropped (ESRI 1999).

After the SPOT NDVI layers were resampled to the 79 m cell size of the Landsat MSS NDVI layers, the later SPOT layers were subtracted from the earlier Landsat MSS layers using the SUBTRACT operator in the GRID module within ArcInfo. The SUBTRACT operator subtracts the values of the second grid from the values of the first grid on a cell-by-cell iteration (ESRI 1999). The two resampled SPOT NDVI layers were also subtracted from each other for comparison. These computations would create new thematic layers showing the how NDVI values have changed between 1977 and 1989, 1977 and 1995, and 1989 and 1995 respectively. Cells in the difference NDVI layers that have a negative value indicate that the more recent layer had a higher NDVI value than the older layer which would indicate a change for the positive (improvement) in vegetation health. Meanwhile, cells in the differenced NDVI layers that have a positive value indicate that the more recent layer had a lower NDVI value than the older layer which would indicate an adverse change in vegetation health. The computed NDVI difference layers as well as the histograms for each of the

difference layers produced are shown and discussed in Chapter 4.

3.6 Rainfall and Temperature Data Characteristics

In order to successfully determine trends in rainfall and surface temperature for Hawai'i Island, a time series with sufficient temporal and spatial resolution was needed. It was decided to use monthly surface data between (and including) 1969 and 1999 as this would create a sample size of 31 years with roughly an equal distribution before and after Kilauea began its current long-term eruption in January 1983. The rainfall and temperature data were acquired from the National Climatic Data Center (NCDC) in Asheville, NC. using their interactive web-based search engine.

3.6a Precipitation Data

The NCDC search produced a list of 142 individual sites that reported any total monthly precipitation values during the 31 year study period. Each station's period of record was inspected to assess its completeness. It was decided that only sites that had records for all 31 years and having no more than one month's precipitation value missing would be included in the exploratory analysis. This produced a total of 15 sites; 10 with complete records and 5 which were missing only one month's value. Data for missing months were interpolated by using the computed average of the value from the prior and subsequent month. Finally, data that were flagged as accumulated, trace, and estimated monthly rainfall values were accepted as being the "actual" value measured. Figure 3.5 shows the location and spatial distribution of the selected rainfall sites used in the analysis.



Figure 3.5: Location of precipitation stations used in trend analysis.

3.6b Temperature Data

The temperature search of the NCDC database comprised of sites that reported monthly mean temperatures, monthly mean minimum temperature, and monthly mean maximum temperatures during the 31 year study period. The search produced a list of 35 individual sites, and again each station's period of record was inspected to assess it completeness. None of the site records were complete for the whole 31 year time-line, with most missing several years of data. Moreover, many of the stations that did have records for the 31 year period had substantial missing data (over 6 continuous months). The final acceptable criterion was that the site had reported data for the complete 31 year period with no more than 3 months of data being missing in any particular year. This drastically reduced the site total to 3 sites. Data values for a missing single month were interpolated by using the computed average of the value from the prior and subsequent month. When three consecutive months of data were missing, a 6^{th} order polynomial curve was fitted to the three prior and subsequent months to interpolate the missing values. The stations and their spatial location are shown in Figure 3.6.

3.7 Exploratory Statistical Analysis of Monthly Rainfall and Temperature Data

Linear regression is commonly used in trend analysis. For this study, the exploratory statistical techniques used were based on those used in a study by Morrissey and Graham (1996) in which they examined trends in monthly rainfall using accumulated daily precipitation in the Tropical Pacific. Before they began their analysis, they applied a filter to the daily values to remove the annual cycle signal by

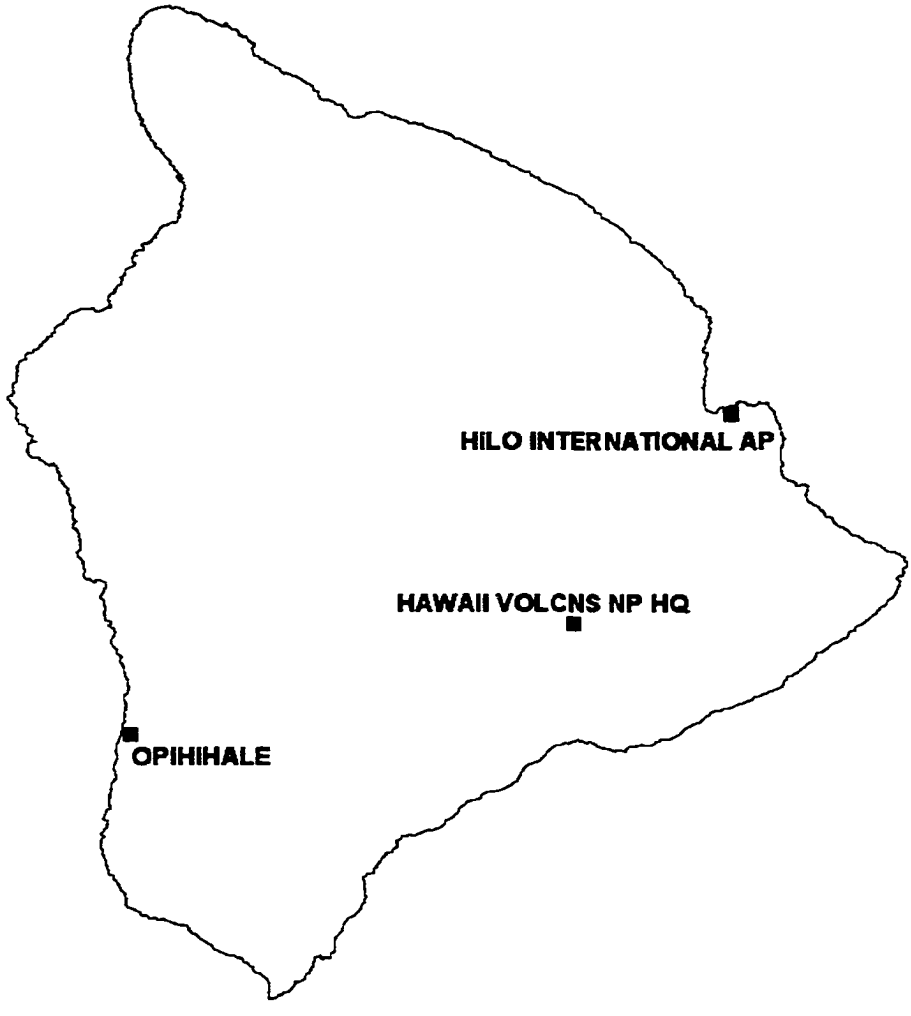


Figure 3.6: Location of temperature sites used in trend analysis.

subtracting long-term monthly rainfall averages from each station. Morrissey and Graham then applied a simple linear regression to each time series for all rain gauge stations.

For this study, mean yearly precipitation values were derived from the total monthly precipitation data. Linear regression was applied to the complete yearly mean time series; thus it was not necessary to remove the annual cycle from the data set. The same was done for the monthly mean temperature, monthly mean minimum temperature, and monthly mean maximum temperature. The time series of precipitation and temperature data were separated into pre- and post-eruption years and a regression line was fitted to these "sub" samples of time series as well. Microsoft's Excel software was used to calculate all statical analysis and to make the corresponding graphs. The resulting regression equations along with corresponding r^2 values are shown in Tables 3.2, 3.3, 3.4, 3.5, 3.6, and 3.7.

The goodness of fit of the regression line can be determined by looking at the population correlation coefficient (ρ), the coefficient of determination (ρ^2), and the standard error (σ). The values of these true regression model parameters are not really known; thus point estimates of the parameters are used in applications of regression analysis instead. These estimates include the simple correlation coefficient (r), the coefficient of determination (r^2), and the standard error of estimate ($S_{x \cdot y}$), which are defined by the following (Burt and Barber 1996):

$$r = \frac{\sum_{(i-1)}^{n} (X_i - \overline{X})(Y_i - \overline{Y})}{\sqrt{\sum_{i=1}^{n} (X_i - \overline{X})^2} \sqrt{\sum_{i=1}^{n} (Y_i - \overline{Y})^2}} \qquad (3.12)$$

Site	Regression Eq.	r^2	S_b	t (* indicates it is significant)
Hawaii Volcns NP HQ	y = -1.2707x + 923.06	0.0031	9.054	-0.140
Hilo International AP	y = 1.0531x + 1049.1	0.0014	13.902	0.076
Kainaliu	y = -4.8934x + 534.62	0.1412	2.512	-1.948*
Kapapala Ranch	y = -1.8495x + 545.46	0.007	8.311	-0.222
Keaau	y = -3.0193x + 1219.3	0.0096	16.190	-0.186
Kona Village	y = -0.6336x + 102.16	0.0126	0.541	-1.172
Kulani Camp	y = -2.3378x + 951.91	0.0074	12.715	-0.184
Lanihau	y = -7.459x + 600.66	0.1889	4.118	-1.811*
Mauna Loa Obs	y = -0.5954x +164.41	0.0043	1.418	-0.42
Middle Pen	y = -0.7657x + 132.11	0.0194	0.510	-1.50
Naalehu	y = -0.9514x + 416.7	0.0043	3.615	-0.263
Opihihale	y = -2.5992x + 365	0.0674	1.613	-1.612
Paauilo	y = 1.8286x + 817.11	0.0037	15.373	0.119
Papaikou	y = -8.5557x + 1340.6	0.0642	18.387	-0.465
Waiakea	y = 1.321x + 1640.1	0.0011	1.864	0.709

Table 3.2: List of precipitation sites along with each station's corresponding regression equation, r^2 value, S_b value, and calculated *t* value for the complete 31 year time series. Those that are significant (P=0.95) are indicated by *.

Site	Regression Eq.	r^2	S_b	t (* indicates it is significant)
Hawaii Volcns NP HQ	y = 6.5866x + 880.7	0.0389	44.685	0.147
Hilo International AP	y = -7.994x + 1106.7	0.0191	136.38	-0.059
Kainaliu	y = 13.835x + 416.05	0.1917	33.632	0.411
Kapapala Ranch	y = 22.885x + 387.56	0.2789	56.426	0.406
Keaau	y = 0.6967x + 1208.7	0.0001	190.49	0.004
Kona Village	y = 2.8908x + 78.89	0.0488	6.786	0.426
Kulani Camp	y = 6.7026x + 904.78	0.027	67.564	0.099
Lanihau	y = 13.099x + 467.32	0.1042	61.441	0.213
Mauna Loa Obs	y = 12.419x + 78.249	0.3383	12.57	0.99
Middle Pen	y = 3.2242x + 101.43	0.0854	4.636	0.695
Naalehu	y = 4.9526x + 373.28	0.043	22.719	0.218
Opihihale	y = 9.7531x + 285.82	0.1749	18.7	0.522
Paauilo	y = 16.564x + 700.97	0.0512	212.01	0.078
Papaikou	y = 3.1687x + 1275.8	0.0015	271.8	0.012
Waiakea	y = 6.2332x + 1621.2	0.0073	218.96	0.028

Table 3.3: List of precipitation sites along with each station's corresponding regression equation, r^2 value, S_b value, and calculated *t* value for the 14 years prior to current eruption. Those that are significant (P=0.95) are indicated by *.

Site	Regression Eq.	r^2	S_b	t (* indicates it is significant)
Hawaii Volcns NP HQ	y = 3.1634x + 851.71	0.004	84.101	0.038
Hilo International AP	y = 0.648x + 1075.9	0.0001	100.794	0.006
Kainaliu	y = -3.6922x + 437.27	0.0614	6.946	-0.532
Kapapala Ranch	y = -0.9594x + 488.82	0.0005	59.509	-0.016
Keaau	y = 4.0688x + 1099.1	0.0053	102.73	0.04
Kona Village	y = -0.9165x + 93.231	0.009	3.072	-0.298
Kulani Camp	y = 3.6132x + 848.61	0.0037	115.69	0.031
Lanihau	y = -7.8352x + 482.45	0.1434	12.224	-0.641
Mauna Loa Obs	y = -1.7647x + 157.17	0.0135	7.59	-0.233
Middle Pen	y = -3.3938x + 145.67	0.0194	3.403	-0.997
Naalehu	y = -3.7864x + 428.19	0.015	31.433	-0.12
Opihihale	y = -2.3282x + 315.09	0.0239	7.39	-0.315
Paauilo	y = -9.3785x + 948.21	0.0363	77.8	-0.121
Papaikou	y = -2.8409x + 1150.5	0.003	90.08	-0.032
Waiakea	y = 8.1308x + 1582.5	0.0093	3968.5	0.002

Table 3.4: List of precipitation sites along with each station's corresponding regression equation, r^2 value, S_b value, and calculated *t* value for the 17 years since Kilauea began erupting in 1983. Those that are significant (P=0.95) are indicated by *.

Table 3.5a

Site (mean monthly temp)	Regression Eq.	r^2	S_b	t (* indicates it is significant)
Hawaii Volcns NP HQ (lt)	y = 0.9522x + 679.28	0.3643	0.011	56.769*
Hawaii Volcns NP HQ (be)	y = 1.1947x + 595.74	0.3553	0.108	11.073*
Hawaii Volcns NP HQ (ae)	y = -0.077x + 616.23	0.0035	0.056	-1.366

Table 3.5b

Site (mean monthly minimum temp)	Regression Eq.	r^2	S_b	t (* indicates it is significant)
Hawaii Volcns NP HQ (lt)	y = 0.2652x + 522.19	0.0783	0.014	18.588*
Hawaii Volcns NP HQ (be)	y = -0.2723x + 526.3	0.0328	0.091	-2.986*
Hawaii Volcns NP HQ (ae)	y = 0.6058x + 522.77	0.0941	0.118	5.145*

Table 3.5c

Site (mean monthly maximum temp)	Regression Eq.	r^2	S_b	t (* indicates it is significant)
Hawaii Volcns NP HQ (lt)	y = 0.9522x + 679.28	0.3643	0.027	34.9*
Hawaii Volcns NP HQ (be)	y = 2.7009x + 664.8	0.6432	0.169	16.02*
Hawaii Volcns NP HQ (ae)	y = -0.7494x + 709.05	0.1752	0.088	-8.50*

Table 3.5: Station's corresponding regression equation, r^2 value, S_b value, and calculated *t* value for the complete 31 year time series (lt), for the 14 years prior to the eruption (be), and the 17 years since eruption began (ae) calculated from monthly temperature data. Those that are significant (P=0.95) are indicated by *.

Table 3.6a

Site (mean monthly temp)	Regression Eq.	r^2	S_b	t (* indicates it is significant)
Hilo International AP (lt)	y = 0.1355x + 738.65	0.0223	0.014	9.785*
Hilo International AP (be)	y = 05429x + 736.08	0.1316	0.081	6.70*
Hilo International AP (ae)	y = 0.1671x + 739.86	0.0075	0.123	1.359

Table 3.6b

Site (mean monthly minimum temp)	Regression Eq.	r^2	S_b	t (* indicates it is significant)
Hilo International AP (lt)	y = 0.3737x + 660.27	0.1992	0.010	36.6*
Hilo International AP (be)	y = 1.1396x + 645.79	0.3553	0.05	22.889*
Hilo International AP (ae)	y = 0.0835x + 667.91	0.0035	0.078	1.07

Table 3.6c

Site (mean monthly maximum temp)	Regression Eq.	r^2	S_b	t (* indicates it is significant)
Hilo International AP (lt)	y = -0.1035x + 816.55	0.0071	0.026	-4.007*
Hilo International AP (be)	y =-0.0553x + 816.9	0.0006	0.230	-0.24
Hilo International AP (ae)	y =0.2492x + 811.34	0.0105	0.196	1.274

Table 3.6: Station's corresponding regression equation, r^2 value, S_b value, and calculated *t* value for the complete 31 year time series (lt), for the 14 years prior to the eruption (be), and the 17 years since eruption began (ae) calculated from monthly temperature data. Those that are significant (P=0.95) are indicated by *.

Table 3.7a

Site (mean monthly temp)	Regression Eq.	r^2	S_b	t (* indicates it is significant)
Opihihale (lt)	y = 0.5882x + 688.36	0.2487	0.018	32.635*
Opihihale (be)	y = 1.3255x + 680.82	0.4582	0.087	15.312*
Opihihale (ae)	y = -0.8895x + 711.54	0.2436	0.082	-10.859*

Table 3.7b

Site (mean monthly minimum temp)	Regression Eq.	r^2	S_b	t (* indicates it is significant)
Opihihale (lt)	y = 0.4966x + 599.37	0.1428	0.026	19.466*
Opihihale (be)	y = -0.3183x + 601.43	0.0372	0.109	-2.917*
Opihihale (ae)	y = -1.2031x + 624.96	0.3083	0.108	-11.112*

Table 3.7c

Site (mean monthly maximum temp)	Regression Eq.	r^2	S_b	t (* indicates it is significant)
Opihihale (lt)	y = 0.6999x + 776.32	0.2543	0.025	28.267*
Opihihale (be)	y = 2.9856x + 759.18	0.7662	0.113	26.347*
Opihihale (ae)	y = -0.5743x + 797.59	0.1098	0.089	-6.439*

Table 3.7: Station's corresponding regression equation, r^2 value, S_b value, and calculated *t* value for the complete 31 year time series (lt), for the 14 years prior to the eruption (be), and the 17 years since eruption began (ae) calculated from monthly temperature data. Those that are significant (P=0.95) are indicated by *.

where X_i is the i^{th} observation of variable X; $\bar{x}$ is the mean of all X_i ; Y_i is the i^{th} observation of variable Y; and $\bar{y}$ is the mean of all Y_i.

$$r^2 = 1 - \frac{ESS}{TSS} = \frac{RSS}{TSS} \qquad (3.13)$$

where *ESS* is the error variation; *TSS* is the total variation of Y; and *RSS* is the explained variation (regression sum of squares).

$$S_{x \cdot y} = \sqrt{\frac{\sum_{i=1}^{n} \left(Y_i - \bar{Y}_i \right)^2}{n-2}} \qquad (3.14)$$

where Y_i is the i^{th} observation of variable Y; $\bar{y}$ is the mean of all Y_i; and *n* is the number of observations.

The significance of the correlation between X (time) and Y (precipitation) can be determined by performing a t-test. In this case, the null hypothesis (H_0) is $\beta = 0$. The equation used for the t-test is (Burt and Barber 1996):

$$t = \frac{b - \beta}{S_b} \qquad (3.15)$$

where β represents the true slope in the regression model; *b* is the slope from the calculated regression line; S_b is the estimate of standard error of the sampling distribution of *b*, and is defined as:

$$S_b = \frac{S_{x \bullet y}}{\sqrt{\sum_{i=1}^{n} X_i^2 - \left[\sum_{i-1}^{n} X_i\right]^2 / n}} \qquad (3.16)$$

For (H_0) : $\beta = 0$, therefore the equation for *t* can be reduced to:

$$t = \frac{b}{S_b} \qquad (3.17)$$

Furthermore, a confidence interval can be constructed from the point estimate *b* such that:

$$b - t_{\alpha/2,n-2} S_b \leq \beta \leq b + t_{\alpha/2,n-2} S_b \qquad (3.18)$$

If zero is contained in the above interval, then we must accept the null hypothesis that $\beta = 0$, and therefore the trend created by the regression line can be the result of random values and precipitation is not significantly correlated with time. For both precipitation and temperature, the t-test was performed, with the PROB-VALUE (p) < 0.05. If the t-value is higher than the lowest listed probability of 0.05, then it is considered significant, i.e. one may be 95% certain that the trend is not random.

For the precipitation data, the annual cycle was plotted. as well as plots of the annual cycle subtracted from the total monthly precipitation, to visually investigate variances in rainfall over the study period. Only annual cycle plots were created for the surface temperature data.

CHAPTER 4

RESULTS AND DISCUSSION

This chapter presents the results from the data analysis performed on the satellite imagery, monthly precipitation data, and monthly temperature data. This chapter also discusses what can be ascertained from the results.

4.1 Analysis of NDVI Scenes Prior to Differencing

Inspection of each image's pre-NDVI differencing frequency histogram provides information related to the distribution and range of NDVI values. Two NDVI frequency histograms were generated for the 1977 Landsat MSS scene since a NDVI was computed using both IR bands (bands 6 and 7). Figure 4.1 is the frequency histogram of NDVI values generated from MSS bands 7 and 5, while Figure 4.2 is the histogram of NDVI values produced from MSS bands 6 and 5. Figure 4.1 shows a negative skew distribution with values ranging from approximately -0.52 to 0.70. The strong spike at 0 is caused by "no data" pixel values present in the pre-NDVI scene. Most of the NDVI cell values are greater than zero, with the modal peak located approximately between 0.4 to 0.5. The histogram created from the band 6 and band 5 NDVI combination (Figure 4.2) also exhibits a negative skew distribution and shows the same "no data" spike at zero. The data range shown is between -0.31 and 0.62, which is narrower than the range produced by the band 7 and band 5 NDVI combination. The band 6 and band 5 NDVI combination is also unimodal with the peak being present in the 0.30 range. For both histograms, the location of most of the pixels is on the positive portion

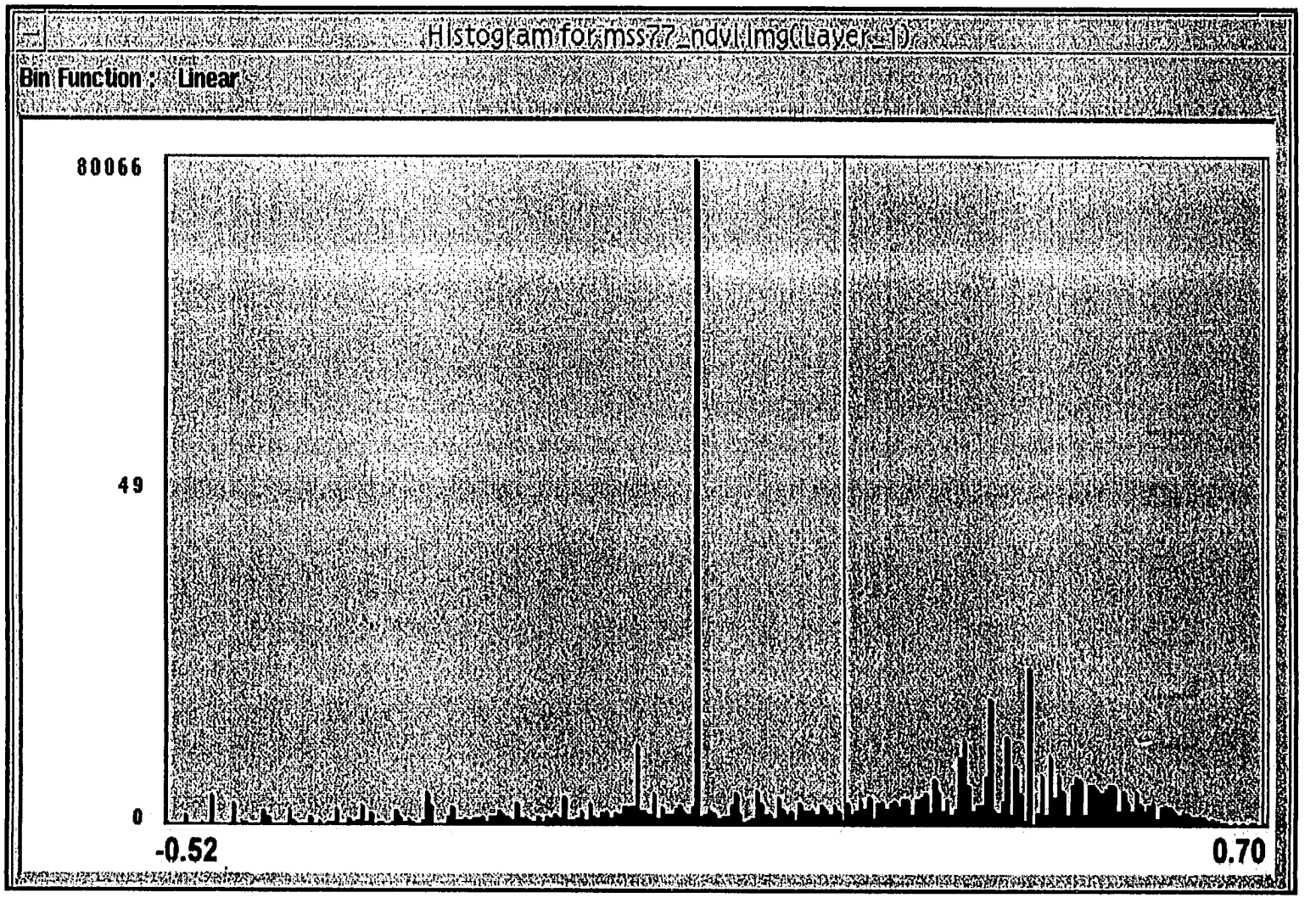


Figure 4.1: Frequency histogram of NDVI values computed from 1977 Landsat MSS sub-scene using band 7 (NIR) and band 5 (red). X-axis is NDVI value; Y-axis is the number of pixels.

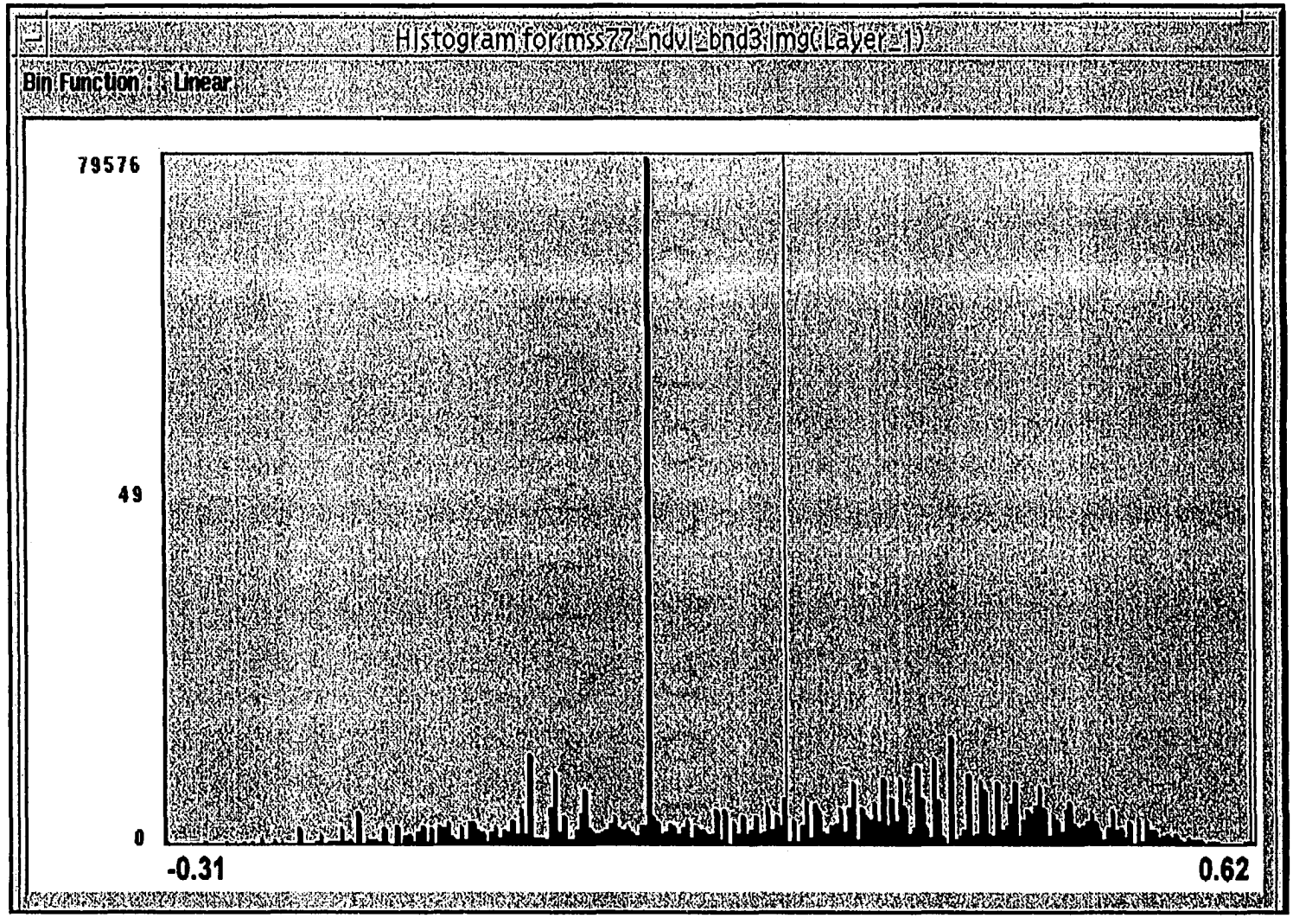


Figure 4.2: Frequency histogram of NDVI values computed from 1977 Landsat MSS sub-scene using band 6 (NIR) and band 5 (red). X-axis is NDVI value; Y-axis is the number of pixels.

of the histogram which implies that a large portion of the area represented by the image is vegetated.

The histograms for the NDVI images produced by the SPOT scenes are very similar to each other (Figures 4.3 and 4.4). Like the histograms produced from the Landsat MSS NDVI computations, the SPOT NDVI histograms exhibit negative skew indicating that most pixel values in the scene have strong positive values. Again, the location of most of the pixels on the positive portion of the histogram implies that most of the region is vegetated. The range of the 1989 SPOT NDVI is from -0.46 to 0.79, and the range of the 1995 SPOT NDVI is from -0.4 to 0.80.

4.2 Analysis of NDVI Scenes: Post-differencing

Maps of the differenced NDVI values and their spatial distribution were created using ArcView 3.2 with the Image Analyst extension. To efficiently gauge the possible changes in pixel NDVI values over time, NDVI difference maps were created by subtracting each of the SPOT NDVI images from the MSS NDVI images. The two SPOT NDVI images were also subtracted from each other. This produces a time series of differenced NDVI maps for the periods 1977 to 1989, 1977 to 1995, and 1989 to 1995. All maps were created with the same scaled legend of NDVI difference values between -1.0 and 1.0. The color scale used to represent the differenced NDVI values was a two colored graduated scale from dark grey (-1.0) to dark red (1.0). Negative NDVI difference values correspond with an increase in the NDVI value from the earliest scene to the latest scene; this would imply that vegetation's health had improved between the pre-eruption time to the post-eruption time. Positive NDVI

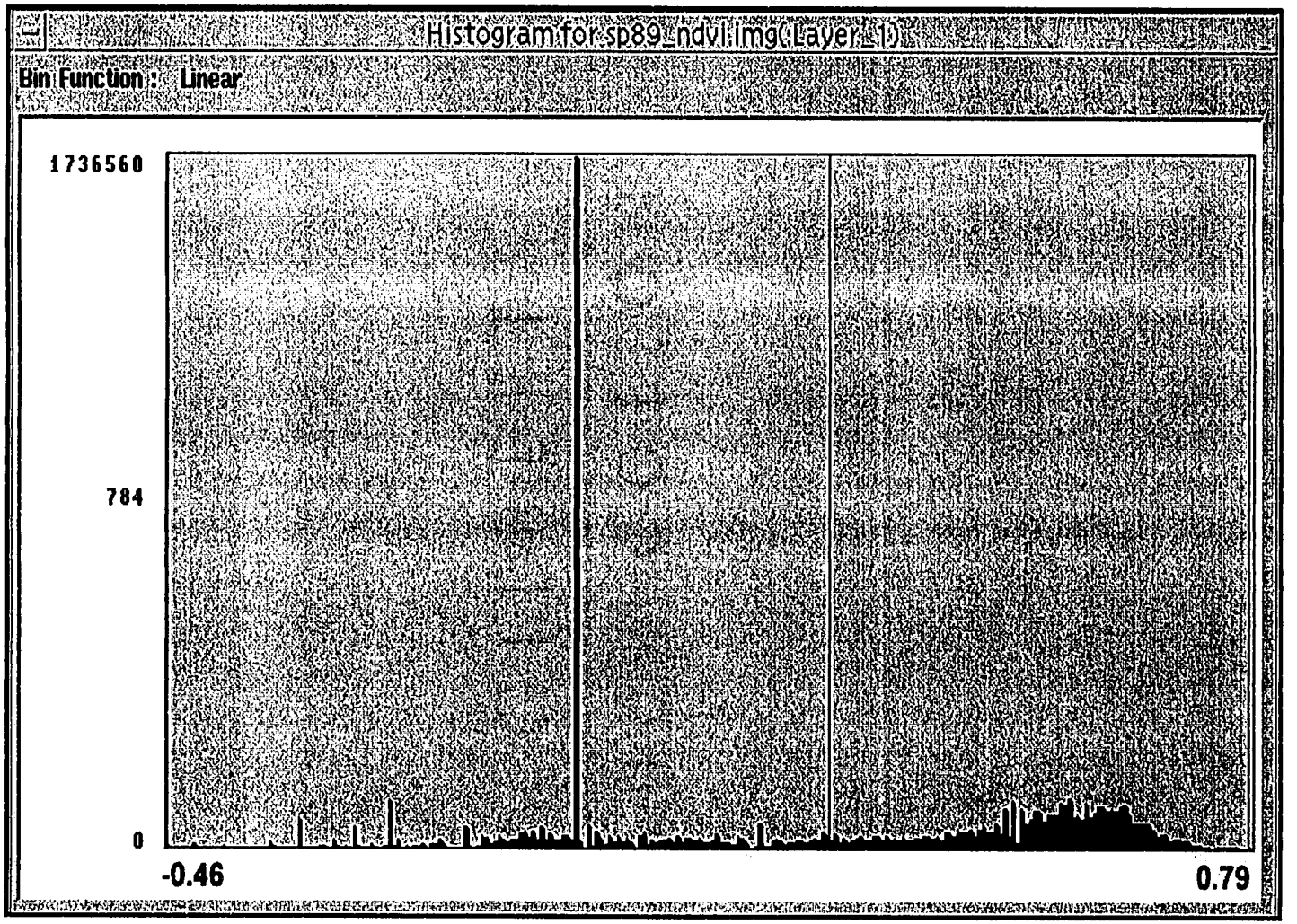


Figure 4.3: Frequency histogram of NDVI values computed from 1989 SPOT HRV sub-scene using band 3 (NIR) and band 2 (red). X-axis is NDVI value; Y-axis is the number of pixels.

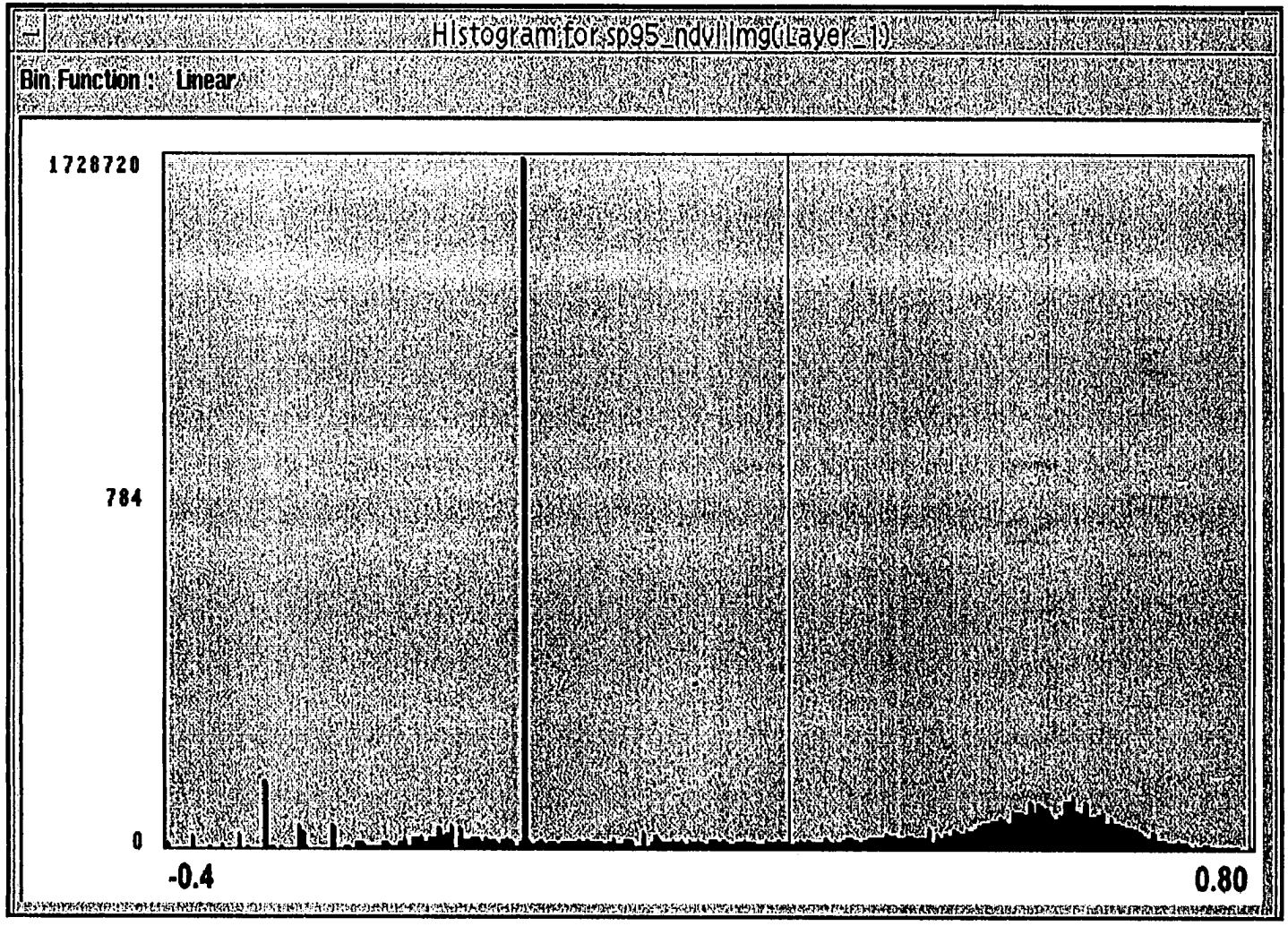


Figure 4.4: Frequency histogram of NDVI values computed from 1995 SPOT HRV sub-scene using band 3 (NIR) and band 2 (red). X-axis is NDVI value; Y-axis is the number of pixels.

difference values correspond to a decrease in the NDVI value from the earliest scene to the latest scene; this would imply that either the vegetation's health had declined between the pre-eruption time to the post-eruption time, or that the land cover had drastically changed between the two dates the satellite images were acquired.

As previously noted, Landsat MSS and SPOT HRV had both spectral and spatial differences. The spatial differences were partially accounted for by resampling the 20 m SPOT HRV to the 79 m resolution of the Landsat MSS. Unfortunately, there is no way to "resample" each image to account for the spectral differences between the two images. The MSS band 7 (NIR) and band 5 (red) combination is the closest to the SPOT HRV band 3 (NIR) and band 2 (red) combination (Table 3.1). But the MSS NIR-band 7 encompasses a larger portion of the electromagnetic spectrum that the SPOT HRV NIR-band 3. This discrepancy in spectral resolution may have impacted the NDVI ratioing and the NDVI differencing. Band 6 of the Landsat MSS sensor is also located in the IR portion of the EMR, thus an NDVI was also computed using the band 6 / band 5 ratio. It should be noted however that only a small fraction of the MSS band 6 corresponds with the SPOT band 3 NIR band (see Table 3.1).

4.2a NDVI differencing between MSS 77 and SPOT 89 scene

Two maps representing differenced NDVI layers were produced from the MSS 77 NDVI image and the SPOT 89 NDVI image. One was the result of using the MSS band 7 and band 5 NDVI combination (Figure 4.5), and the other using the MSS band 6 and band 5 NDVI combination (Figure 4.6). For both maps, the grey in the study area on the maps indicate regions where it is implied that vegetation health has improved between 1977 and 1989. These areas comprised most of the NDVI differencing maps. Areas represented by the color white are regions where there has been little if any change in vegetation health (or land cover), and encompass the second largest portion of the study area. The red color on the map indicate areas where there has been a notable decrease in vegetation health or a change in land cover.

Most of the red regions on Figure 4.5 correspond with areas now covered by lava flows, thus indicating a change in land cover from vegetated rainforest to black pahoehoe or a'a lava. Areas representing decreased NDVI values are also present around the town of Hilo, perhaps giving an indication of how much the town's urban sprawl has expanded between 1977 and 1989. Finally, there are a few red areas indicating decreases in NDVI values in the region between HAVO and Hilo. These are most likely caused by the practices of the various agriculture farms present in that area. It would be hard to correlate the change with the *vog* as it may be due in part to harvesting, plant disease, or simply a change the type of crops being grown.

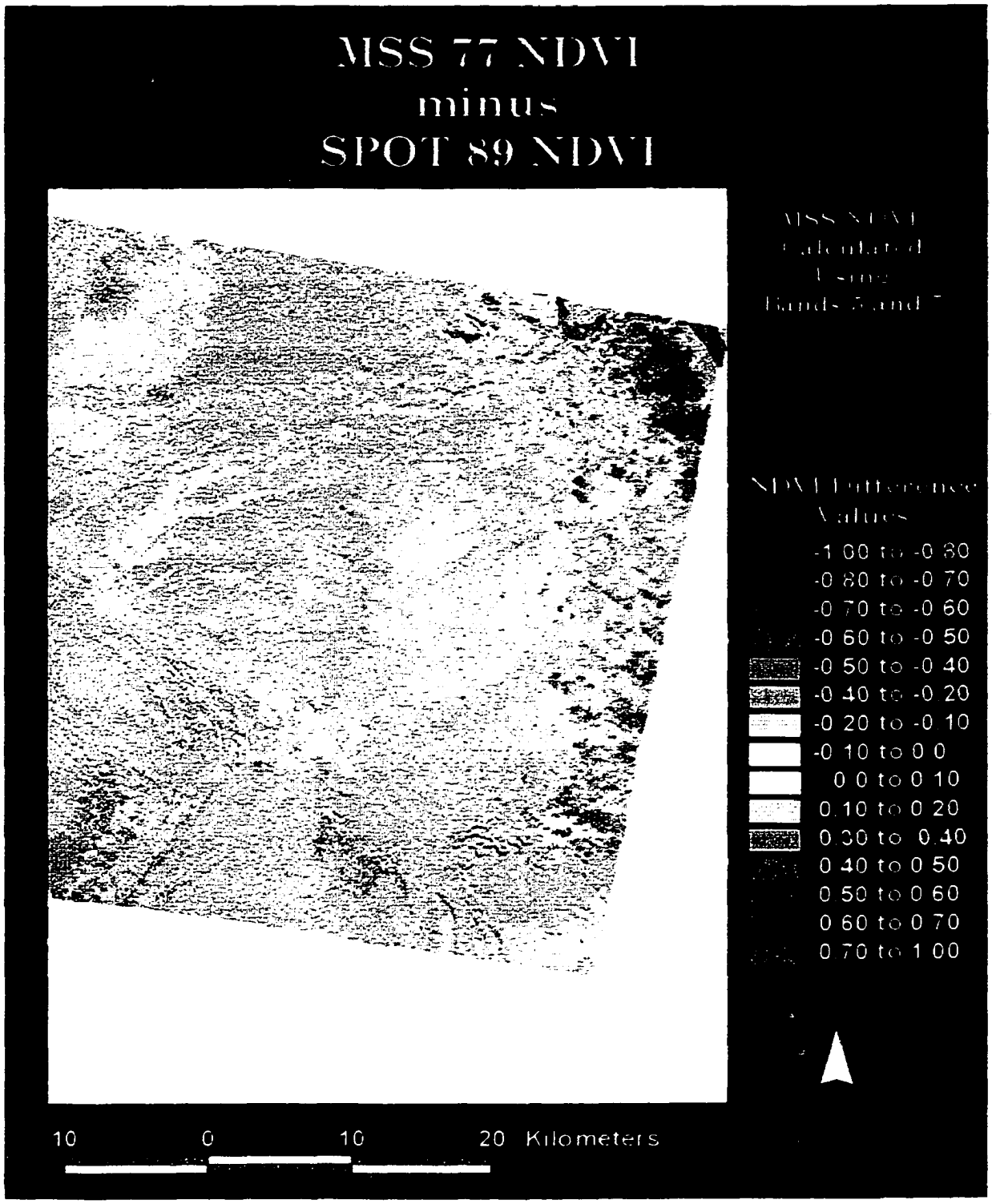


Figure 4.5: Computed difference NDVI layer between MSS 1977 (band 7) NDVI and SPOT HRV 1989 NDVI.

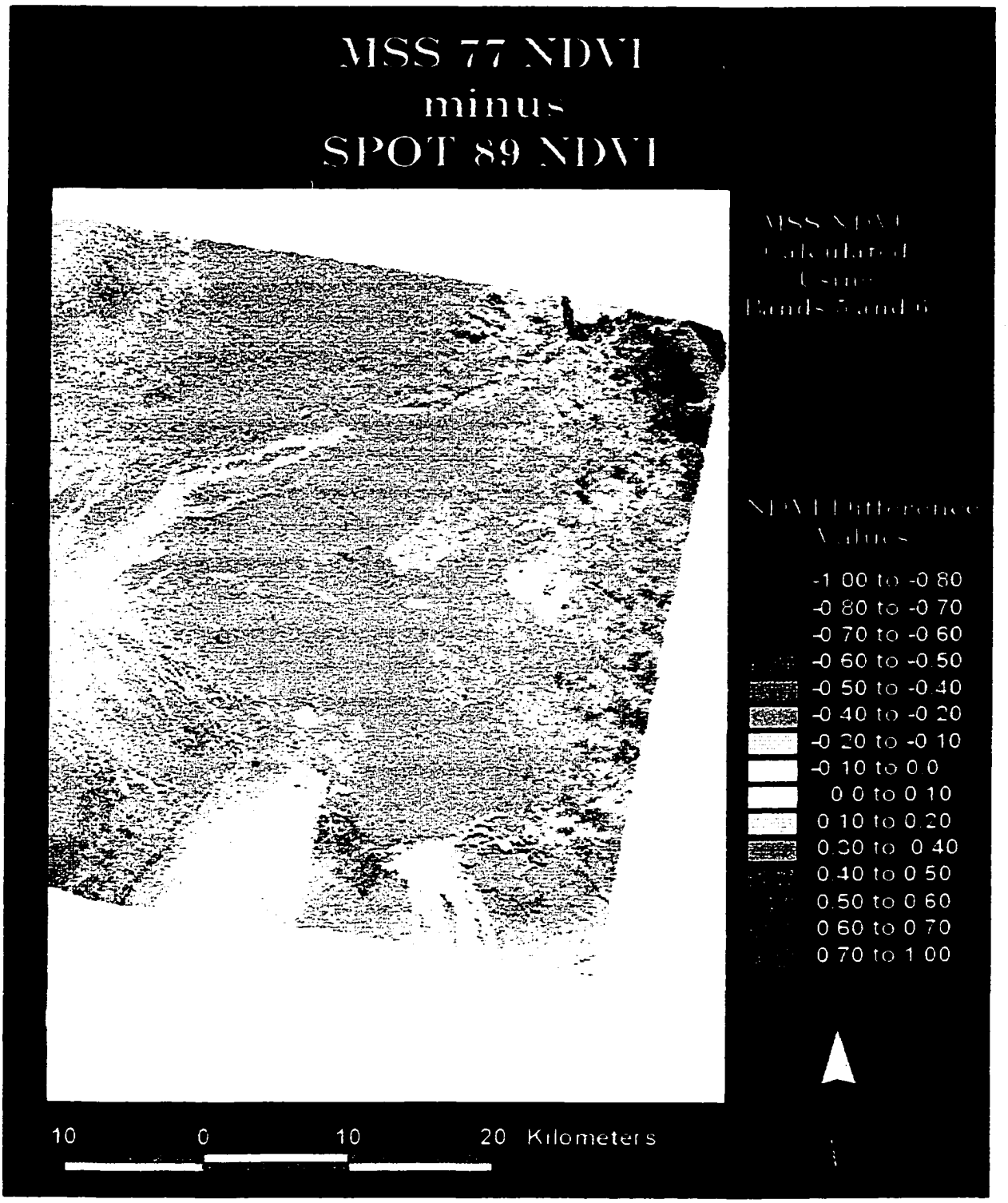


Figure 4.6: Computed difference NDVI layer between MSS 1977 (using band 6) NDVI and SPOT HRV 1989 NDVI.

Investigation of the frequency histogram from the image produced from the MSS (bands 7 and 5) and SPOT 1989 NDVI differencing also provides some clues as to how the land cover has changed between the time the scenes were acquired (Figure 4.7). The range of differenced NDVI values as indicated by the frequency histogram are approximately from -0.75 to 0.85. The histogram also exhibits a slightly bimodal distribution curve, with one high point around 0.35 and the other much larger one around -0.2. Most of the pixel values in the scene are less than zero indicating that the NDVI value increased from 1977 to 1989. The negative NDVI difference values that dominate most of the study implies that the vegetation health had improved between 1977 and1989; or that the land cover had changed such that ratioing its NIR and Red bands would produce a higher NDVI value.

Like the NDVI difference map produced from the MSS NDVI image and SPOT 89 NDVI image using the MSS band 7 and 5 combination, the map of the differenced NDVI values between the MSS 77 NDVI (band 6 and 5) and SPOT 89 NDVI did not reveal any areas where the NDVI had significantly decreased (Figure 4.6). The map did have a smoother texture than the same map produced using the band 7 and band 5 combination, with a majority of the study area being shaded grey indicating that most pixels' NDVI value increased between 1977 and 1989. Again, this implies either an improvement in the health of the vegetation present, or a change in land cover type that would generate a higher NDVI.

The frequency histogram of the differenced NDVI image is bimodal, with the larger peak being around -0.2 and the smaller peak located around 0.40 (Figure 4.8). The range of the histogram was from approximately -0.8 to 0.75. This range

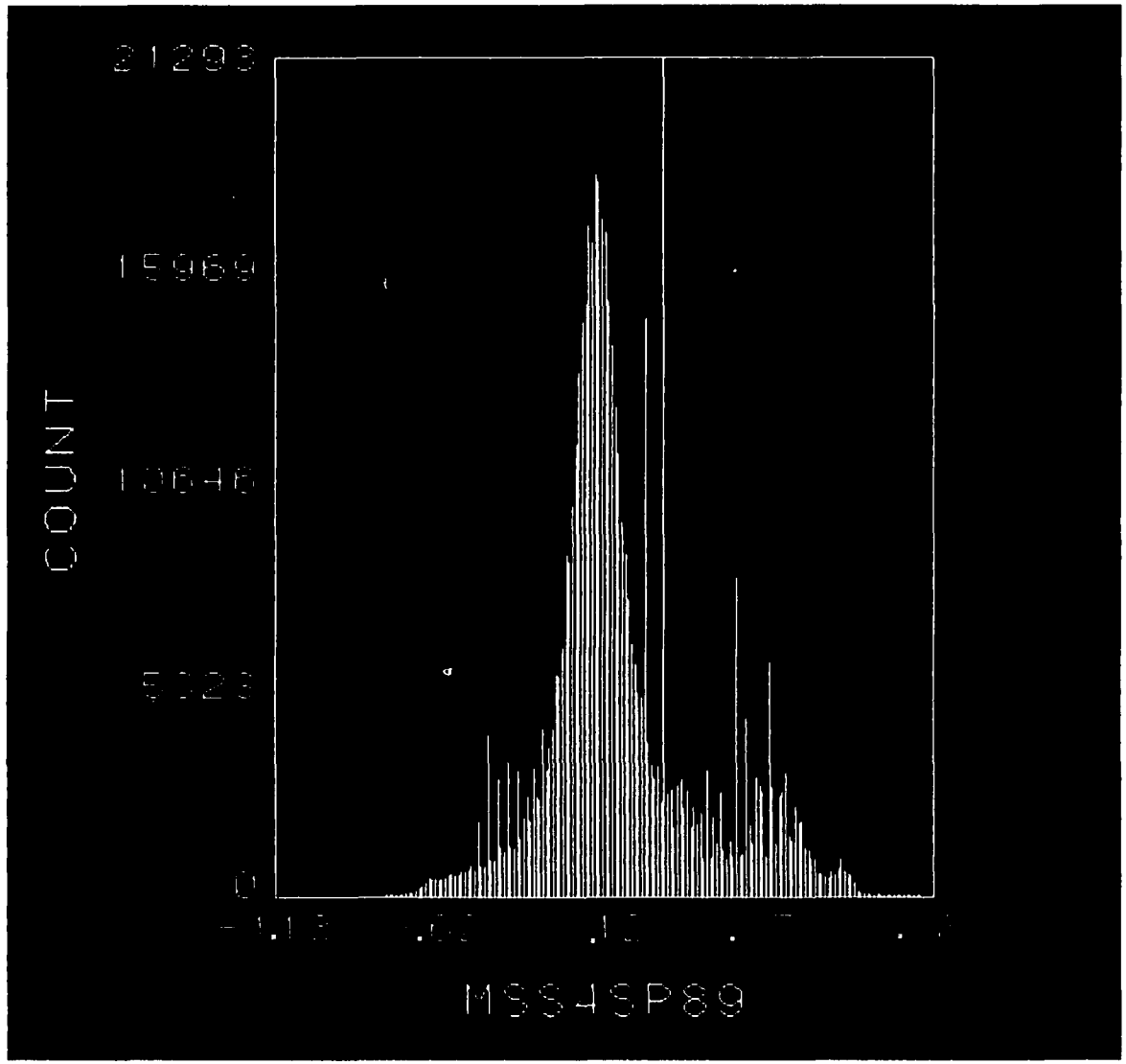


Figure 4.7: Frequency histogram of differenced NDVI layer between MSS 1977 (band 7) and 1989 SPOT HRV. X-axis is NDVI; Y-axis is number of pixels.

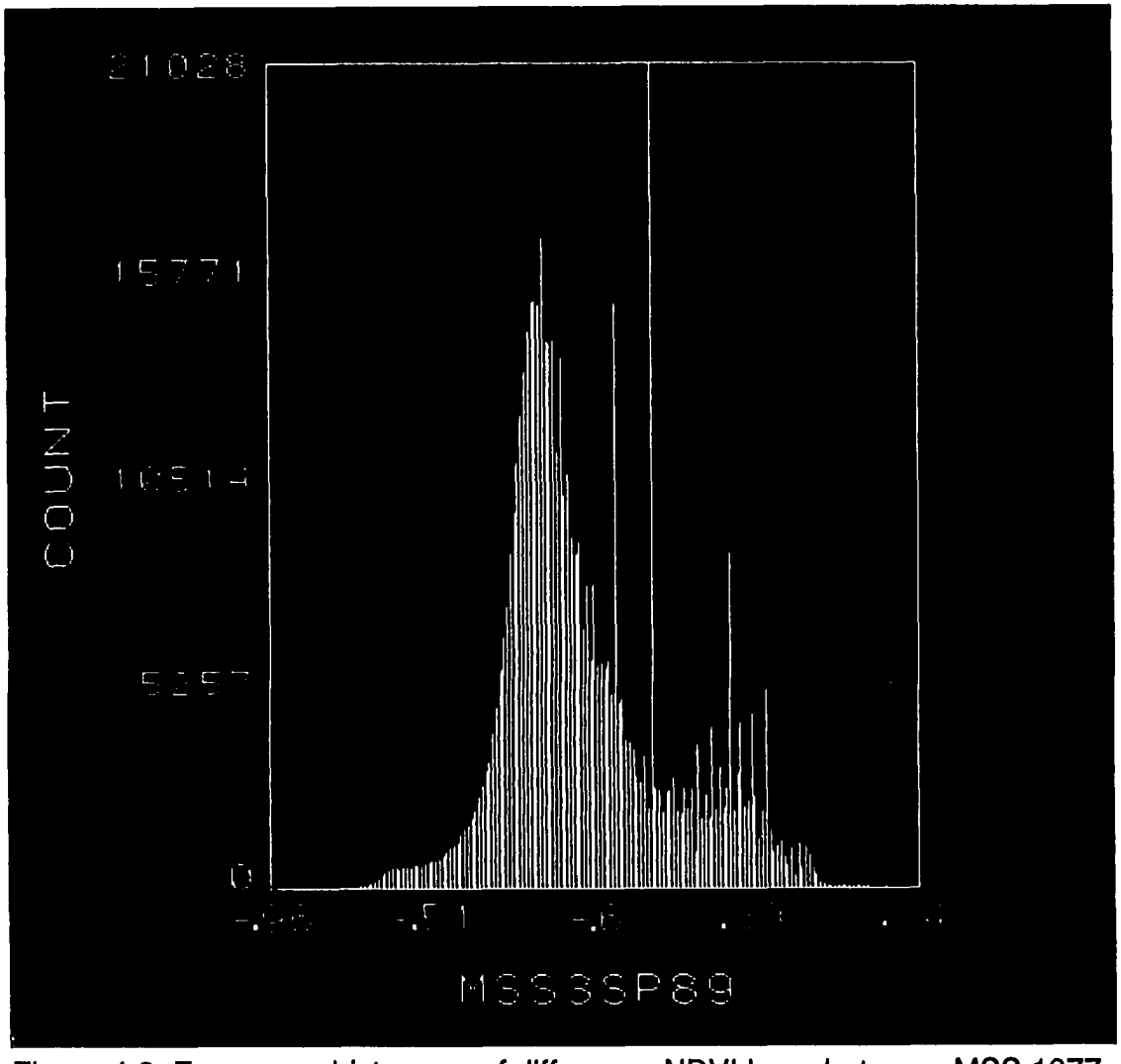


Figure 4.8: Frequency histogram of difference NDVI layer between MSS 1977 (band 6) and 1989 SPOT HRV. X-axis is NDVI; Y-axis is the number of pixels.

is similar to the range of the histogram produced using the band 7 and band 5 combination. Furthermore, most of the pixel values are near or less than zero indicating that most of the land cover in the study area had not changed or that the health of the vegetation had not been impacted.

4.2b NDVI differencing between MSS 77 and SPOT 95 scene

Two differenced maps were also created from the MSS 77 NDVI image and the SPOT 95 NDVI image. One was produced from the MSS band 7 and band 5 combination (Figure 4.9), and the other was made using MSS bands 6 and 5 (Figure 4.10). The differenced map of the Landsat MSS NDVI image (band 7 and 5) and the SPOT 1995 HRV NDVI (Figure 4.9) is very similar to one produced from the differencing of the MSS NDVI image and 1989 SPOT NDVI image. But there are areas in the HAVO region that indicate a greater reduction in land cover NDVI values. Most of these areas have a linear shape implying that they are the result of vegetated areas being replaced by either pahoehoe or a'a. Some also appear to be located along the fringe of the lava flows. This may be the result of the vegetation in those areas being scorched by the lava's heat. Overall though, there are no prominent vegetated regions that display stress through a reduced NDVI value between 1977 and 1995.

The frequency histogram of differenced NDVI image shown in Figure 4.9 is unimodal with its peak around -0.15; thus most of the pixel values are around or below zero implying that there was not much change in the land cover between 1977 and 1995 (Figure 4.11). The range of the histogram values are from approximately -0.75

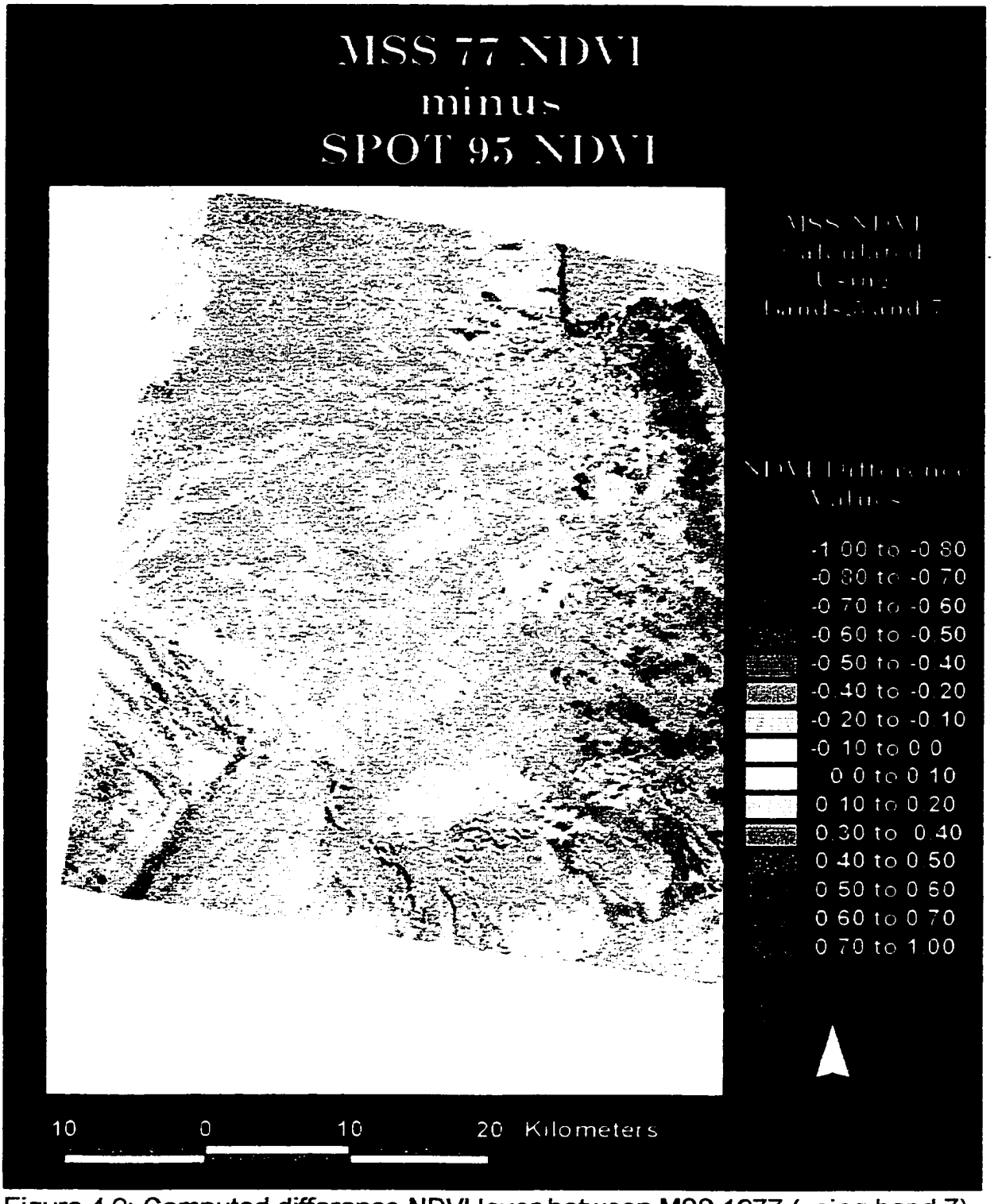


Figure 4.9: Computed difference NDVI layer between MSS 1977 (using band 7) NDVI and SPOT HRV 1995 NDVI.

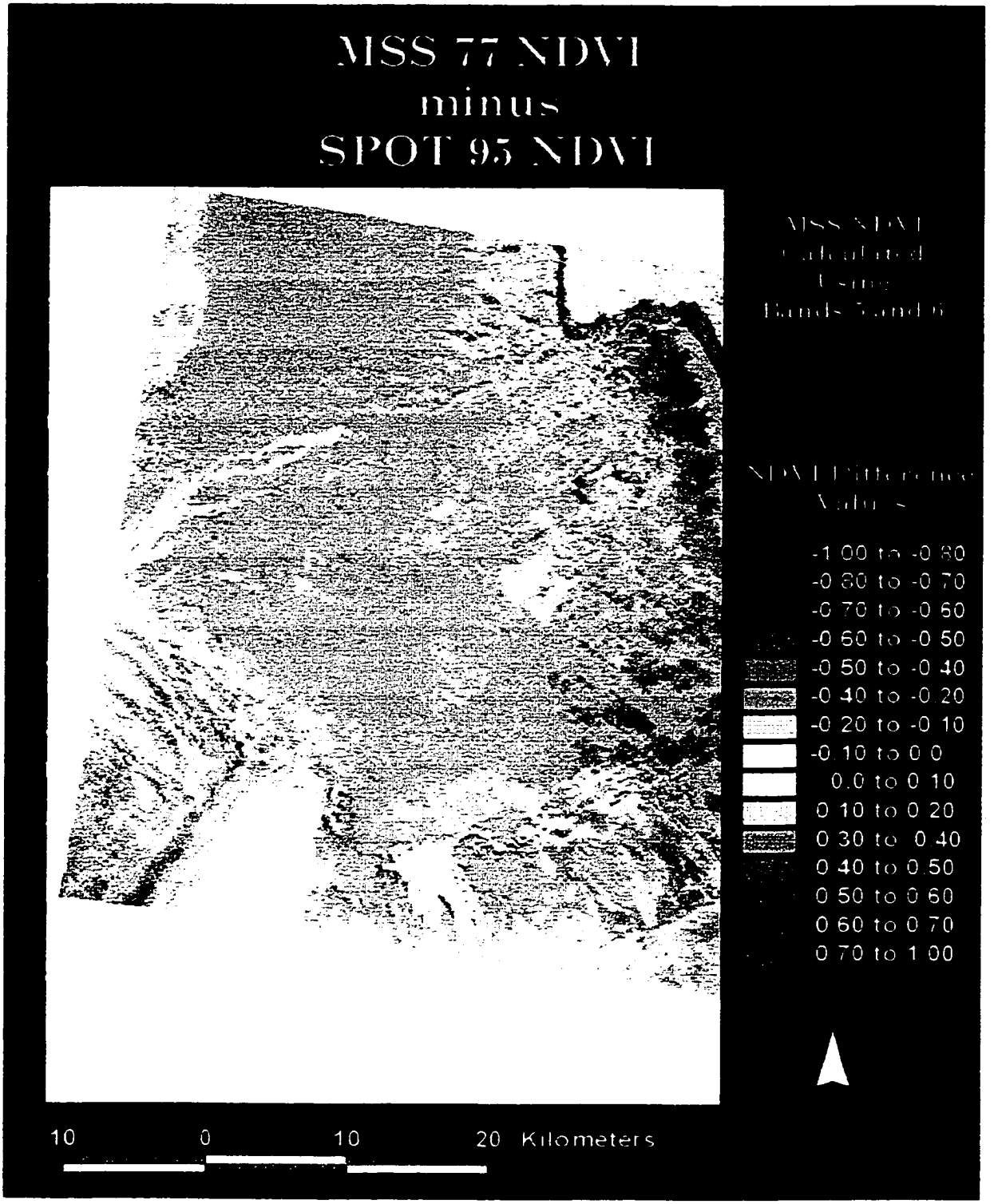


Figure 4.10: Computed difference NDVI layer between MSS 1977 (using band 6) NDVI and SPOT HRV 1995 NDVI.

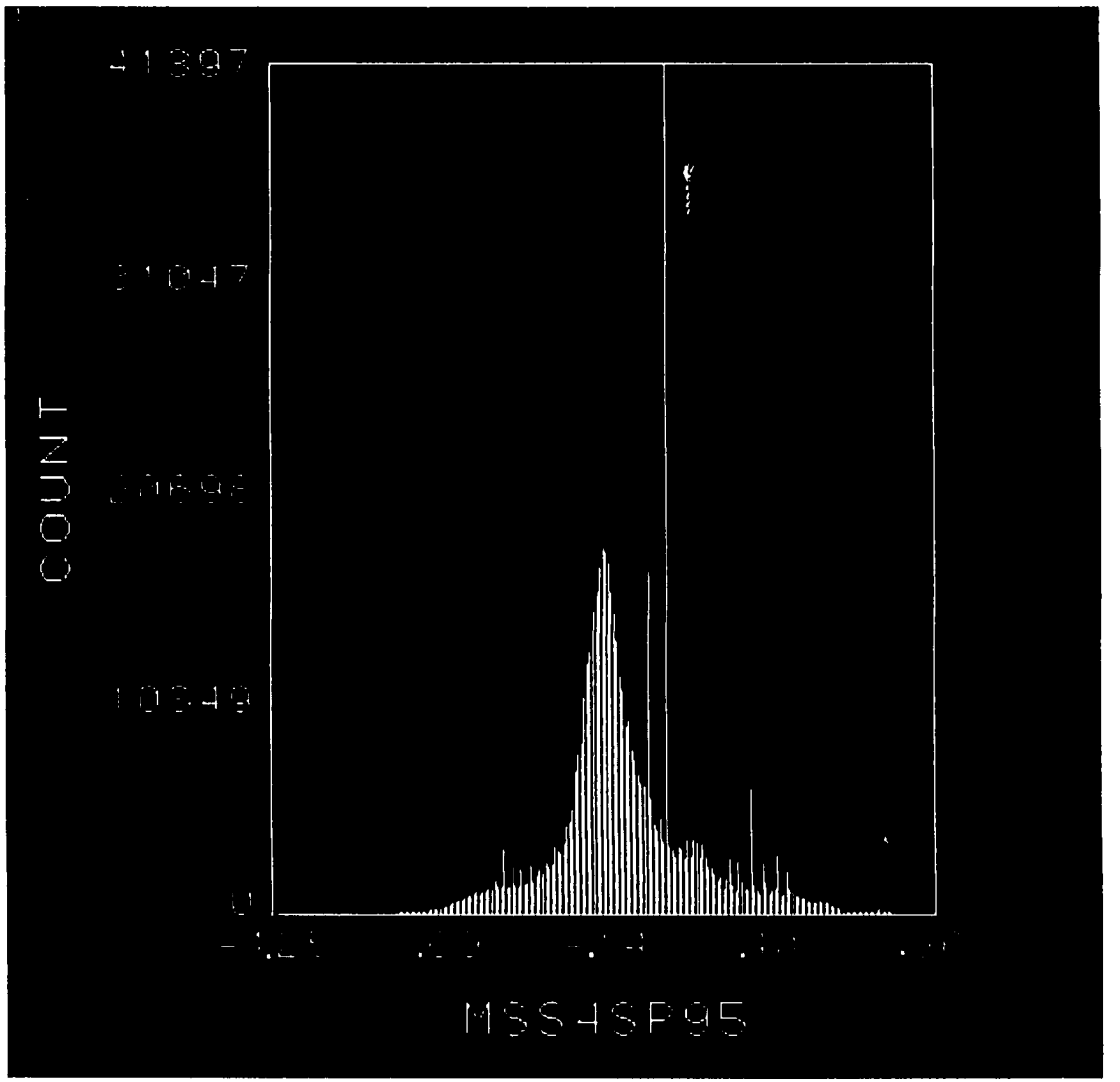


Figure 4.11: Frequency histogram of differenced NDVI layer between MSS 1977 (band 7) and 1995 SPOT HRV. X-axis is NDVI value; Y-axis is number of pixels.

to 0.90, which is close to the range of the histogram of the differenced MSS NDVI and SPOT 1989 NDVI. Again it should be noted that differences in the spectral resolution between the MSS NIR band 7 the SPOT NIR band 3 may have impacted the NDVI differencing.

The differenced map of the Landsat MSS NDVI image (band 6 and 5) and the SPOT 1995 HRV NDVI (Figure 4.10) did not indicate any areas where there had been a notable change in vegetation health or land cover, other than the areas that were covered by lava flows between 1977 and 1995 and the increase in urbanization around Hilo. The map is dominated by grey areas hinting that the land cover NDVI value increased between 1977 and 1995. The MSS band 6 and band 5 NDVI combination when differenced with the SPOT 95 NDVi image produced a smooth image similar to the one created by the differencing of the MSS band 6/band 5 NDVI with the SPOT 89 NDVI image. The smooth texture of the band 6/band5 combination implies that it does not distinguish changes in vegetation as well as the band7/band 5 combination.

The histogram of the differenced MSS NDVI image (band 6/band 5) and SPOT 1995 NDVI image is unimodal with its peak around -0.30 (Figure 4.12). The range of the histogram is from approximately -0.75 to 0.75. The histogram is also positively skewed; thus most of the pixel values are below zero implying that there was an increase in pixel NDVI values between 1977 and 1995. This implies that where vegetation is present, its health actually improved. More likely though this signal is due to the MSS band 6 (NIR) band only overlapping with a very small portion of the SPOT NIR band.

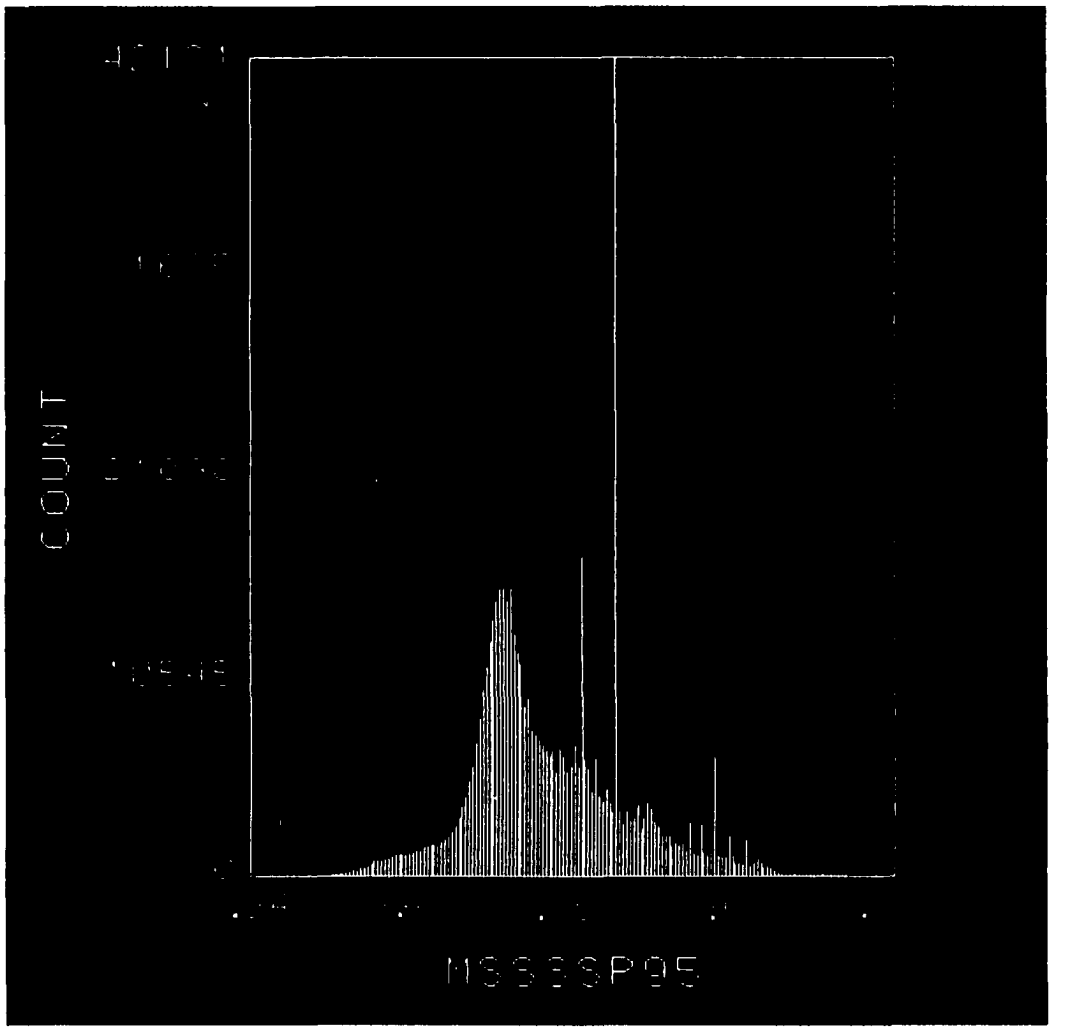


Figure 4.12: Frequency histogram of differenced NDVI layer between MSS 1977 (band 6) and 1995 SPOT HRV. X-axis is NDVI value; Y-axis is number of pixels.

4.2c NDVI differencing between SPOT 89 and SPOT 95 scene

Even though the current eruption of Kilauea began in 1983, the change in NDVI pixel values between 1989 and 1995 was investigated as long-term changes in vegetation health may still have been occurring 5 years after the eruption started. For example, one species may have had its population reduced in a particular area due poor resistance to the *vog*, and another more resistant species could have spread and began to exhibit its dominance in the same area. Depending on the spectral resolution of the sensor and the plant's own spectral radiance curve, not only a change in vegetation health but a change in the type of plant species in an area may be detected using remotely-sensed data. Thus, besides detecting stressed vegetation, the SPOT 89 and SPOT 95 NDVI differencing may show areas where the vegetation population dynamics have changed.

The two SPOT NDVI images used to create the NDVI differencing map had been created from the SPOT scenes that were resampled from their original 20 m resolution to the 79 m resolution of the Landsat MSS scene. The reason for looking at the differenced SPOT NDVI using the coarser scale was so that the map could be properly compared to the other maps created by the MSS and SPOT NDVI images. Finally, even though the differenced SPOT NDVI map used the same 79 m spatial resolution as the other maps, it provided more spatial detail related to pixels (and thus areas) that had a change in NDVI values.

The map of the differenced SPOT NDVI images uses the same color and numerical scale as the maps that were created using the Landsat MSS NDVI images (Figure 4.13). Unlike the other maps, the preponderance of white indicates that there is very little to no change in pixel NDVI values for most of the study area. The location of grey areas on the map are closely located to regions where agriculture was prominent, thus hinting that perhaps the increase in the NDVI value between 1989 and 1995 is due to the maturity of the crop grown or a change in the type of crop grown.

Noticeably, there are more areas corresponding to the red portion of the NDVI difference color scale, implying a change in land cover or a decrease in the health of vegetation present in those areas. Due to the linear shape, it is obvious that some of the red is indicating regions where vegetation was replaced by pahoehoe or a'a. The red area near the Pu'u O`o vent is the signature of a volcanic plume that is present in the 1995 SPOT scene but not the 1989 SPOT scene (Figures 3.2 and 3.3). As with the other NDVI differenced images, the urban sprawl of Hilo can also be seen by the smattering of red (reduced NDVI pixel values) near the city. The areas that are located along the southern boundary of the Ka`u Desert and Mauna Loa's southwest rift zone are noteworthy as their shape and location would not correspond with vegetated land cover being replaced by lava flows. Thus, these regions would be a good start to perform fieldwork concerning the type, number, and physical appearance as related to the health of the vegetation species that populate the area.

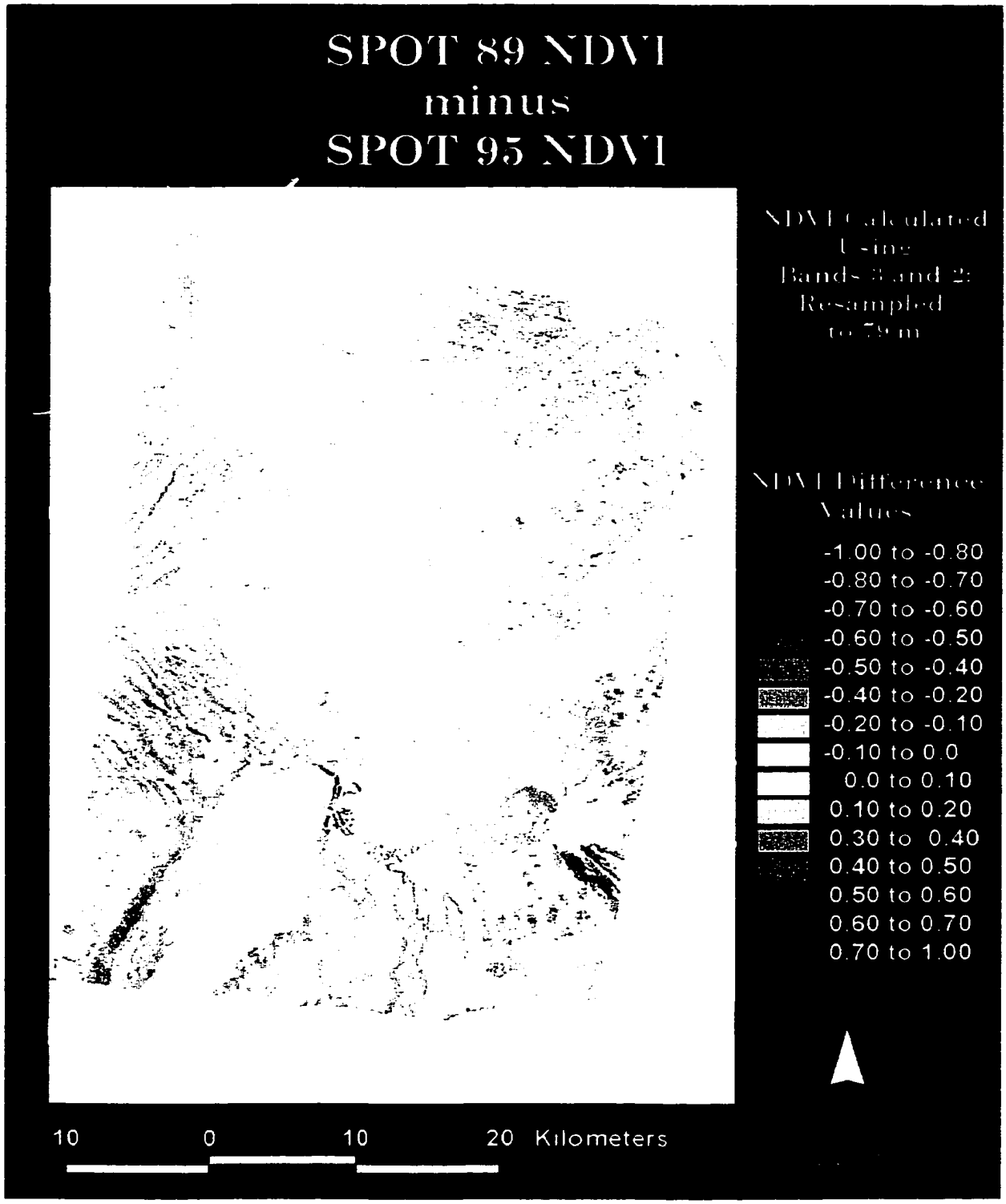


Figure 4.13: Computed difference NDVI layer between SPOT HRV 1989 NDVI and SPOT HRV 1995 NDVI.

The frequency histogram of the differenced SPOT NDVI image is bimodal, with its range being approximately from -0.80 to 0.79 (Figure 4.14). The larger peak is centered approximately at 0.0, while the smaller peak is located approximately at -0.60. This distribution further supports that most of the NDVI values did not change between 1989 and 1995.

The NDVI differencing performed between the two SPOT images produced much more decipherable and visible results than the NDVI differencing that incorporated the Landsat MSS NDVI images. The likely reason for this is due to the similarity in spectral and spatial resolution, which is discussed in more detail in Chapter 5.

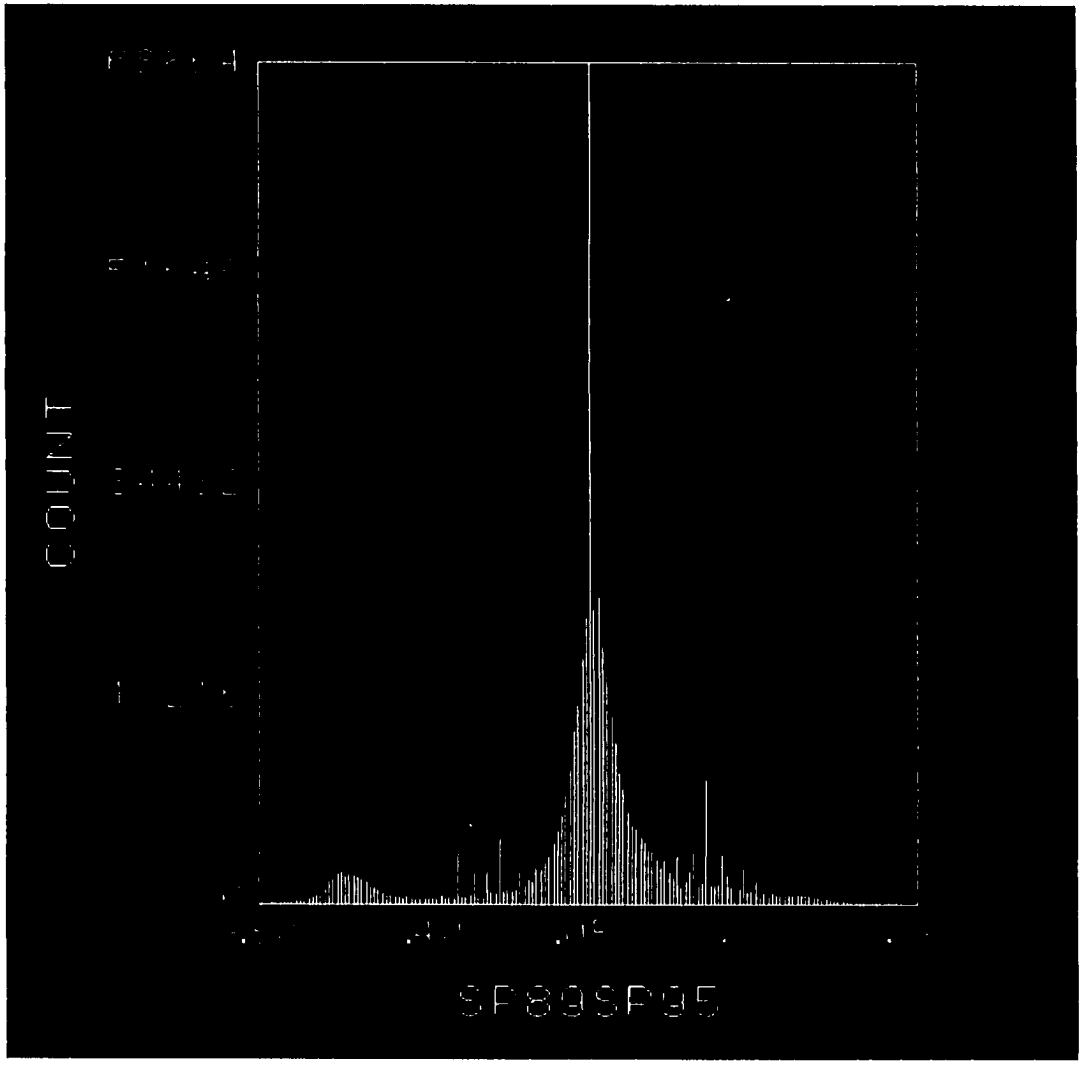


Figure 4.14: Frequency histogram of differenced NDVI layer between 1989 SPOT HRV and 1995 SPOT HRV. X-axis is NDVI value; Y-axis is number of pixels.

4.3 Results of Exploratory Analysis of Rainfall Data

Aerosols, such as sulfates, can come from anthropogenic and natural sources, and are important in the formation of clouds as they act as cloud condensation nuclei (CCN) (Miller 1998). Depending on the size of the CCN, they may act as an inhibitor of rainfall or they may behave as a catalyst to produce more rainfall than normal (Hobbs et al. 1970). For example, sulfates are known to increase the lifetime of clouds, while also altering the development of precipitation (Chuang et al. 1997). The *vog* produced by Kilauea is mostly composed of sulfate particulates; thus one would expect to see a negative trend in rainfall in certain locations around the Island. Moreover, a change in rainfall may also lead to a change in surface temperatures.

There are other considerations one should be aware of when trying to attribute changes in rainfall to the presence of the *vog*. The main factor to consider it how the ENSO (El Niño and Southern Oscillation) impacts the regional weather in Hawai`i, especially since there were ENSO episodes during this investigation's period of study (Figure 4.15). Typically, during an ENSO event a drought is experienced as it creates a dry situation in the normally wet winter-time, which in turn is followed by a drier summer season. Another possibly devastating impact of the ENSO is that there is an increase in the frequency of tropical cyclones forming in the region around Hawai`i (NOAA OGP 2001).

Since the ENSO phenomenon would affect regional rainfall in the same manner as the *vog* is hypothesized to affect rainfall, a methodology had to be developed to try and mask out the ENSO signal. The approach taken by this study was the assumption that if the ENSO was responsible for decreasing trends in rainfall, these trends would

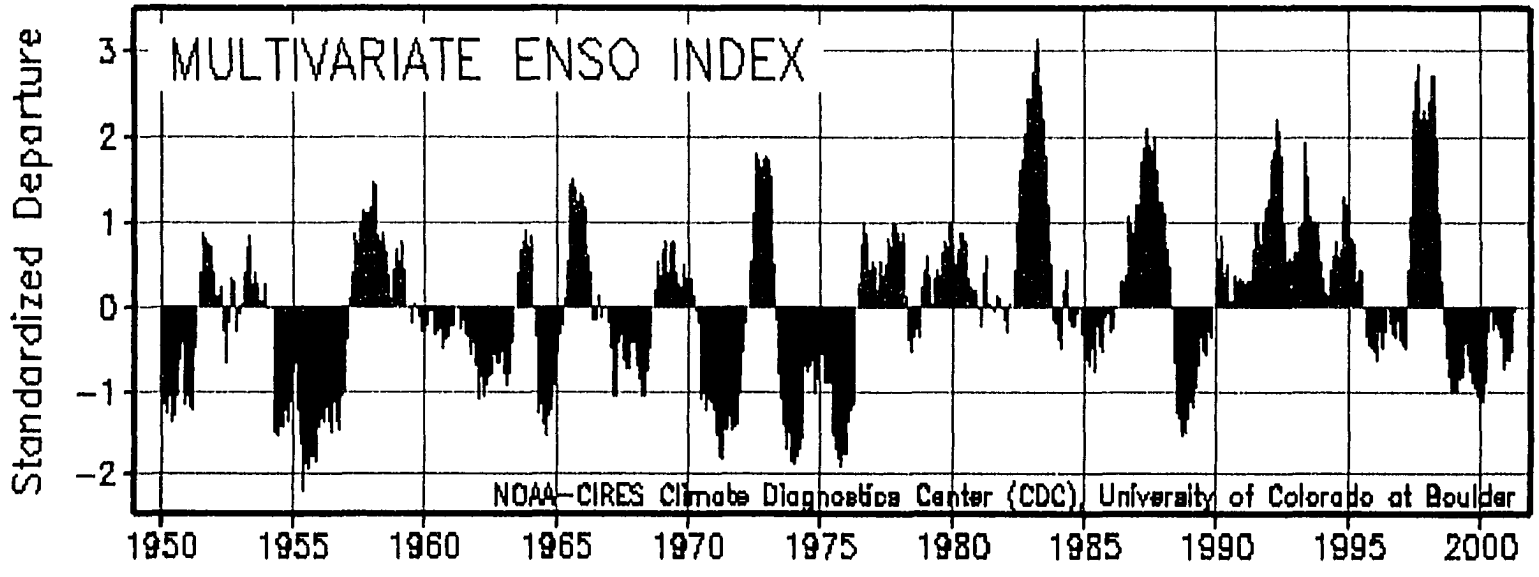


Figure 4.15: Graphic showing ENSO events. Taken from the CDC (University of Colorado) web page.

be apparent all over the island. But if the *vog* was responsible for decreasing trends in rainfall, a stronger signal would be seen in locations on the leeward side of the island where the *vog* tends to hang due to the wind dynamics produced by the shape of the of the Big Island (Sutton et al. 1994).

4.3a Rainfall Trends for the Complete Time Series

Most of the fifteen rainfall sites reflected a negative rainfall trend between 1969 and 1999 (See Table 3.2); the only stations that exhibited a positive rainfall trend were Waiakea, Paauilo, and Hilo International Airport. Out of the twelve rainfall sites that had a negative trend, only two were significant for P=0.95: Lanihau (Figure 4.16) and Kainaliu (Figure 4.17). But if P=0.90, two additional stations would be significant: Middle Pen (Figure 4.18) and Opihihale (Figure 4.19). None of the stations exhibited a significant positive rainfall trend. Analysis of the time series graphs of yearly rainfall averages for each station reflects the expected decrease in rainfall during ENSO years, with the magnitude of decrease varying among stations.

An interesting attribute of the stations that exhibited a negative trend (whether significant or not) is their geographic location on the Island (Figure 4.20). The two stations that showed a significant negative trend are located on the leeward side of the island, where the *vog* tends to accumulate due to the predominate trade winds and physical landscape of the Big Island.

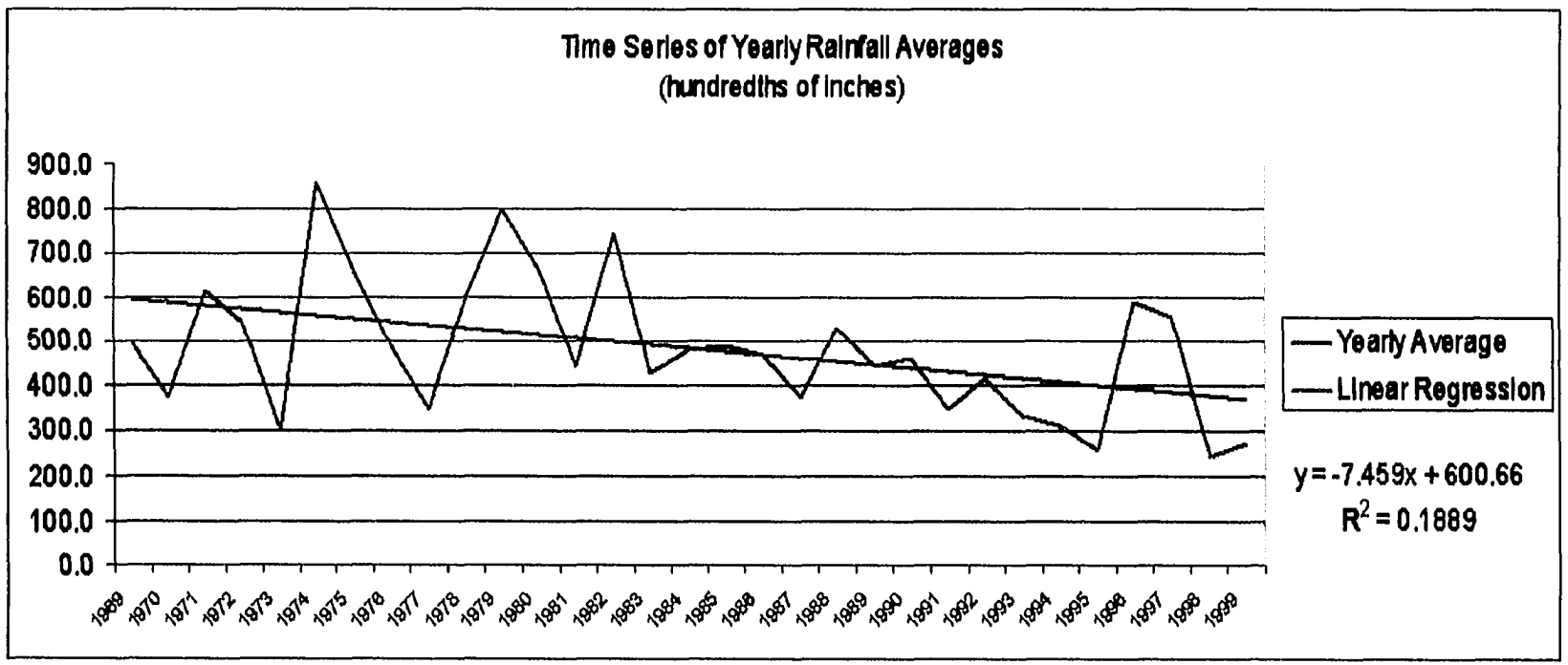


Figure 4.16: Graph of mean annual rainfall for Lanihau site.

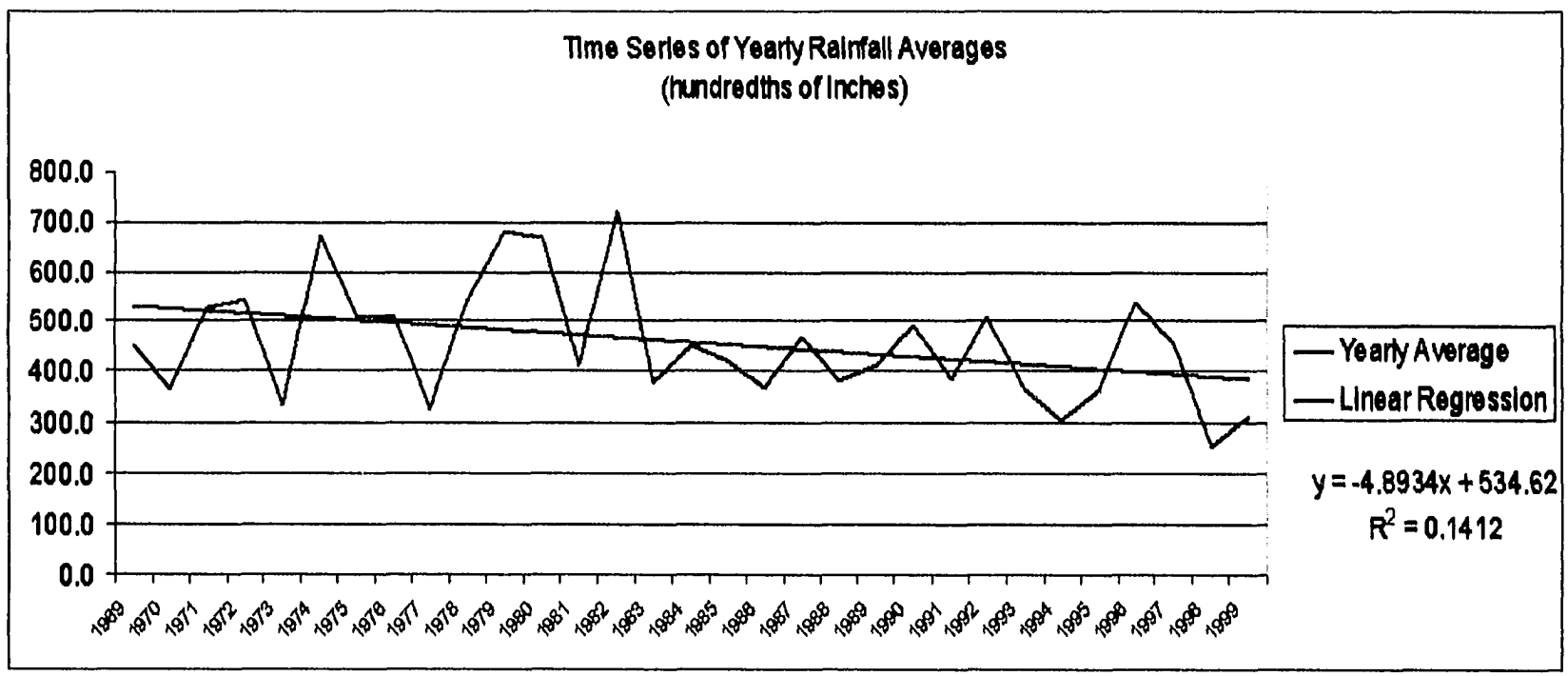


Figure 4.17: Graph of mean annual rainfall for Kainaliu site.

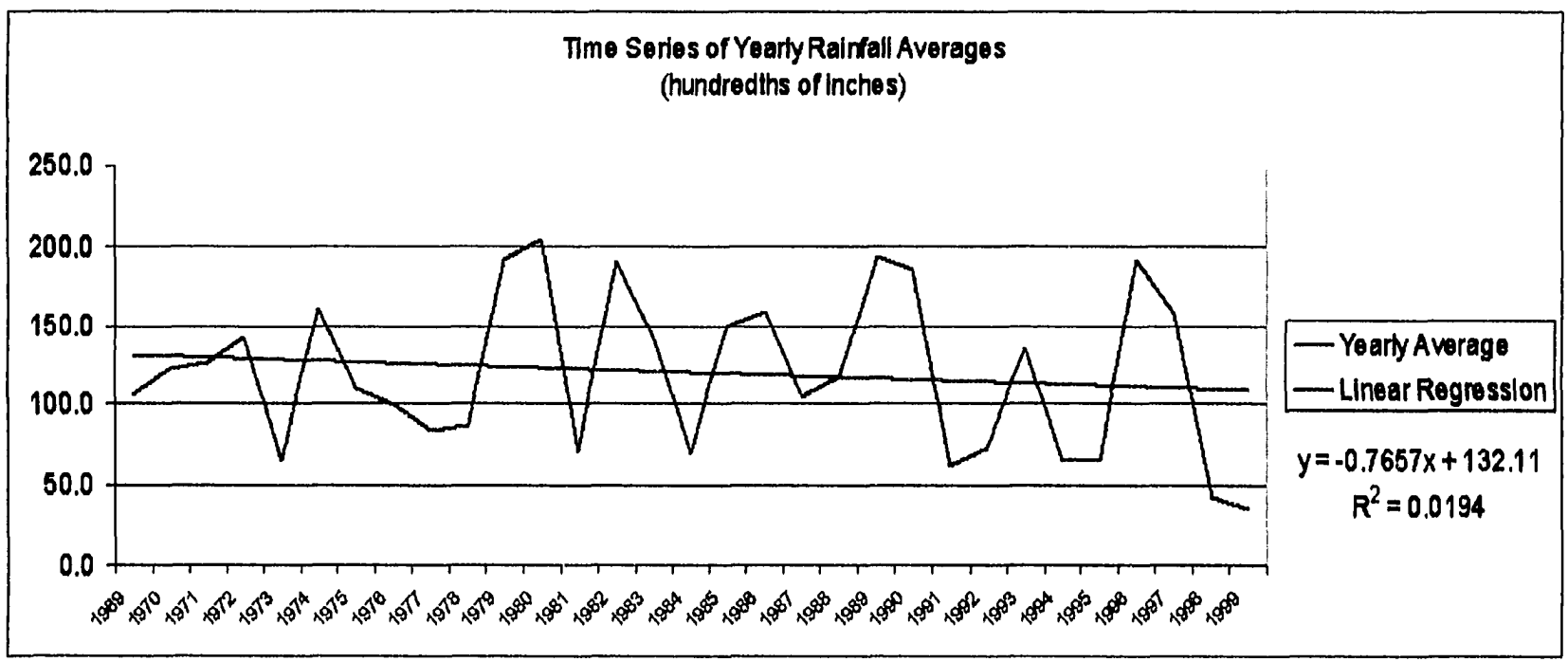


Figure 4.18: Graph of mean annual rainfall for Middle Pen site.

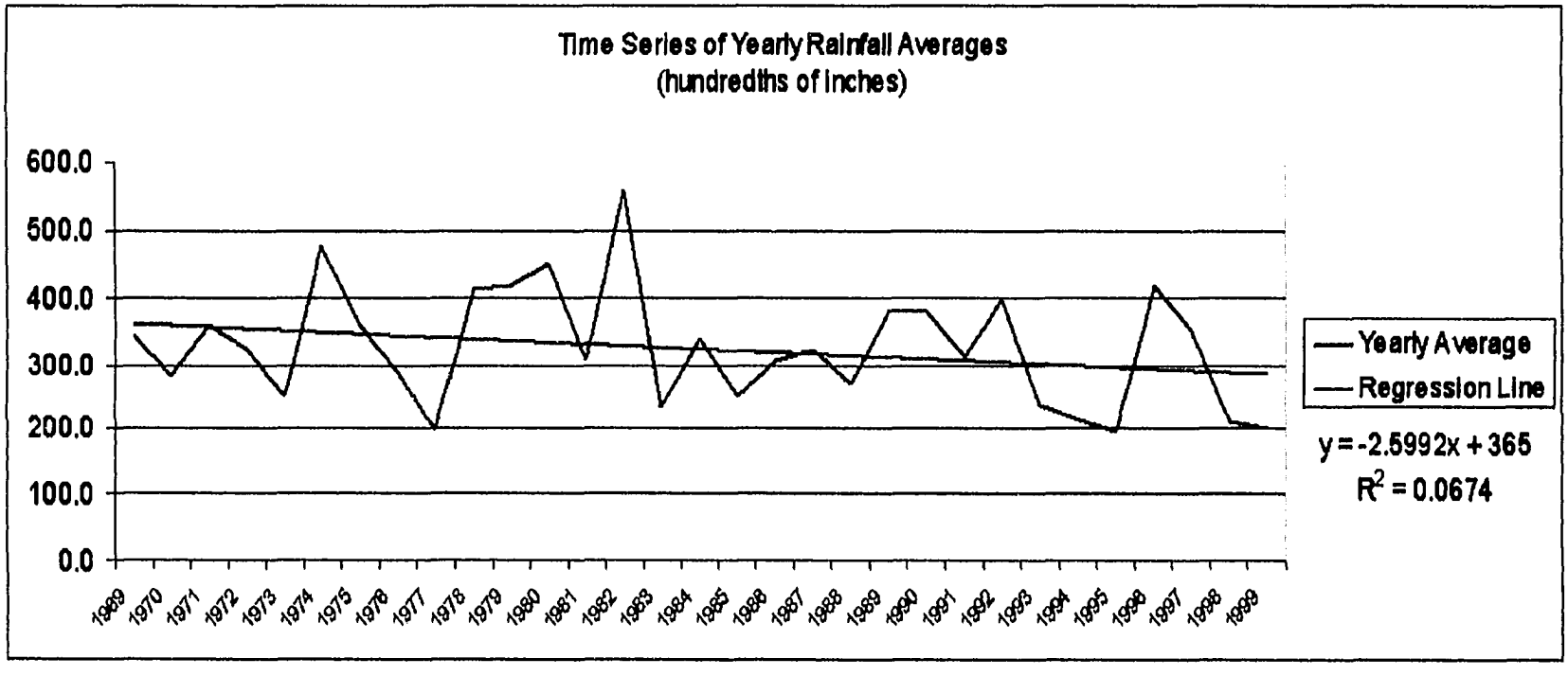


Figure 4.19: Graph of mean annual rainfall for Opihihale site.

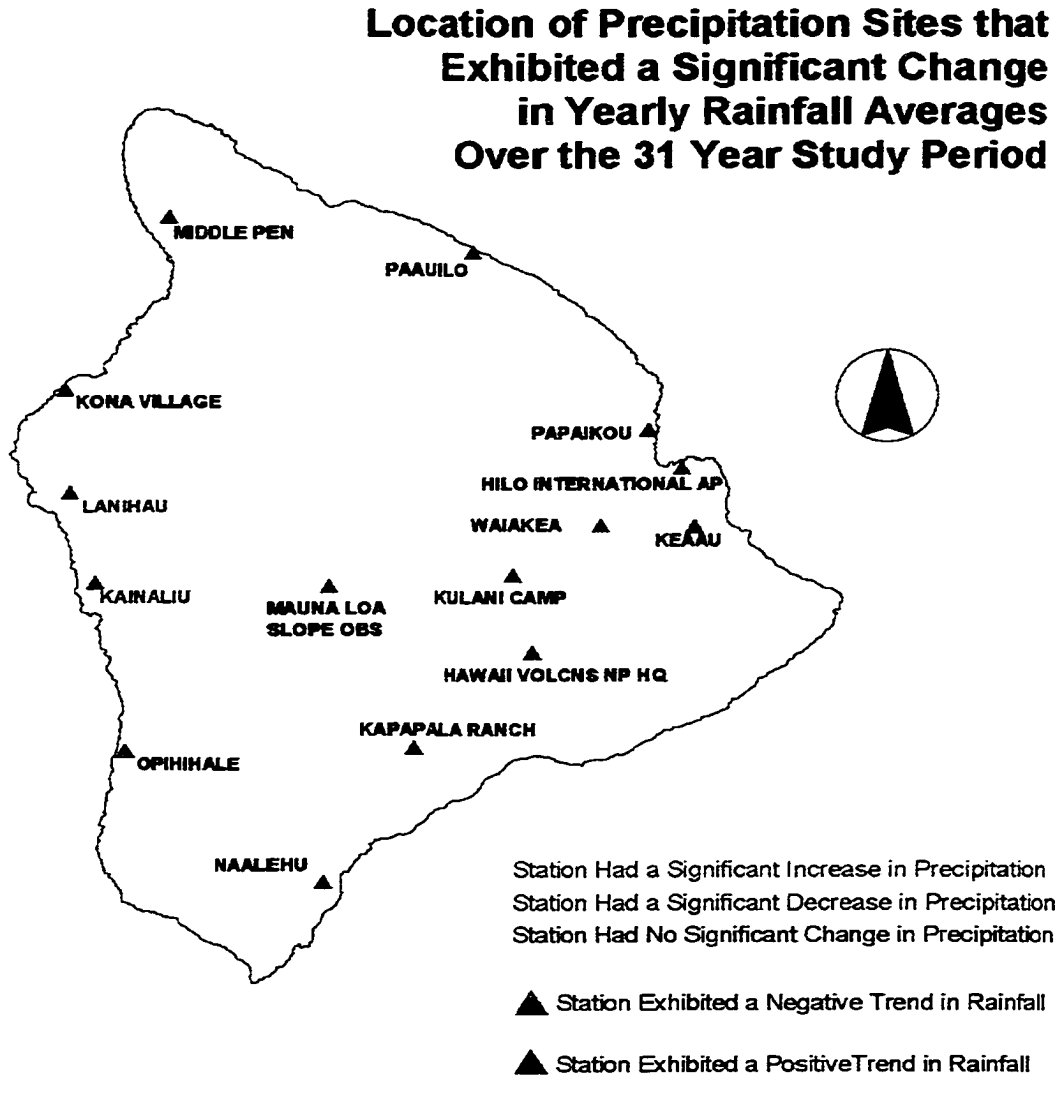


Figure 4.20: Map of rainfall stations with significant changes in precipitation trends between 1969 and 1999. Also shows the relative geographic location of stations with negative trends vs. positive trends (regardless of significance).

4.3b Rainfall Trends for Pre-eruption vs. Post-eruption Time Series

The result of the pre-eruption trend analysis showed that all rainfall stations except for one exhibited a positive rainfall trend (Table 3.3). Of the fourteen stations with a positive trend, none were significant. The only station that exhibited a negative trend was Hilo International Airport, but that trend was not significant (Figure 4.21).

The post-eruption analysis results were supportive of the hypothesis of the *vog* reducing rainfall, especially when compared to the results from the pre-eruption analysis. Ten of the fifteen rainfall stations showed a negative trend in rainfall between 1983 and 1999, but none were significant (Table 3.4). Five stations exhibited a positive trend in rainfall, but again none were significant. What should be noted however is the geographic clustering of the stations that did show the positive rainfall trend between 1983 and 1999, verses those that had a negative trend. All five were located on the windward side of the island and are grouped relatively closely to each other (Figure 4.22). Their location on the island may actually help to reduce the amount of *vog* that they received since their position is upwind of the volcano during normal trade wind conditions. During kona winds, these areas would be affected by the *vog*, but these winds are usually variable and not persistent. Moreover, because these sites are located on the windward side of the island, the high frequency of rainfall due to orographic effect would actually help to clean the air by removing the sulfate particulates. One of the five sites that showed a positive trend during the post-eruption time frame, Hilo International Airport, exhibited a negative trend in rainfall for the 14 years prior to the current eruption. This is opposite of what one would expect if the

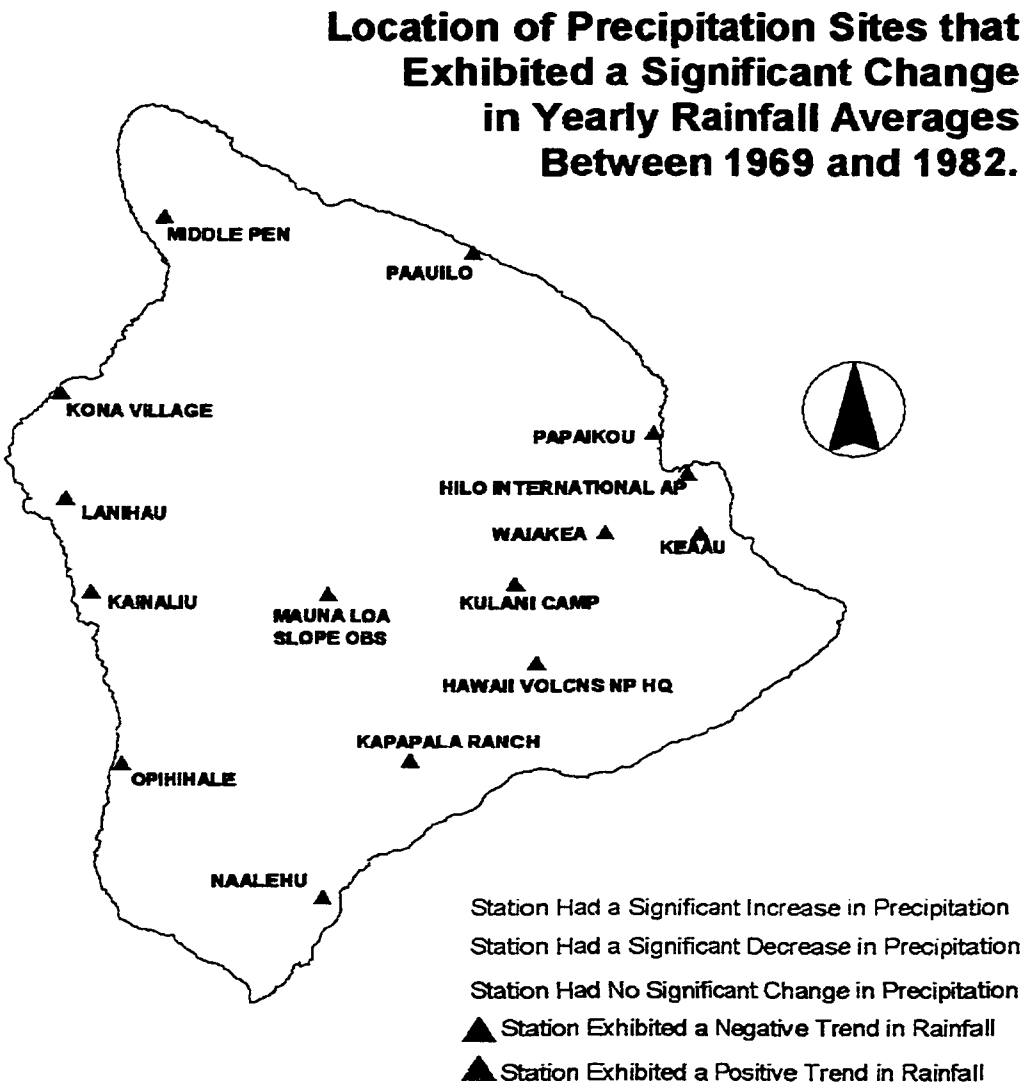


Figure 4.21: Map of rainfall stations with significant changes in precipitation trends between 1969 and 1982. Also shows the relative geographic location of stations with negative trends vs. positive trends (regardless of significance).

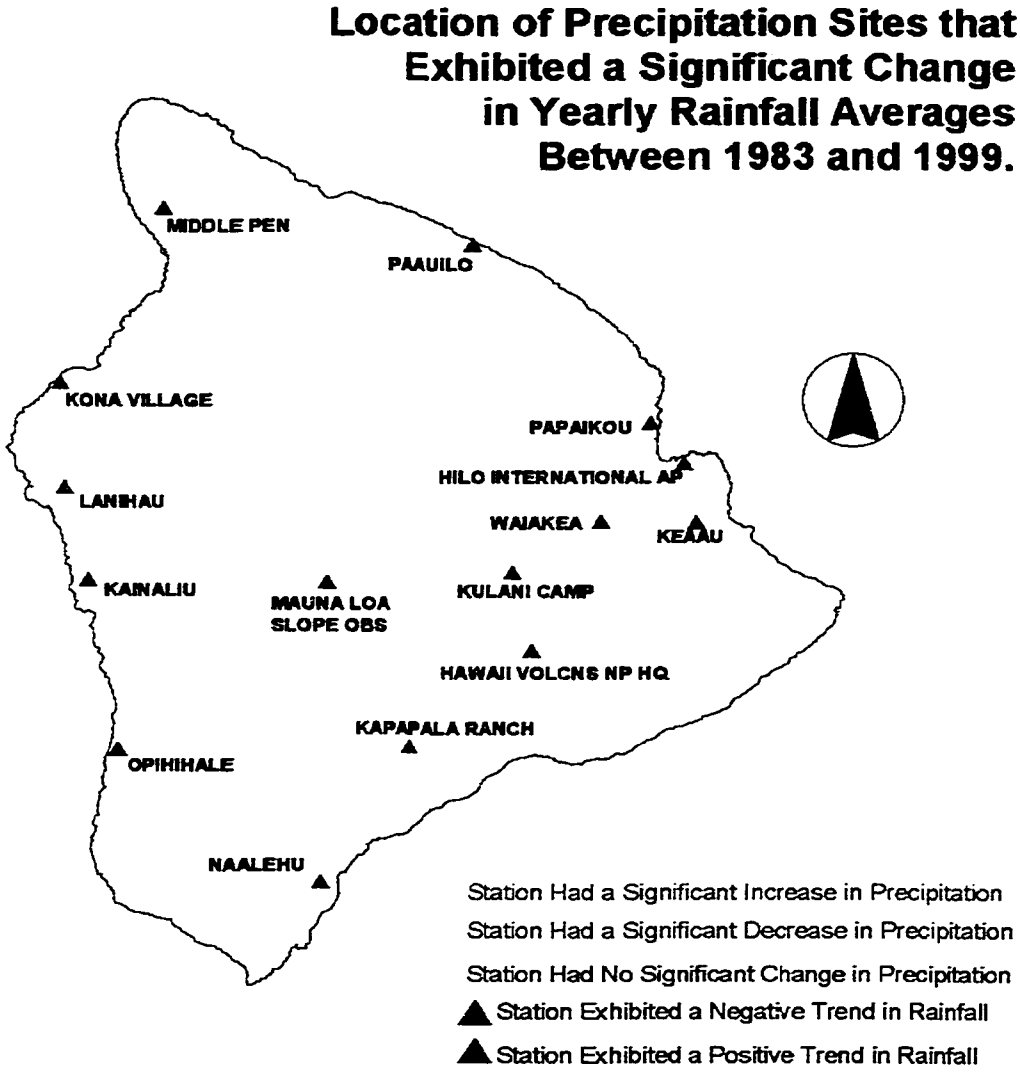


Figure 4.22: Map of rainfall stations with significant changes in precipitation trends between 1983 and 1999. Also shows the relative geographic location of stations with negative trends vs. positive trends (regardless of significance).

changes at that site were due to the *vog*. Since neither case was significant, it could be random or that there are not enough years in the sample to detect the trend. Furthermore, the pre-eruption trend could have been due to rapid urban expansion in Hilo (anthropogenic pollutants), verses the slower increase (perhaps even a decline) in urban expansion since the economic bust of the 1980s.

Furthermore, most of the ten other stations that had a negative trend are located to the west of the volcano. Due to their location, one may infer that if the trend was only due to the increased frequency of ENSOs since 1982, a significant trend would be seen both on the leeward (western) and windward (eastern) sides of the island. Thus it is very possible that the presence of the *vog* on the leeward side of the island has compounded the signal of the ENSO.

4.4 Results of Exploratory Analysis of Surface Temperature Data

The presence of sulfates in the troposphere can affect the local climate both directly and indirectly (Miller 1998). Sulfate aerosols can reflect solar radiation back into space, inducing direct cooling of the Earth's surface. As mentioned earlier, sulfates also act as cloud condensation nuclei (CCN) and increase the reflectivity and lifetime of clouds; thus sulfates also indirectly act as a cooling agent (UCAR 1995; Chuang et al. 1997;Miller 1998). Due to the above properties, an impact that one would expect the *vog* to trigger is a decrease of the island's surface temperatures.

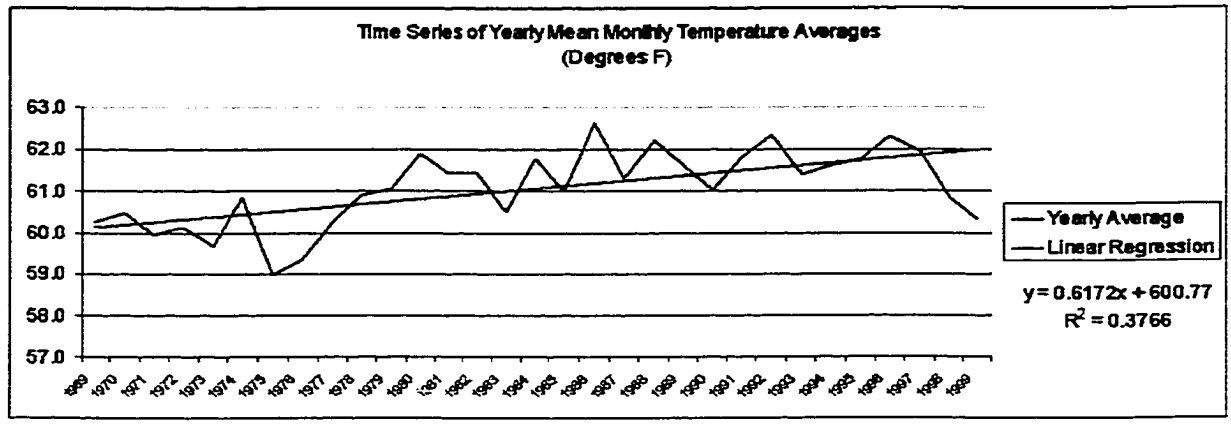
Only three data points with sufficient data were available for the temperature trend analysis. Fortunately the three sites were located across dissimilar climate regimes and different districts of the island (See Figure 3.6) so any bias due to

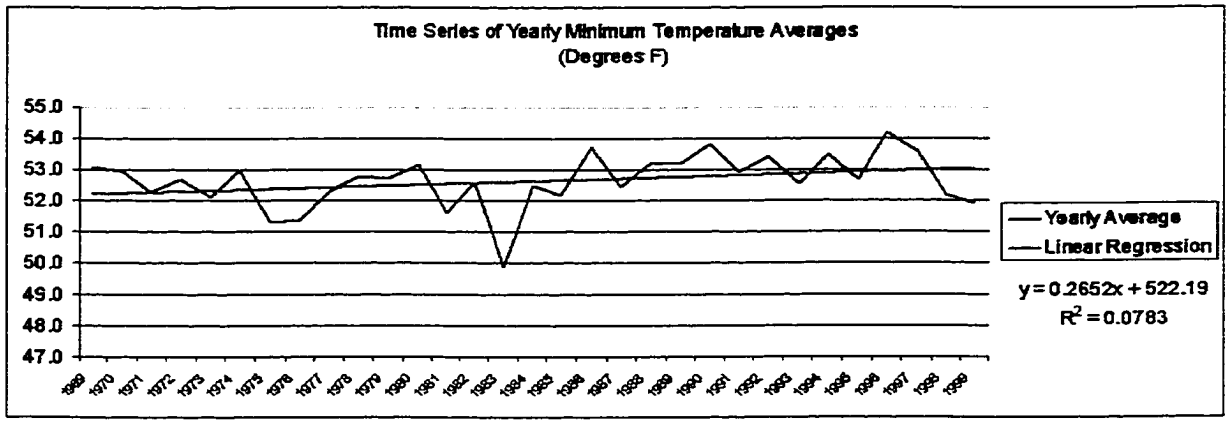
location should be minimal.

4.4a Temperature Trends for the Complete Time Series

All three sites showed a significant positive trend in yearly mean monthly temperature and yearly mean monthly minimum temperature for the complete 31-year time series. The Hawaii Volcanoes NP and Opihihale sites had a significant increase in yearly mean monthly maximum temperature (Figures 4.23 and 4.24), but the Hilo International AP site exhibited a significant decrease in yearly mean monthly maximum temperature (Figure 4.25). These results are not what would be expected if the *vog* was having an effect on the island's surface temperature. The Hilo International AP site is located on the windward side of the island, and therefore it would be expected that the *vog* effects would be minimal due to the dominant northeasterly trade winds. The station that would be expected to show the strongest signal (negative trend) is Opihihale due to its location on the leeward side of the island.

The overall results of the trend analysis for the complete 31-year time period do not readily support the hypothesis that the *vog* is impacting the island's temperature. Reasons for this include the obvious - the *vog* is not impacting the surface temperatures on the Big Island. Another possibility is that the global warming signature is so strong that it overcomes the weaker cooling signal due to the presence of sulfate particulates in the troposphere. By breaking up the complete time series into a pre- and post-eruption time series, a more distinct cooling signal from the *vog* may be detected.





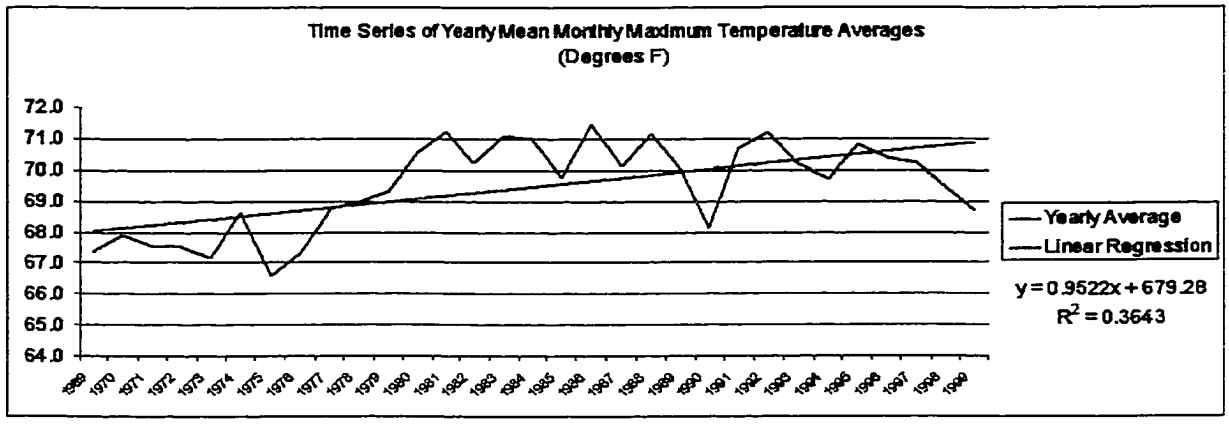
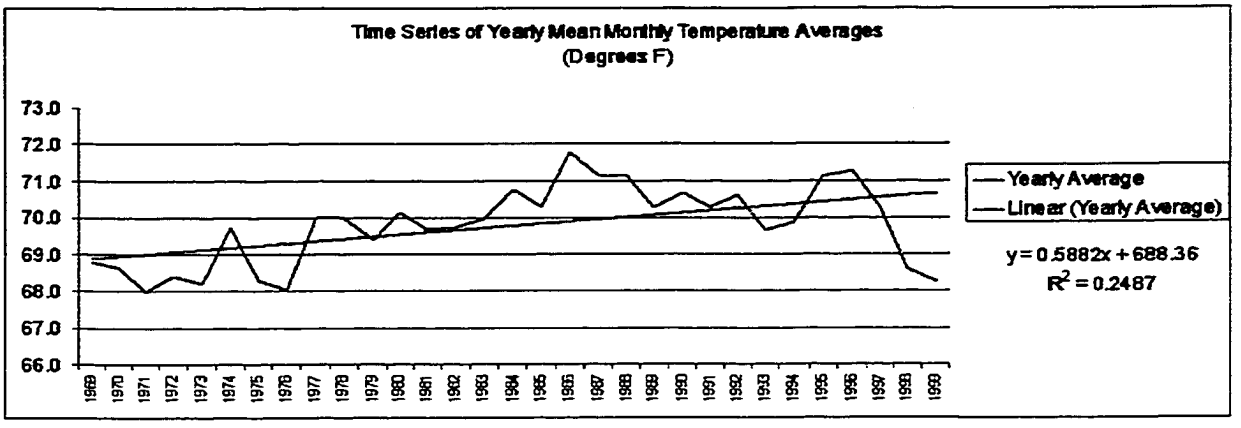
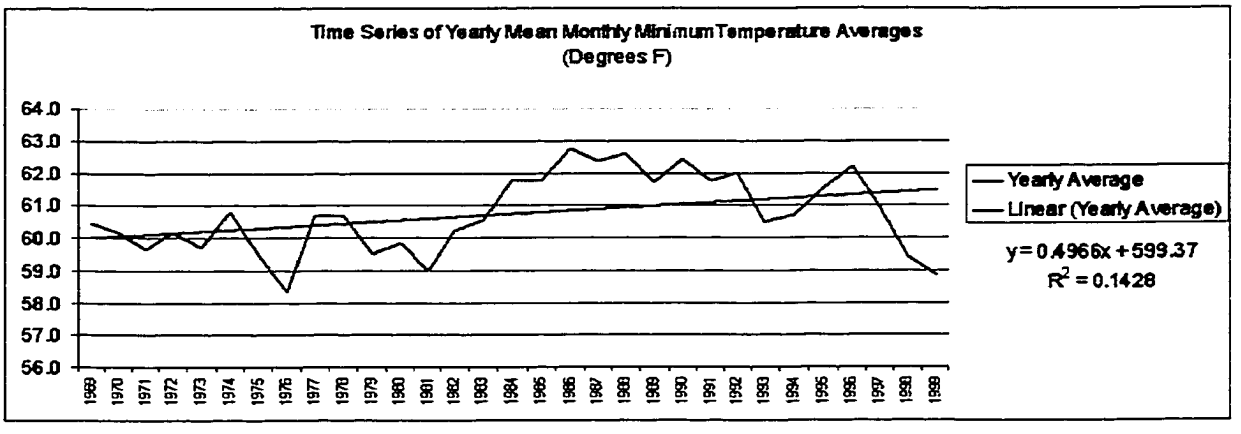


Figure 4.23: Graphs of yearly mean monthly temperature, yearly mean monthly minimum temperature, and yearly mean monthly maximum temperature (1969 to 1999) for the Hawaii Volcanoes NP station.





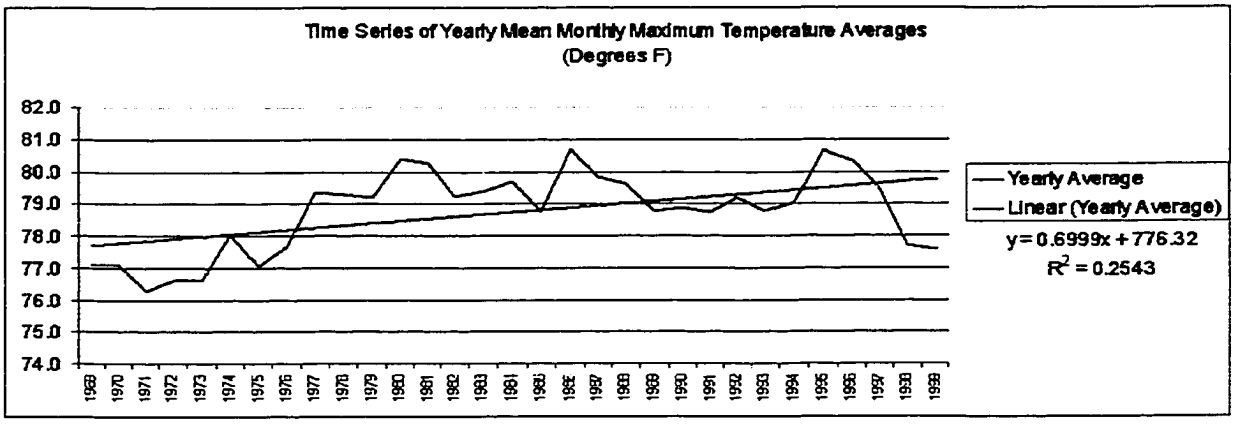


Figure 4.24: Graphs of yearly mean monthly temperature, yearly mean monthly minimum temperature, and yearly mean monthly maximum temperature (1969 to 1999) for the Opihihale station.

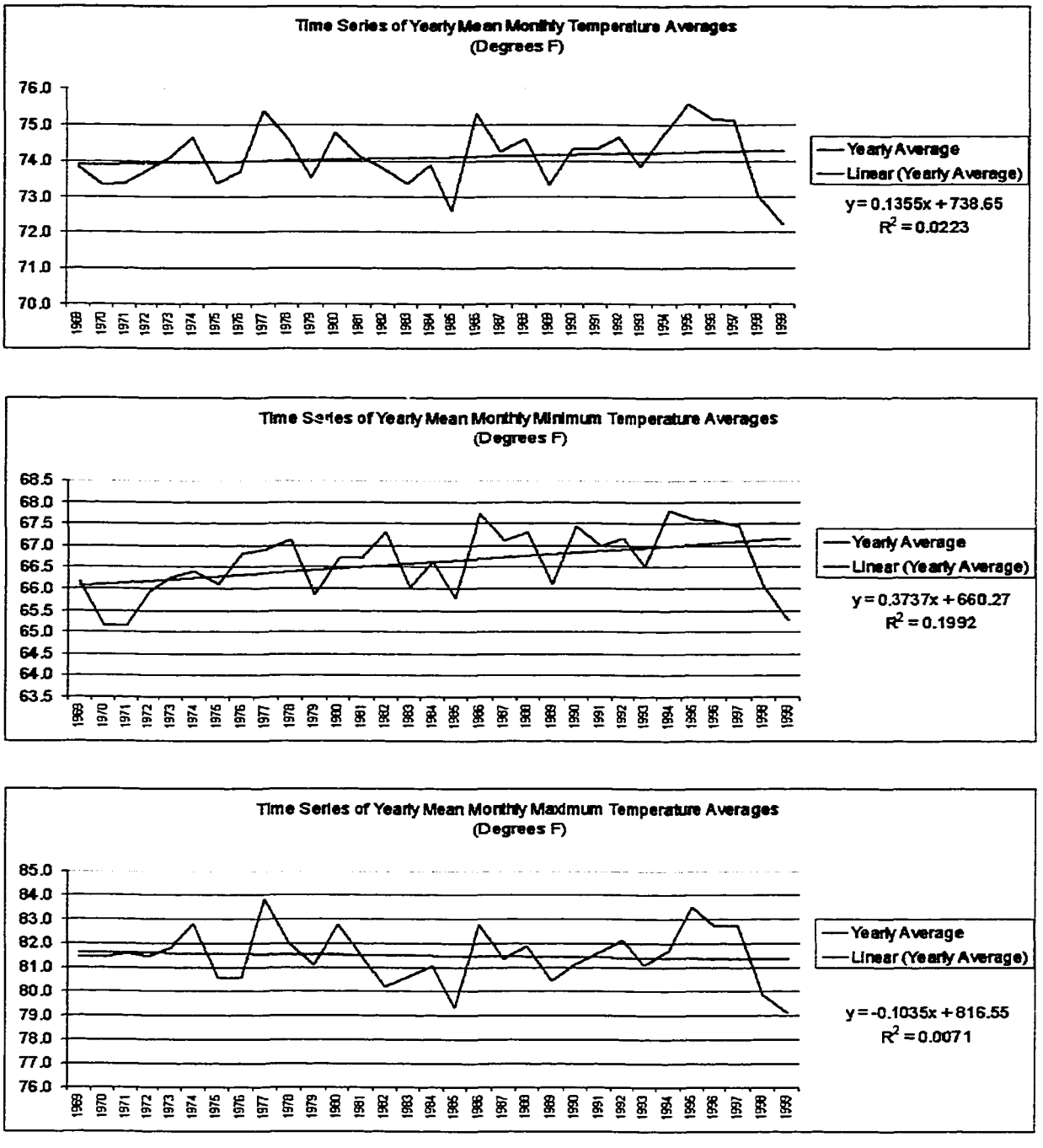
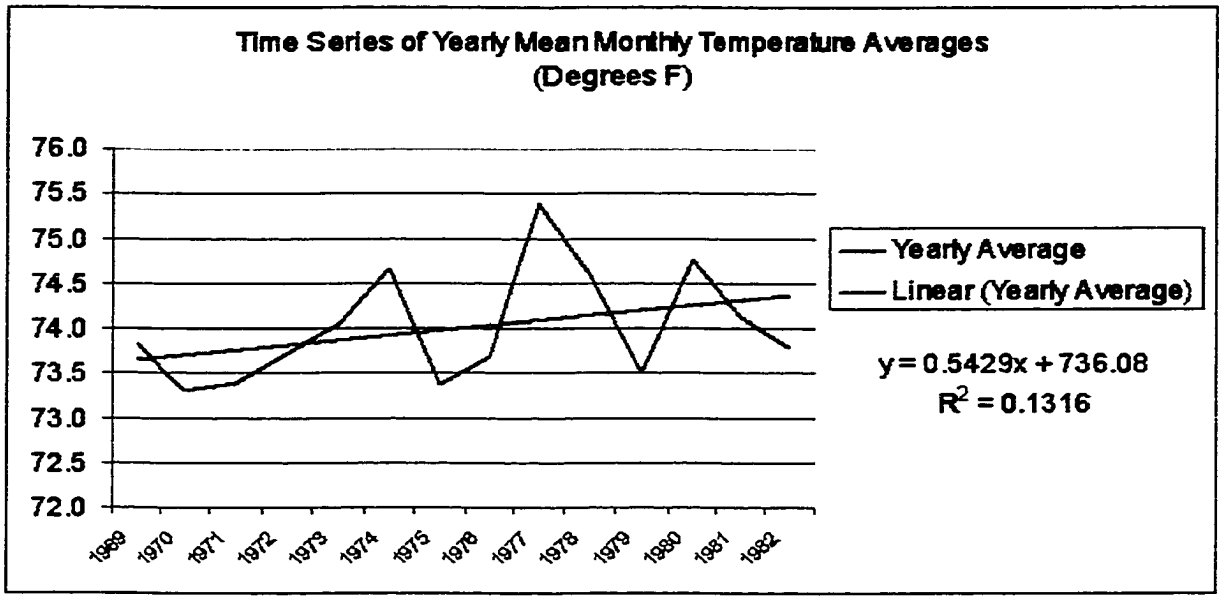


Figure 4.25: Graphs of yearly mean monthly temperature, yearly mean monthly minimum temperature, and yearly mean monthly maximum temperature (1969 to 1999) for the Hilo International AP station.

4.4b Temperature Trends for Pre-eruption vs. Post-eruption Time Series

All the sites exhibited a significant positive trend in the yearly mean monthly temperature for the 14 years prior to the start of the current eruption (Figures 4.26, 4.27, and 4.28). The Hilo International AP showed a significant positive trend in yearly mean monthly minimum temperature (Figure 4.29), but the Hawaii Volcanoes NP and Opihihale sites exhibited a significant negative trend (Figures 4.30 and 4.31). The Hawaii Volcanoes NP and Opihihale sites had a significant positive trend in yearly mean monthly maximum temperature (Figures 4.32 and 4.33), while the Hilo International AP station reflected a negative trend which was not significant (Figure 4.34).

These results show an overall steady increase in yearly mean monthly temperatures, yearly mean monthly minimum temperatures, and yearly mean monthly maximum temperatures prior to 1983 when Kilauea began it current eruption. This may be a result of global warming or simply the increased urbanization of the island (i.e. local urban heat island effect). The decreasing trend in yearly mean monthly minimum temperatures found at the Hawaii Volcanoes NP and Opihihale sites is not as easy to explain and it is not sure what would cause a such a decrease. One logical possibility is that there was a decrease in night-time cloud cover which would allow more long-wave infrared energy to radiate from the Earth's surface back into space; but that is just a hypothesis and requires more investigation. The decreasing trend in yearly mean monthly maximum temperatures at Hilo International AP is also not very readily explained.



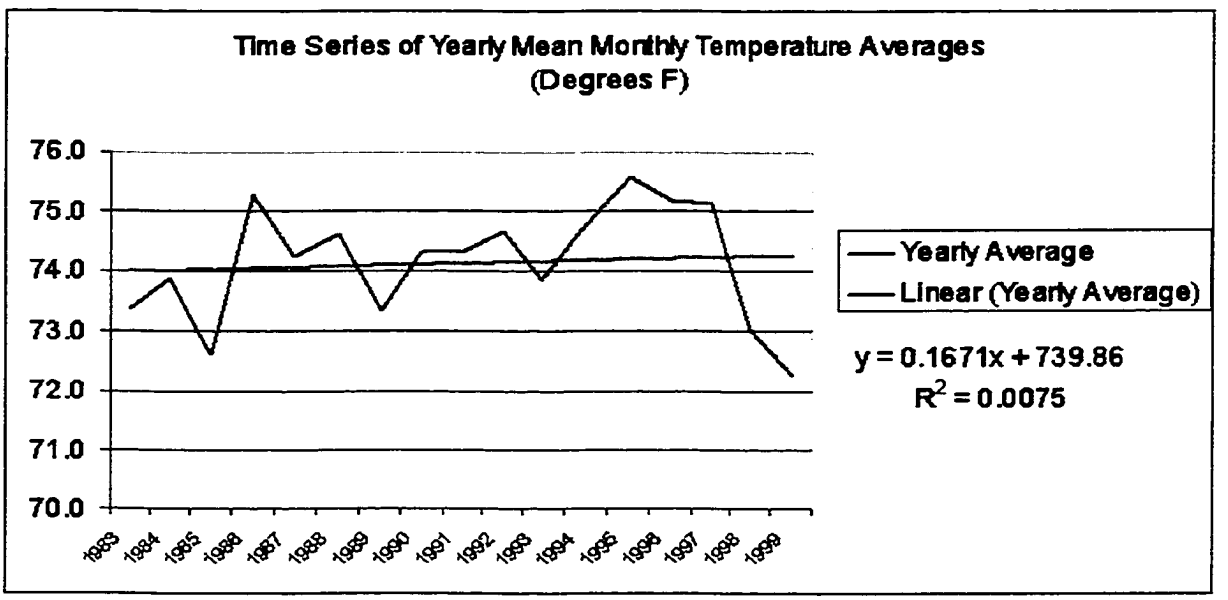
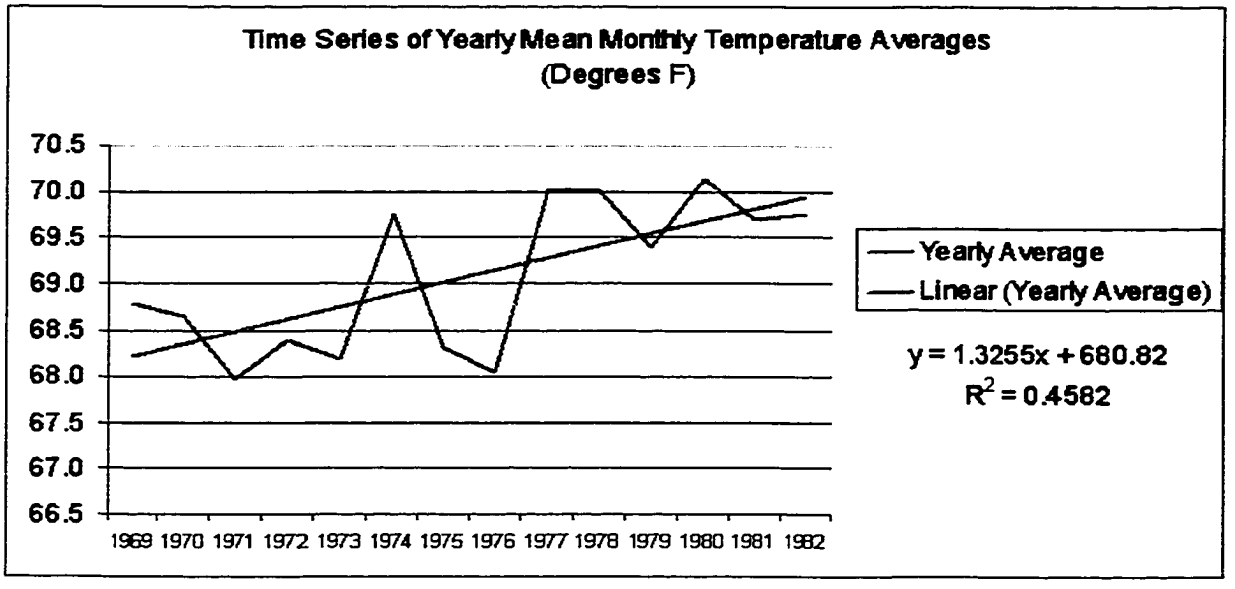


Figure 4.26: Graphs of yearly mean monthly temperature for the Hilo International AP station for pre-eruption (1969 to 1982) and post-eruption (1983 to 1999) time periods.



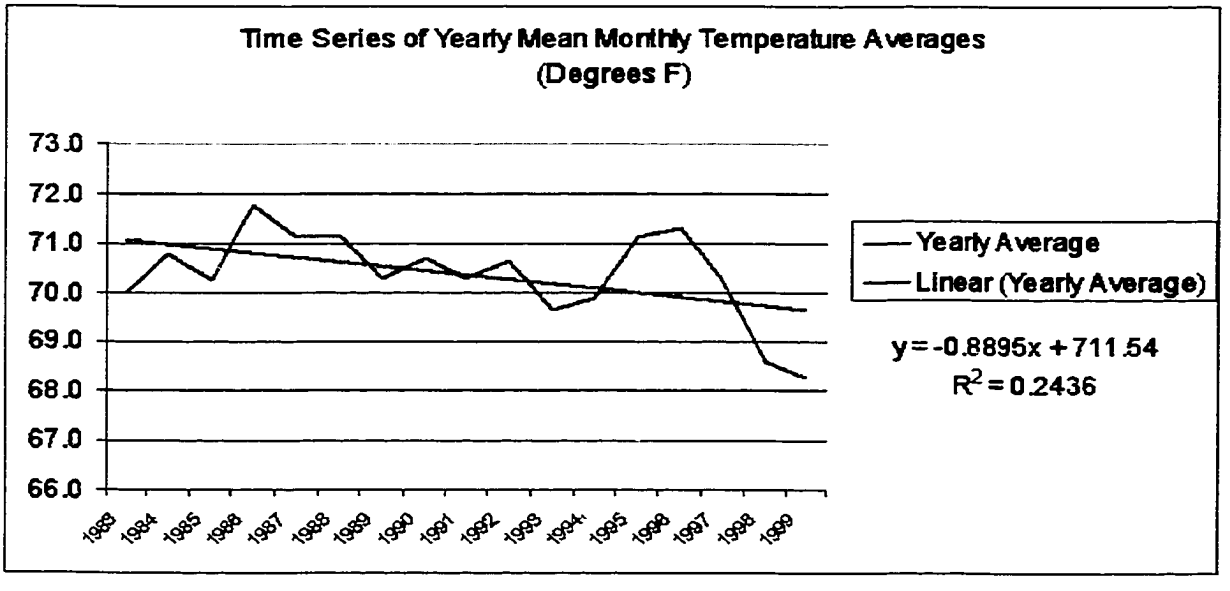
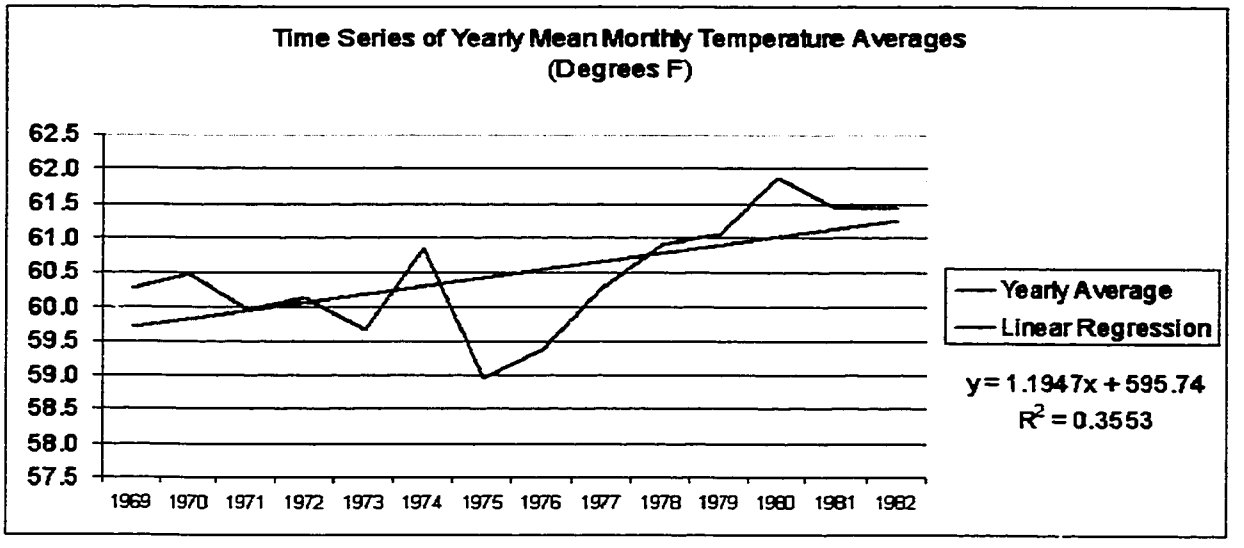


Figure 4.27: Graphs of yearly mean monthly temperature for the Opihihale station for pre-eruption (1969 to 1982) and post-eruption (1983 to 1999) time periods.



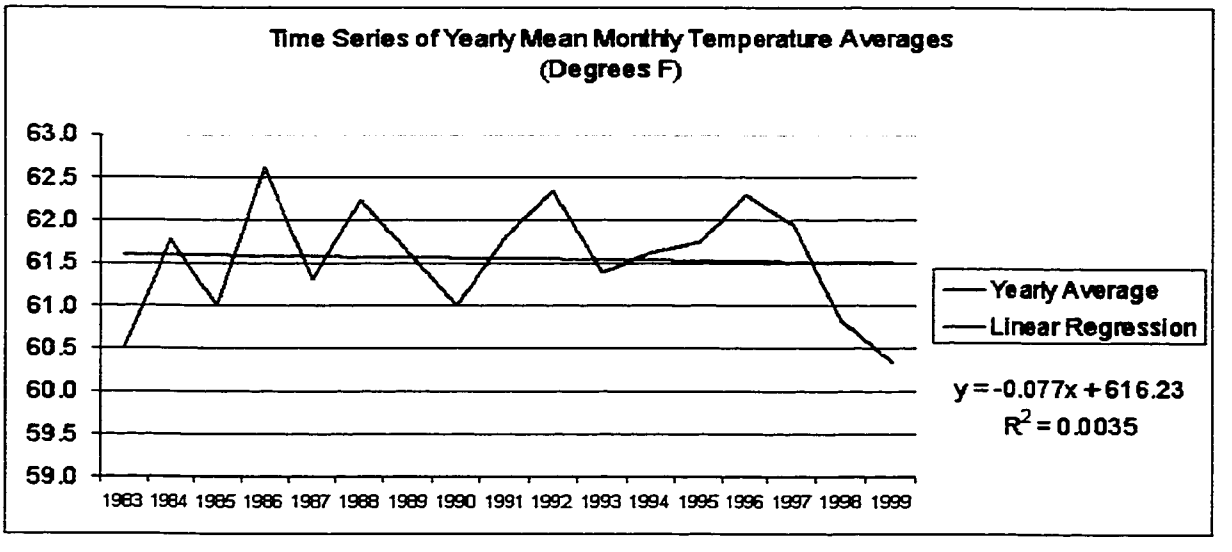
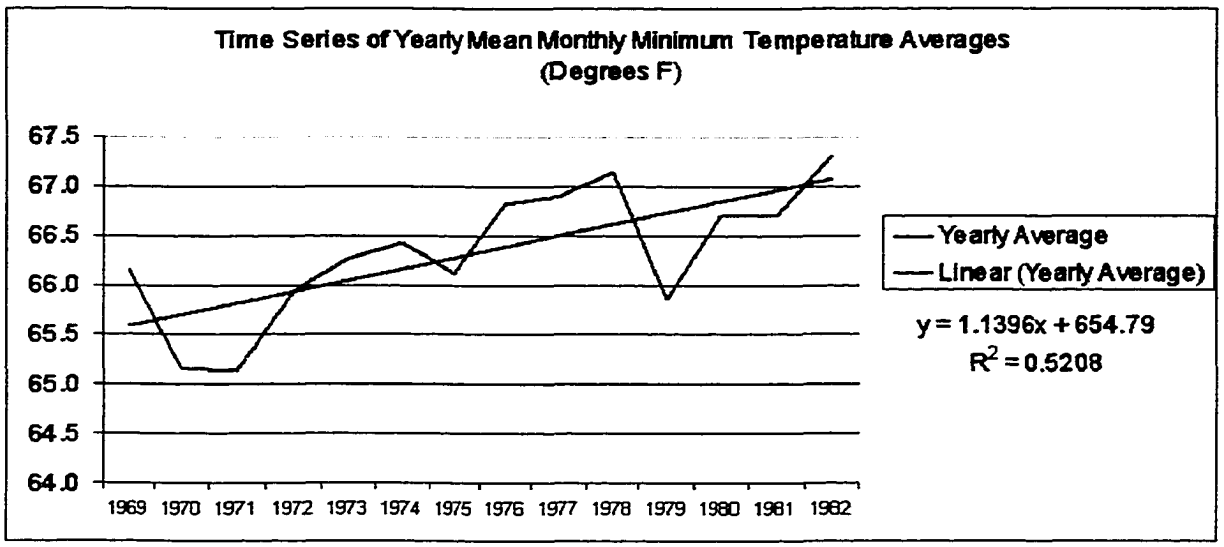


Figure 4.28: Graphs of yearly mean monthly temperature for the Hawaii Volcanoes NP station for pre-eruption (1969 to 1982) and post-eruption (1983 to 1999) time periods.



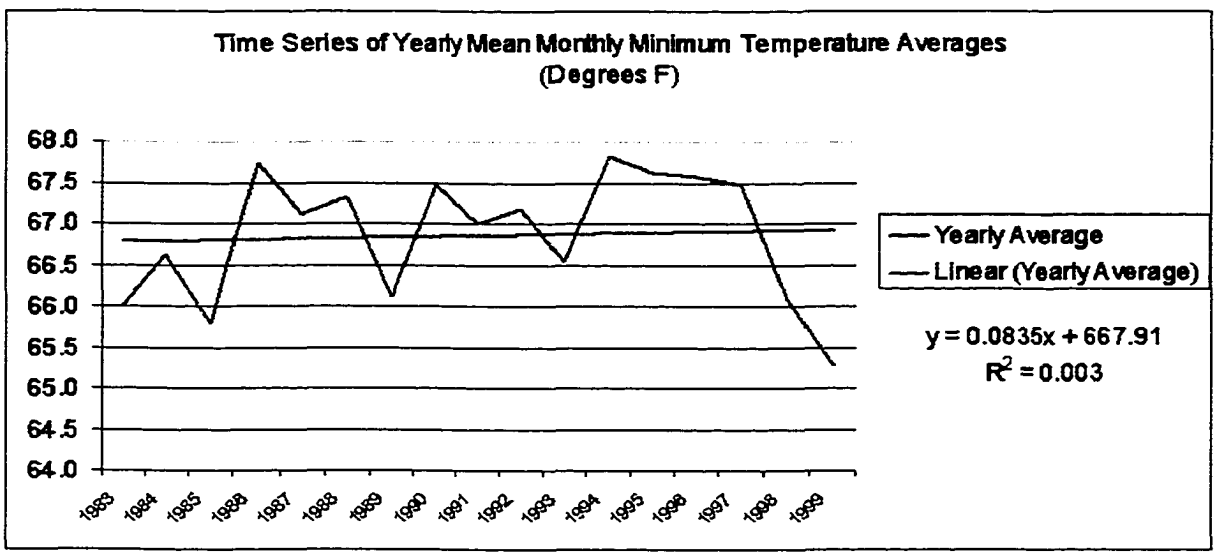
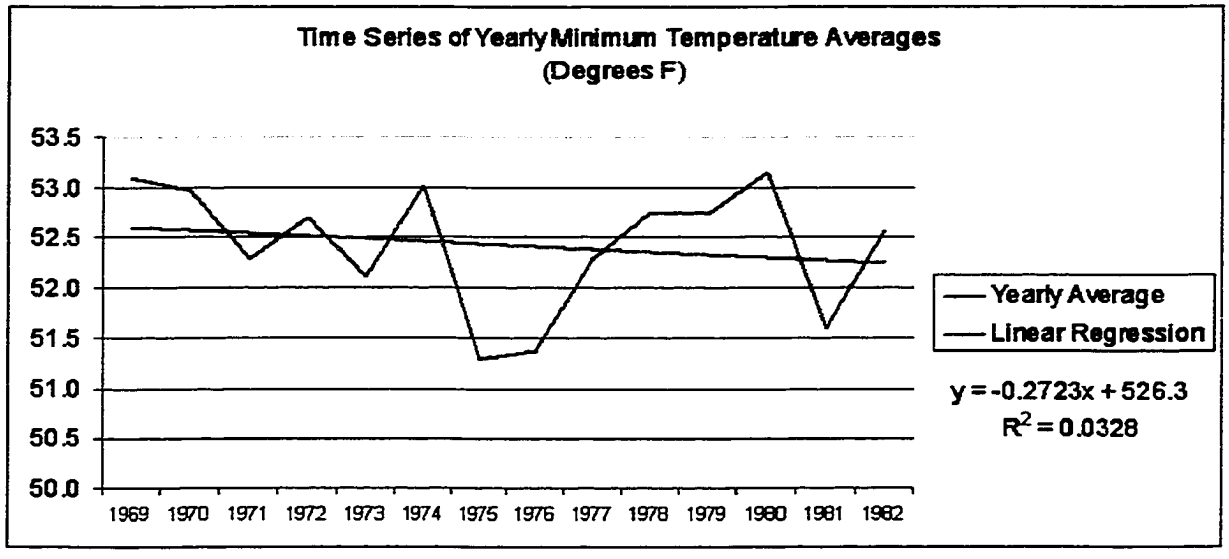


Figure 4.29: Graphs of yearly mean monthly minimum temperature for the Hilo International AP station for pre-eruption (1969 to 1982) and post-eruption (1983 to 1999) time periods.



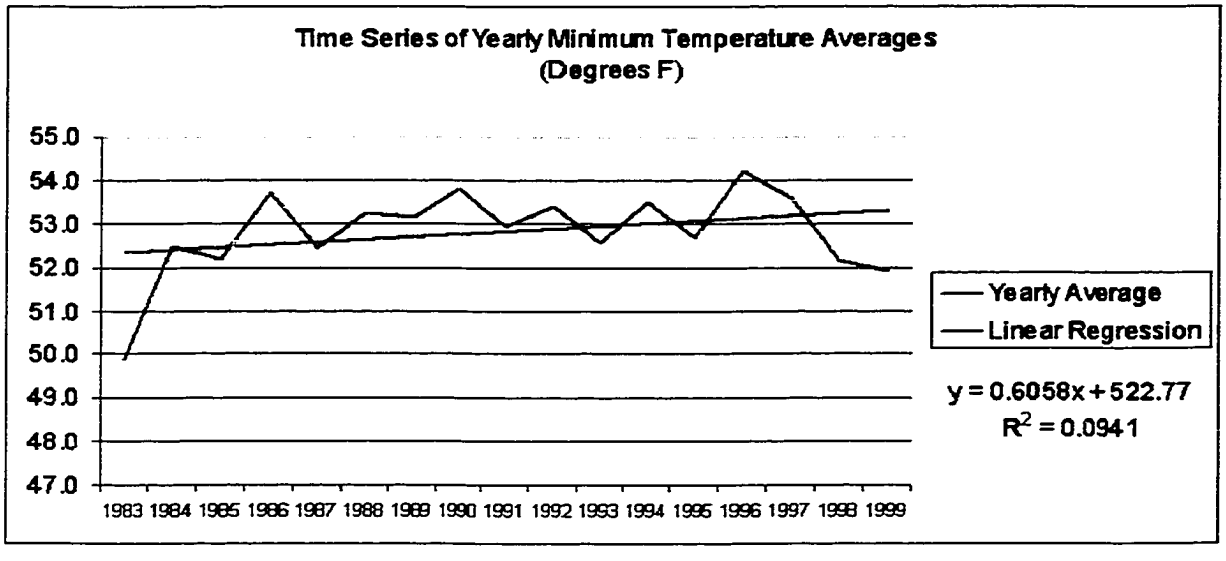
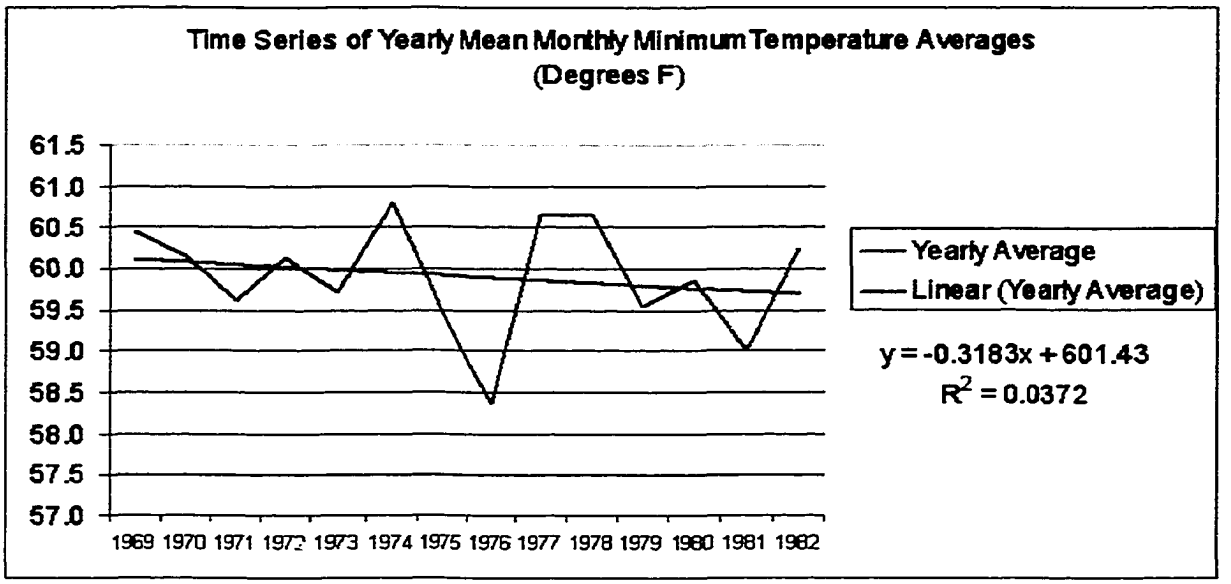


Figure 4.30: Graphs of yearly mean monthly minimum temperature for the Hawaii Volcanoes NP station for pre-eruption (1969 to 1982) and post-eruption (1983 to 1999) time periods.



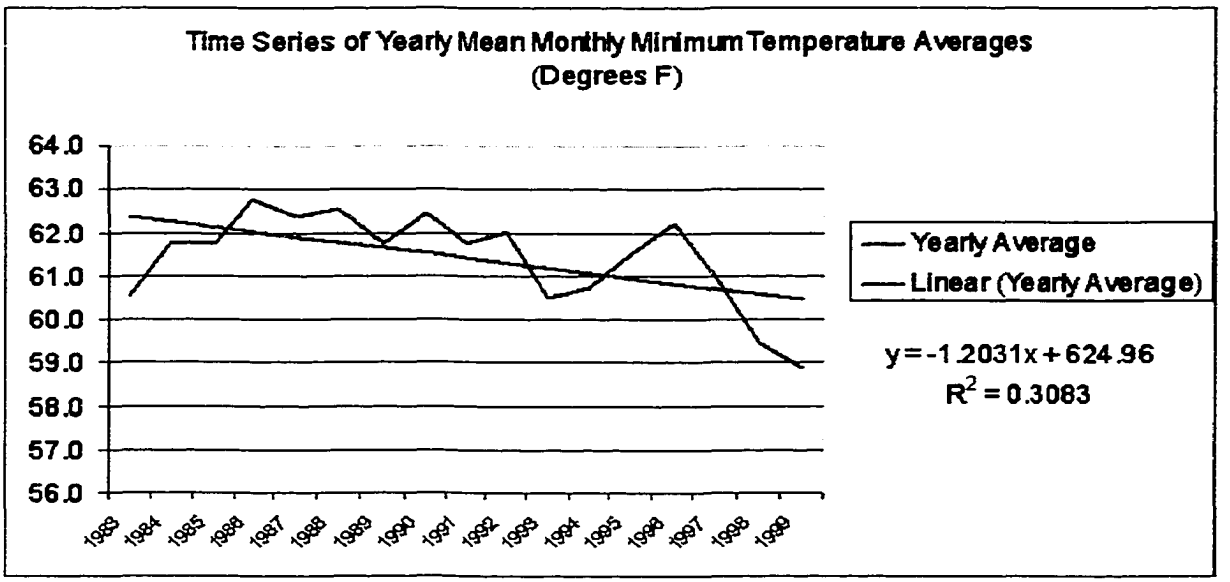
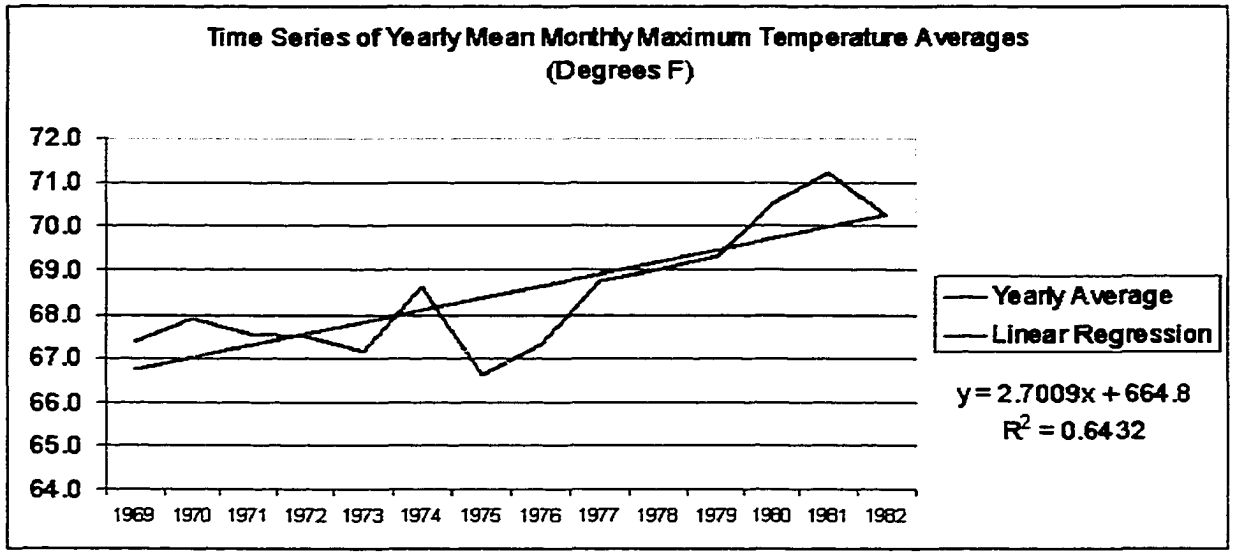


Figure 4.31: Graphs of yearly mean monthly minimum temperature for the Opihihale station for pre-eruption (1969 to 1982) and post-eruption (1983 to 1999) time periods.



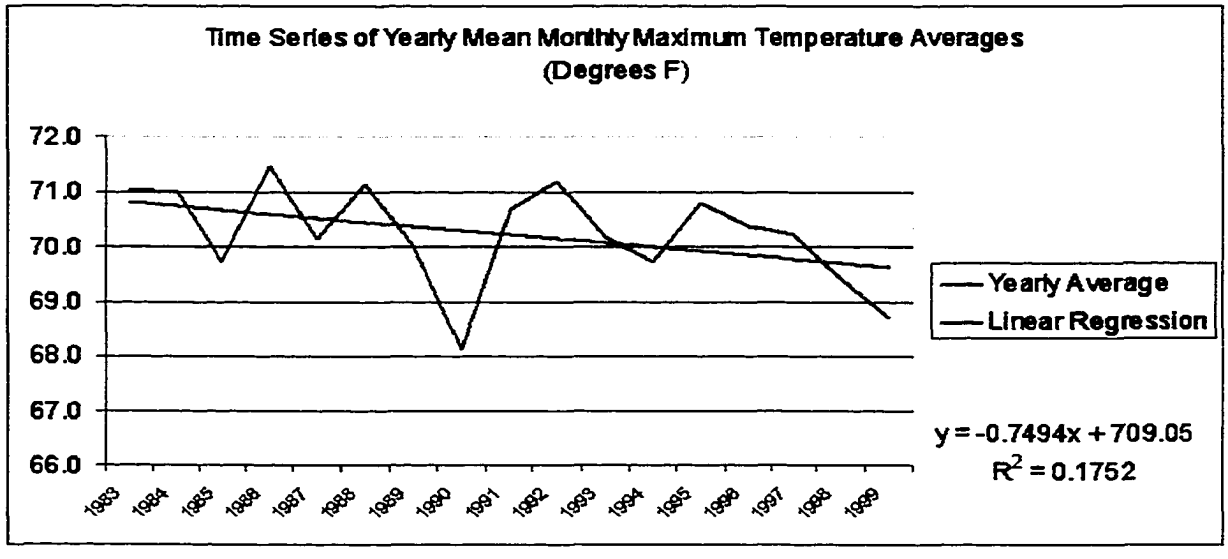
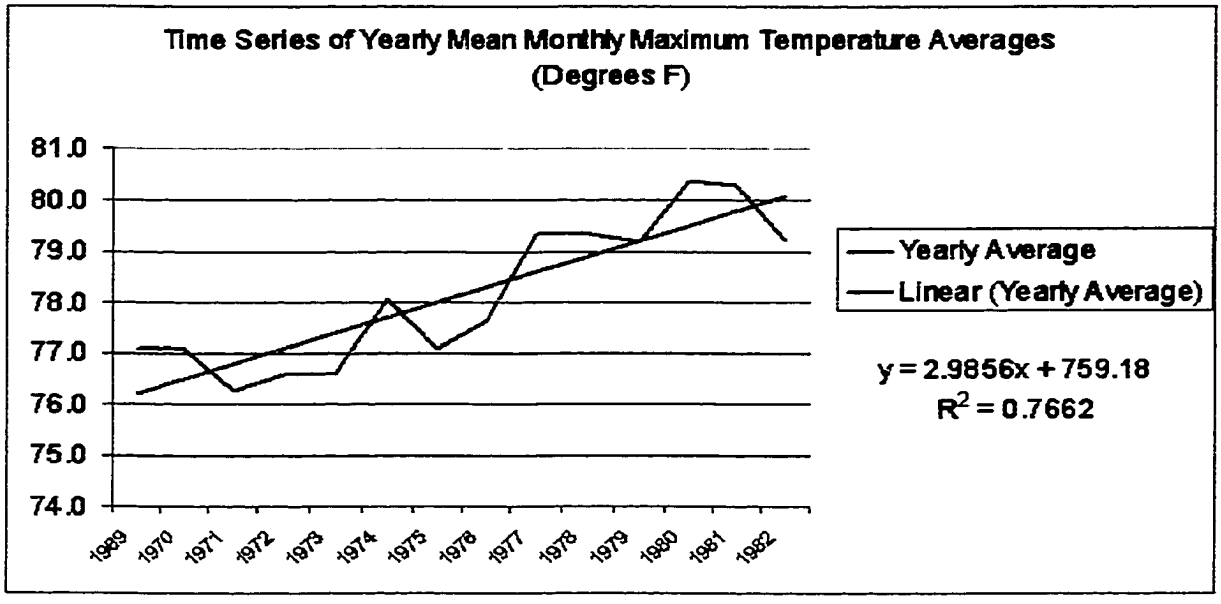


Figure 4.32: Graphs of yearly mean monthly maximum temperature for the Hawaii Volcanoes NP station for pre-eruption (1969 to 1982) and post-eruption (1983 to 1999) time periods.



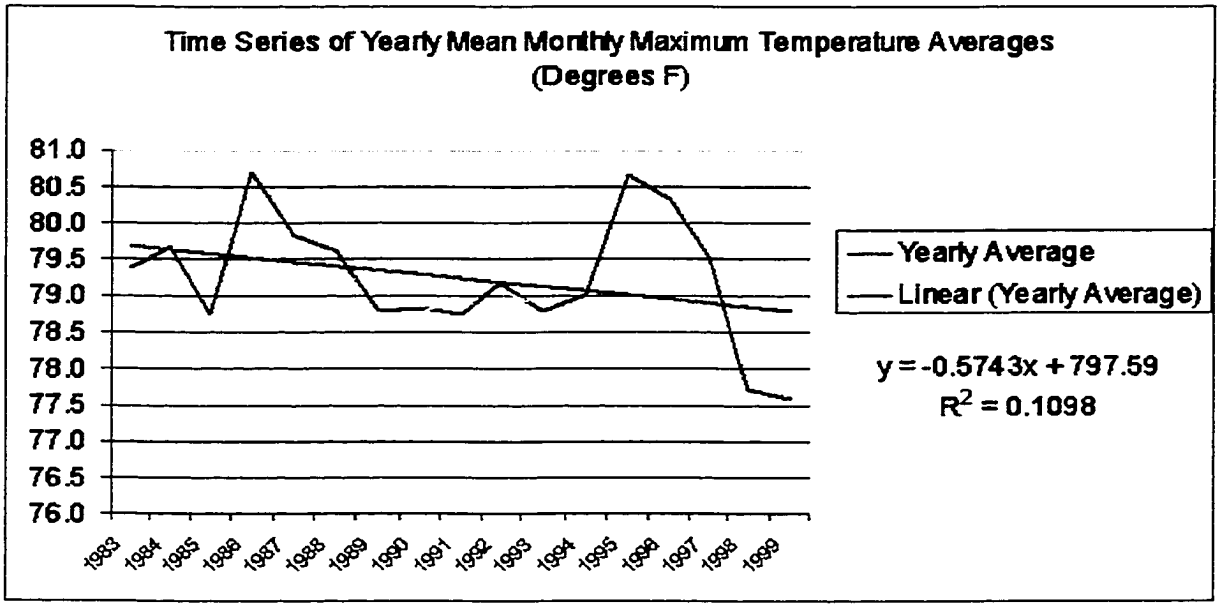
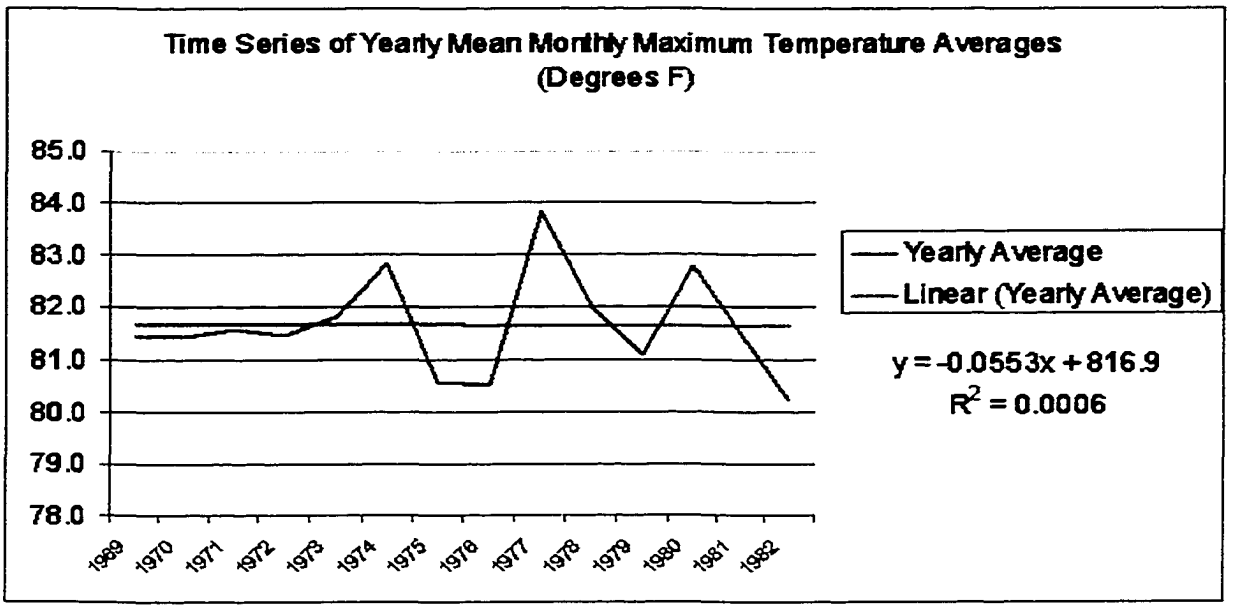


Figure 4.33: Graphs of yearly mean monthly maximum temperature for the Opihihale station for pre-eruption (1969 to 1982) and post-eruption (1983 to 1999) time periods.



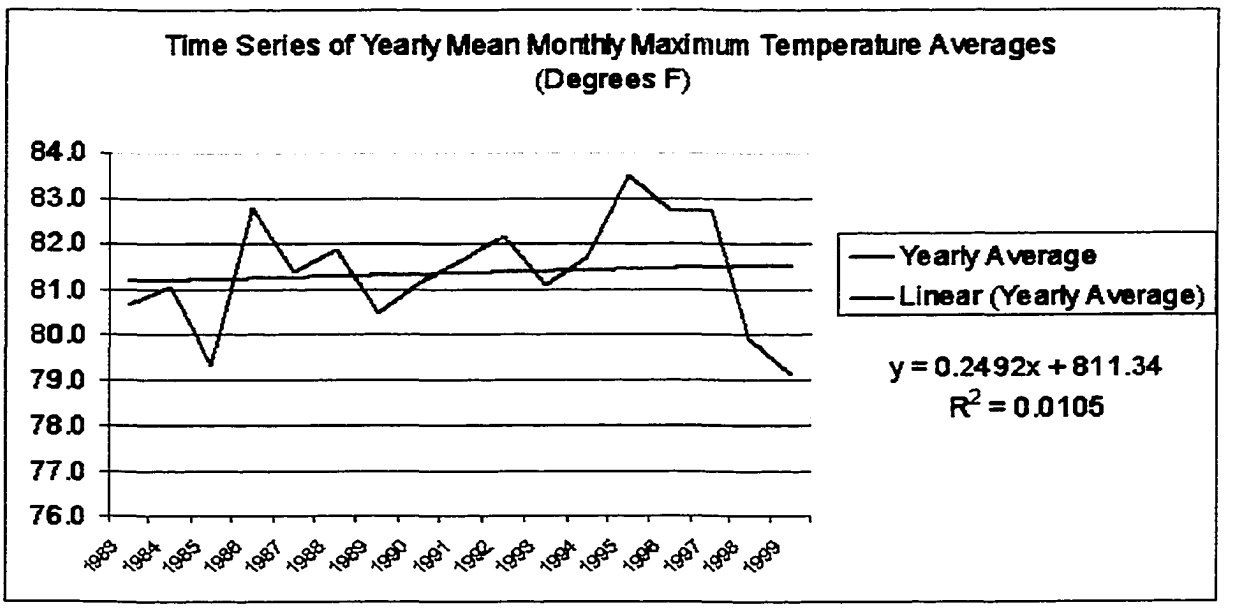


Figure 4.34: Graphs of yearly mean monthly maximum temperature for the Hilo International AP station for pre-eruption (1969 to 1982) and post-eruption (1983 to 1999) time periods.

For the post-eruption time series (1983-1999), the trends detected were mixed. Opihihale showed a significant negative trend for yearly mean monthly temperatures, yearly mean monthly minimum temperatures, and yearly mean monthly maximum temperatures (Figures 4.27, 4.31, 4.33). The Hilo International AP station reflected a non-significant positive trend for yearly mean monthly temperatures, yearly mean monthly minimum temperatures, and yearly mean monthly maximum temperatures (Figures 4.26, 4.29, 4.34). Finally, the Hawaii Volcanoes NP site was mixed with it showing a non-significant decrease in yearly mean monthly temperatures and a significant decrease in yearly mean monthly maximum temperatures (Figures 4.28 and 4.32), but a significant increase in yearly mean monthly minimum temperatures (Figure 4.30).

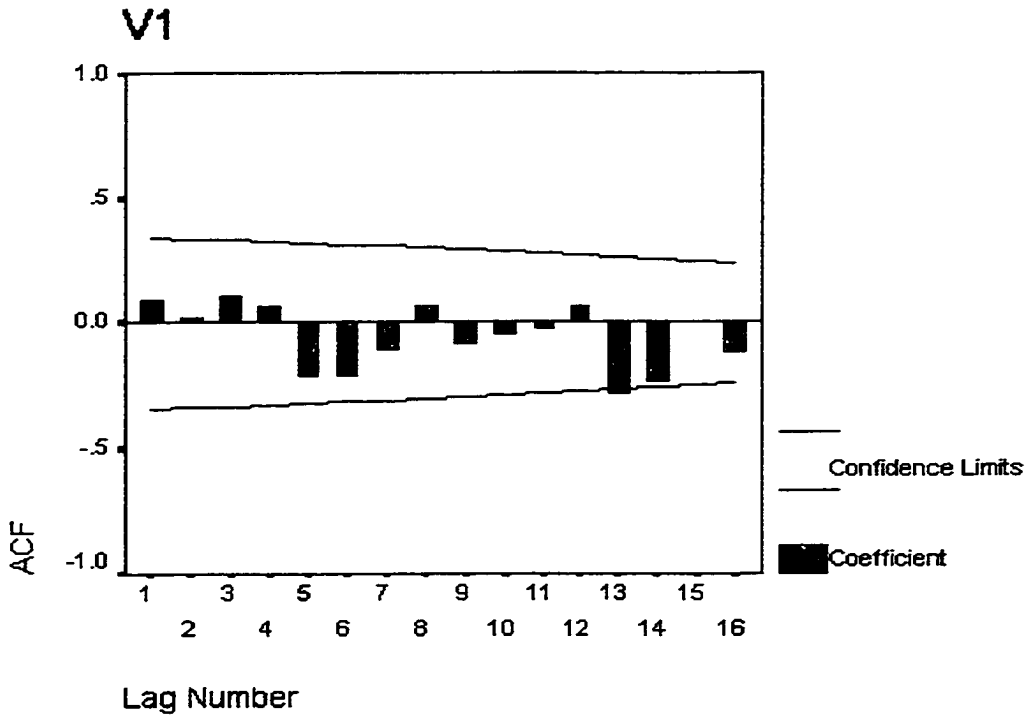
Due to its location on the leeward side of the Big Island, Opihihale would be expected to show a strong cooling signature due to sulfate particulates in the troposphere. It did show a significant cooling trend between 1983 and 1999. The Hilo International AP site's location on the windward side of the Big Island would lessen if not diminish the impacts of the *vog* on surface temperature. Thus, one would expect to see little or no cooling trend there. This was exhibited by the Hilo International AP site as it reflected a warming (but not significant) trend between 1983-1999. The Hawaii Volcanoes NP station reflected a cooling trend between 1983-1999 for yearly mean monthly temperatures and yearly mean monthly maximum temperatures, which would be expected if the *vog* was impacting the local surface temperatures. But the yearly mean monthly minimum temperatures exhibited a significant warming trend between 1983-1999. This may be explained by an increase in clouds in the area due

to sulfates which do not dissipate rapidly after sunset; thus the night time clouds help to keep long-wave radiation being emitted by the Earth's surface from escaping into space. Again, this is only a hypothesis and would require more study.

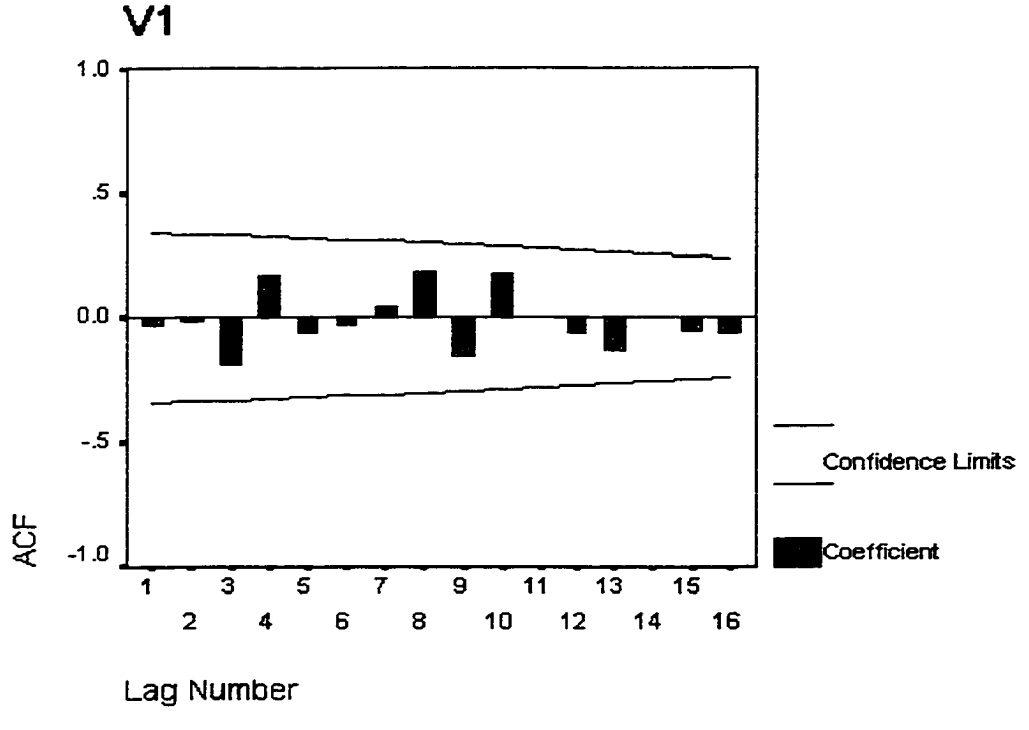
4.5 Autocorrelation Results for Rainfall and Temperature Data

Since time series data were used in the regression analysis, possible autocorrelation in the data must be addressed. Autocorrelation describes the degree to which the value of an attribute at spatially or temporally adjacent points changes with the distance or time separating the observations (Clark and Hosking 1986). Since the regression function assumes that the data are independent of each other, the variables should be tested for autocorrelation.

No autocorrelation was expected to exist since mean yearly data was used, but the values calculated for both temperature and rainfall were tested. The variables did not show signs of autocorrelation, and therefore supported the assumption that the variables were independent of each other. If daily data were used then the possibility of autocorrelation being significant could have been a factor in the regression analysis. Figures 4.35 and 4.36 show sample graphs of the autocorrelation test results for the mean yearly rainfall and temperature values.

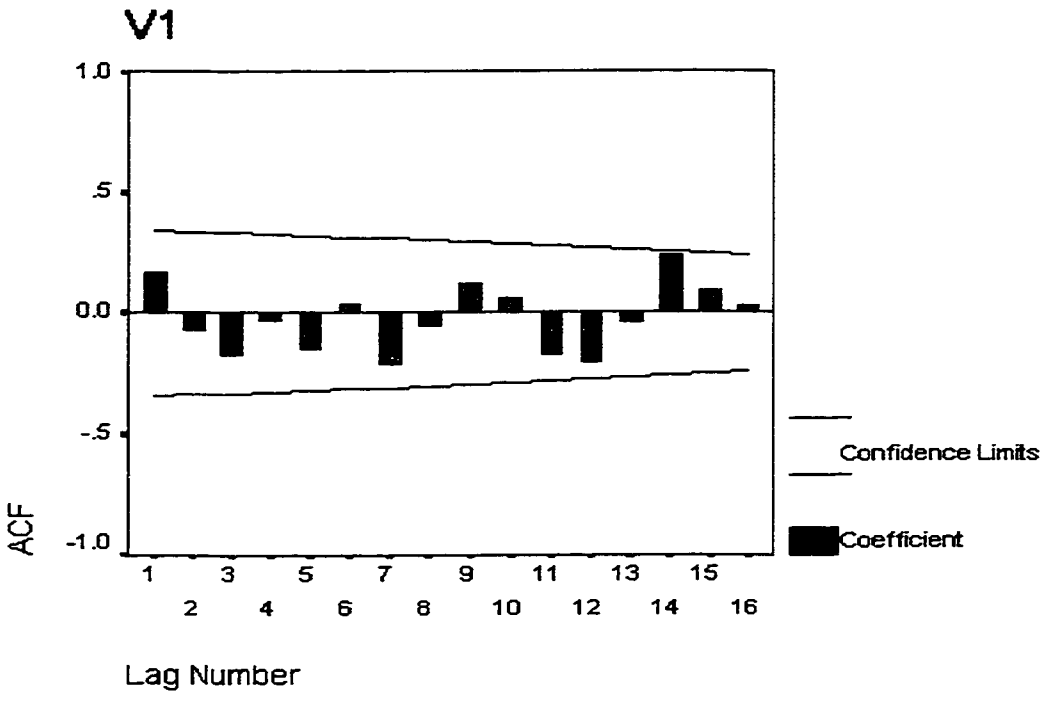


Hilo International Airport

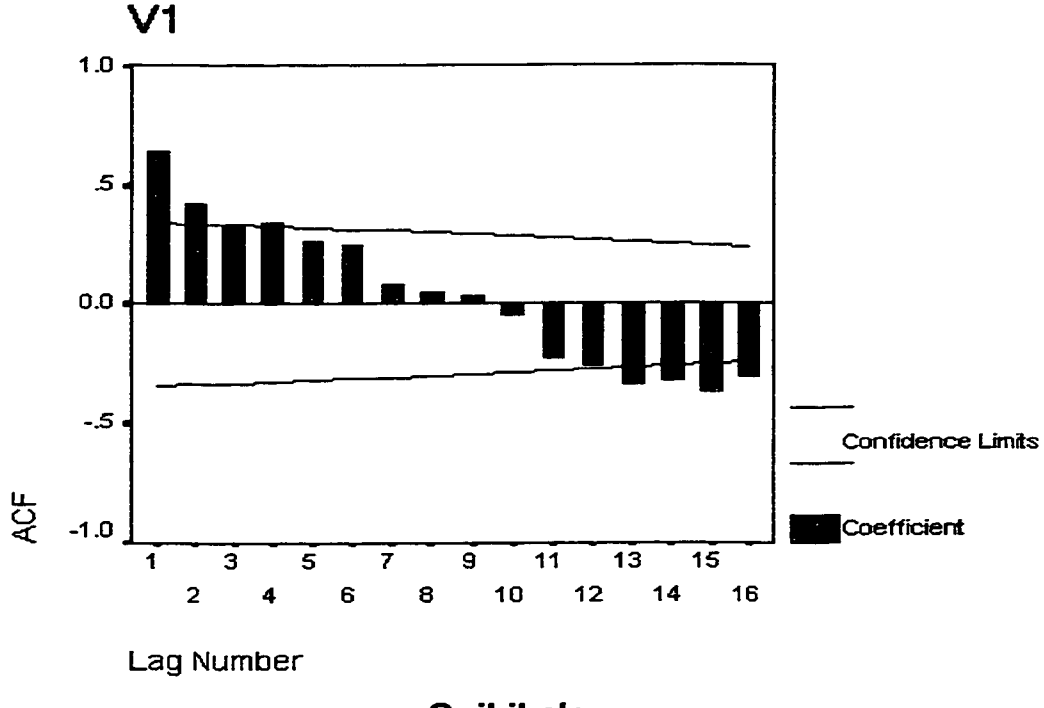


Opihihale

Figure 4.35: Sample graphs showing the results of the autocorrelation test for yearly mean rainfall time series.



Hilo International Airport



Opihihale

Figure 4.36: Sample graphs showing the results of the autocorrelation test for yearly mean temperature time series.

CHAPTER 5

CONCLUSIONS AND SUGGESTED FUTURE RESEARCH

This study attempted to determine if the *vog* produced by Kilauea Volcano on Hawai'i Island was affecting its environmental systems. Specifically, it investigated possible impact to the island's vegetation, rainfall, and temperature. The conclusions from the study's results and possible directions of future research are discussed in this chapter.

5.1 Vegetation Impacts

There were no conclusive results derived from the study which would support the theory that the *vog* had negatively impacted the health of vegetation present in the region of the Hawai'i Volcanoes National Park. The possible reasons why no appreciable changes in vegetation were detected are numerous. First, the spatial resolution of the satellite imagery available prior to when Kilauea began its current eruption is very poor when compared to the size of the vegetation patches being sensed. It is even questionable if the 20 m spatial resolution of the SPOT HRV data used for post-eruption analysis is adequate. Second, the different spectral resolution of the two satellite sensors used provided an unequal comparison of NDVI values between pre- and post-eruption scenes. Moreover, the radiometric resolution of the sensors was also unmatched: Landsat MSS scene was 6-bit while the SPOT HRV scene was 8-bit data. It is certain that the cumulation of all these differences created

an unsatisfactory comparison; but due to the lack of usable satellite data present for the island, there was no other alternative if one wished to use multispectral imagery. One option for future studies would be to use aerial photography, though a different technique such as texture analysis would need to be used since it is single band data.

The Landsat MSS and SPOT NDVI differencing produced inconclusive or even negating results. Yet the NDVI differencing done between the two SPOT scenes did reveal some areas where it is likely that some change has occurred to vegetation health. Unfortunately the dates of both SPOT scenes are sufficiently after the beginning of Kilauea's eruption that it would require much more investigation and analysis to determine if vegetation health was actually impacted and if it was the result of the *vog's* presence.

Finally, it is possible that no noteworthy impacts to vegetation were detected because there was none. The soils in the study area are predominately Andisols and Histosols. Andisols are not considered to be very acidic and can have a pH around 6.0, while the Histosols may have a pH around 4.5. But the relative pH of each soil order in Hawai'i is not as important as the actual elements and their relative amounts in the soil. For example, the Histosols' low pH is not considered to be toxic since there is little aluminum in the soil which can be taken up by plants (Uehara et al. 1997). Therefore the soils' properties allow the *vog* to have little or no long-term effect on vegetation health. It should be noted however that immediate impacts to vegetation due to volcanic emissions when Kilauea begin its eruption are probable, but can not be measured due to the lack of data available.

5.2 Rainfall Impacts

The presence of excessive amounts of sulfate particulates in the troposphere, such as the *vog* on Hawai'i Island, would be expected to cause a reduction in the amount of rainfall. The El Niño phenomenon is also known to be responsible for inhibiting rainfall on Hawai`i, and it must also be considered when attributing significant decreasing trends to the *vog*. The geographic location of each station was utilized to help filter out the signal due to El Niño. For example, locations on the windward side of the island would be expected to be impacted to a lesser degree since the *vog* tends to accumulate on the leeward side of the Big Island.

The trend analysis of the complete mean rainfall time series (1969-1999) showed that some portions of the Big Island experienced a significant negative trend in rainfall. These locations were on the leeward side of the island, which is where the presence of the *vog* is the strongest. The geographic location of these trends would imply that the yearly mean rainfall amounts were decreasing in part due to the presence of the *vog*, and not just the El Niño phenomenon.

Analysis of mean rainfall between 1969-1982 and 1983-1999 were performed to compare pre- and post-eruption rainfall trends. The pre-eruption time series showed most stations having a positive trend, but it none were significant. The post-eruption time series analysis revealed that most stations have a negative trend, although none were significant. There were five sites on the windward side of the island that showed a positive trend, but none of those were significant. Even though all of the stations did not have significant trends, the geographical location of the

positive trends vs. the negative trends may be consequential. Again, the leeward sites reflected negative trends (reduced rainfall), while the windward sites were dominated by positive trends (increased rainfall). This geographical distinction supports the theory that the *vog* is reducing rainfall for portions of the Big Island. Suggested future studies include determining if perhaps the *vog* is compounding ENSO-related droughts for certain locations on the Big Island.

5.3 Temperature Impacts

If the *vog* was impacting the Big Island's surface temperatures, one would expect to see a negative trend (cooling effect) in the data. Yearly mean monthly temperatures, and yearly mean monthly minimum temperatures, and yearly mean monthly maximum temperatures were used in the temperature trend analysis because just using the monthly mean data would not have been thorough. For example, there may not have been a trend on the mean monthly data, but there may have been a change in the trend of the mean monthly minimum data or mean monthly maximum data. The results of the trend analysis for the complete 31-year time series does not support the theory that the *vog* is having a cooling effect on the island's surface temperatures. The results from the pre-and post-eruption comparison does lend support to the *vog* having a cooling affect for certain portions of the island, i.e. the leeward coast. The availability of more data points would be ideal, but the lack of continuous data make this unfeasible.

Suggested future studies would include breaking down the data to its seasonal

components so that more data points (sites) could be used. It should be stressed that the cooling signature of the *vog* may not be detectable due to the stronger signal of global warming. Chuang et al. (1997) note that anthropogenic sulfates may be reducing the magnitude of global warming in some regions. Thus global warming may be masking any cooling trend due to the *vog* from Kilauea Volcano. Using AVHRR polar orbiting imagery to measure changes in the type and amount of cloud cover over Hawai'i between years prior and after the current eruption may allow an indirect measurement of the *vog's* cooling effect on the Island. This approach may be a method to remove the global warming signature.

REFERENCES

Anderson J, Hardy E, Roach J, Witmer R. 1976. *A land use and land cover classification system for use with remote sensor data.* Washington D.C.: U.S. Geological Survey Professional Paper 964, 28 p.

Asrar G, Dozier J. 1994. *EOS: Science strategy for the Earth Observing System.* AIP Press (NASA). 119 p.

Bergin W. Personal letter to Mr. Hind, Livestock Manager, Parker Ranch, Kamuela, Hawaii. January 12, 1990.

Burt J, Barber G. 1996. *Elementary statistics for geographers*, 2nd ed. New York: Guilford Press. 640 p.

Carson H. 1998. Evolution. In: Juvik S, Juvik J, editors. *Atlas of Hawai'i.* 3rd edition. Honolulu: University of Hawai'i Press. p. 107-110.

Casadevall T, Stokes J, Greenland L, Malinconico L, Casadevall J, Furukawa B. 1987. SO_2 and CO_2 emission rates at Kilauea volcano, 1979-1984. *Volcanism on Hawaii; U.S. Geological Survey Professional Paper 1350,*Ch. 29.

Charleson R, Wigley T. 1984. Sulfate aerosol and climate change. *Scientific American*, February: 48-57.

Chen Z, Elvidge C, Groeneveld D. 1998. Vegetation change detection using high spectral resolution vegetation indices. In R. Lunetta and C. Elvidge, editors. *Remote sensing change detection.* Sleeping Bear Press, p 181-190.

Chuang C, Penner J, Taylor K, Grossman A, Walton J. 1997. An assessment of the radiative effects of anthropogenic sulfate. *Journal of Geophysical Research.* 102(D3): 3761-3778.

Clague D. 1998. Geology. In: Juvik S, Juvik J, editors. *Atlas of Hawai'i.* 3rd edition. Honolulu: University of Hawai'i Press. p. 37-46.

Clark H. Vog suspect in sick cattle: 2 Big Island veterinarians call for tests. Advertiser Big Island Bureau Sept. 4, 1990.

Clark W, Hosking P. 1986. *Statistical methods for geographers.* New York: John Wiley & Sons. 518 p.

Coppin P, Bauer M. 1996. Digital change detection in forest ecosystems with remote sensing imagery. *Remote Sensing Reviews* 13:207-234.

Decker R, Decker B. 1989. *Volcanoes.* New York: W. H. Freeman and Company. 285 p.

Department of Planning and Economic Development. 1981. *Landsat Project State of Hawaii Final Report.* 54 p.

Department of Panning and Economic Development. 1998. *NASA land use/land cover project.* http://www.hawaii.gov/dbedt/gis/nasa.htm.

Duggin M, Robinove C. 1990. Assumptions implicit in remote sensing data acquisition analysis. *International Journal of Remote Sensing* 11(10):1669-1694.

Dutton E, Christy J. 1992. Solar radiative forcing at remote surface sites and evidence for global cooling following the eruption of Pinatubo. *EOS Transactions*, American Geophysical Union 73: 632.

Elias T, Sutton AJ, Stokes J, Casadevall T. 1997. Sulfur dioxide emission rates of Kilauea Volcano, Hawai'i, 1979-1999. USGS Open File Report 98-462.

EPA. 2000. What is Acid Rain? http://www.epa.gov/airmarkets/acidrain/index.html#what (accessed 10 June 2001).

ERDAS. 1994. *ERDAS Field Guide.* Atlanta: ERDAS Inc. 628p.

ERDAS. 1999. *Multispectral classification training reference manual.* Atlanta: ERDAS, Inc. 164p.

ESRI. 1999. *ArcDoc* 8. Redlands: ESRI.

Gavenda R, Smith C, Vollrath N. 1998. Soils. In: Juvik S, Juvik J, editors. *Atlas of Hawai'i.* 3rd edition. Honolulu: University of Hawai'i Press. p. 92-96.

Gerlach T, Graeber E. 1985. Volatile budget of Kilauea volcano. *Nature* 313: 273-277.

Giambelluca T, Nullet M, Schroeder T. 1986. *Rainfall Atlas of Hawai'i.* Report R76. Honolulu: Water Resources Research Center, University of Hawai'i at Manoa. 267 p.

Giambelluca T, Sanderson M. 1993. The Water Balance and Climate Classification. In: M. Sanderson, editor. *Prevailing Trade Winds: Weather and Climate in Hawai'i.* Honolulu: University of Hawaii Press p. 56-72.

Giambelluca T, Schroeder T. 1998. Climate. In: Juvik S, Juvik J, editors. *Atlas of Hawai'i.* Honolulu: University of Hawai'i Press. p. 49-59.

Goward S, Markham B, Dye D, Dulaney W, Yang J. 1991. Normalized difference vegetation index measurements from the advanced very high resolution radiometer. *Remote Sens. Environ.* 35: 257-277.

Harding D, Miller J. 1982. The influence on rain chemistry of the Hawaiian volcano Kilauea. *Journal of Geophysical Research* 87(C2): 1225-1230.

Hobbs P, Radke L, Shumway S. 1970. Cloud condensation nuclei from industrial sources and their apparent influence on precipitation in Washington State. *Journal of the Atmospheric Sciences* 27:81-89.

Hue N, Ikawa H. Acid soils in Hawaii: Problems and management. http://agrss.sherman.hawaii.edu/staff/hue/acid.html (accessed December 1997).

Huete A. 1988. A soil-adjusted vegetation index (SAVI). *Remote Sens. Environ.* 25: 295-309.

Jakosky B. 1986. Volcanoes, the stratosphere, and climate. *Journal of Volcanology and Geothermal Research* 28:247-255.

Jensen J. 1996. *Introductory digital image processing: a remote sensing perspective.* 2nd edition. New Jersey: Prentice Hall. 318 p.

Jordan C. 1969. Derivation of leaf area index from quality of light on the forest floor. *Ecology* 50:663-666.

Juvik J, Singleton D, Clarke G. 1978. Climate and water balance on the Island of Hawai'i. In Mauna Loa Observatory, edited by J. Miller. Twentieth Anniversary Report, U.S. Dept. of Commerce, NOAA Environmental Research Laboratory. p. 129-139.

Juvik J. 1998. Biogeography. In: Juvik S, Juvik J, editors. *Atlas of Hawai'i.* 3rd edition. Honolulu: University of Hawai'i Press. p. 103-106.

Kahan A. 1986. *Acid Rain: Reign of controversy.* Colorado: Fulcrum Inc.

Kauahikaua J, Mangan M, Heliker C, Mattox T. 1992. The death of Kupaianaha vent, Kilauea volcano, Hawaii. *EOS Transactions*: AGU Fall Meeting 73: 629.

Kidwell K. 1990. Global vegetation index user's guide. U.S. Department of Commerce/NOAA/National Environmental Satellite Data and Information Service/NCDC/Satellite Data Services Division.

Kozlowski T. 1985. SO_2 effects on community structure. In: Winner, Mooney, Goldstein, editors. *Sulfur dioxide and Vegetation: Physiology, Ecology, and Policy Issues.* 539 p.

Lamoureux C. 1976. *Trailside plants of Hawai`i's national parks.* Hawai'i: Hawai'i Natural History Association. 79 p.

Lamoureux C. 1983. Plants. In: Armstrong R, editor. *Atlas of Hawaii.* 2nd Edition. Honolulu: University of Hawaii Press. p 69-72.

Lauenroth W, Milchunas D. 1985. SO_2 effects on plant community function. In: Winner W, Mooney H, and Goldstein R, editors. *Sulfur dioxide and Vegetation: Physiology, Ecology, and Policy Issues.* California: Stanford University Press, 539 p.

Likens G, Driscoll C, Buso D. 1996. Long-term effects of acid rain: response and recovery of a forest ecosystem. *Science* 272: 244-246.

Lillesand T, Kiefer, R. 1987. *Remote sensing and image interpretation.* 2nd edition. New York: John Wiley and Sons. 721 p.

Markham B, Barker J. 1986. Landsat MSS and TM Post-calibration dynamic ranges, exoatmospheric reflectances and at-satellite temperatures. *EOSAT Landsat Technical Notes* 1:3-8.

Mather P. 1987. *Computer processing of remotely-sensed images.* New York: John Wiley & Sons. 352 p.

Mattox T, Heliker C, Mangan M, Kauahikaua J. 1992. A year of transition for Kilauea's decade-long eruption. *EOS Transactions*: AGU Fall Meeting 73: 629.

McGee K, Gerlach, T. 1995. *Volcanic Gas.* USGS Open File Report 95-85.

Meisner B. 1976. *A study of Hawaiian and Line Islands Rainfall.* UH-MET 76-04. Department of Meteorology, University of Hawaii. 72 p.

Messina J. 1986. What is Radiance? (Ask Dr. SPOT). *SPOTLight.* Spring/Summer: 8-9.

Miller, J, Yoshinaga A. 1981. The pH of Hawaiian precipitation: a preliminary report. *Geophysical Research Letters* 8(7): 779-782.

Miller, T. 1998. Atmospheric aerosols and their effects on climate. http://www.ghcc.msfc.nasa.gov/overview/aerosols.html (created 9 Oct 1998)

Mohlenbrock R. 1996. This land Hawaii: Hawaii Volcanoes National Park. *Natural History* 105(2):79-81.

Monastersky R. 1995. Attack of the *vog. Science News* 147: 284-286.

Morgan J. 1983. Hawaii. In: Armstrong R, editor. *Atlas of Hawaii.* 2nd Edition. Honolulu: University of Hawaii Press. p 23.

Morgan J. 1996. *Hawaii: a unique geography.* Honolulu: Bess Press. 244 p.

Morrissey M, Graham N. 1996. Recent trends in rain gauge precipitation measurements from the Tropical Pacific: Evidence for an enhanced hydrologic cycle. Bulletin of the American Meteorological Society 77(6):1207-1219.

Mouginis-Mark P, Rowland S, Francis P, Friedman T, Garbeil H, Gradie J, Self S, Wilson L, Crisp J, Glaze L, Jones K, Kahle A, Pieri D, Zebker H, Krueger A, Walter L, Wood C, Rose W, Adams J, Woiff R. 1991. Analysis of active volcanoes from the Earth Observing System. *Remote Sensing of Environment* 36: 1-12.

NASA Factsheet. 1994. Volcanoes and global climate change. NF 220.

National Aeronautics and Space Administration. 1976. *Landsat data users handbook.* Greenbelt, MD: National Aeronautics and Space Administration [variously paged].

National GAP Analysis Program Homepage. 2001. http://www.gap.uidaho.edu/

NOAA Coastal Services Center. 1998. What is NDVI?. http://www.csc.noaa.gov/crs/definitions/NDVI.htm

Peixotoo J, Oort A. 1992. *Physics of climate.* New York: American Institute of Physics. 520 p.

Polovina J, Mitchum G, Graham N, Craig M, Demartini E, Flint E. 1994. Physical and biological consequences of a climate event in the central north Pacific. *Fisheries Oceanography* 3:15-21.

Postawko S, Morrissey M, Gibson B. 1994. The Schools of the Pacific Rainfall Climate Experiment: Combining Research and Education. *Bulletin of the American Meteorological Society* 75(7): 1260-1266.

Purevdor Ts, Tateish R, Ishiyamas T, Honda Y. 1998. Relationships between percent vegetation cover and vegetation indices. *Int. J. Remote Sensing* 19(18): 3519 - 3535.

Pratt H. 1998. *A pocket guide to Hawai`i's trees and shrubs.* Honolulu: Mutual Publishing. 136 p.

Rampino M, Self S. 1984. Sulfur-rich volcanic eruptions and stratospheric aerosols. *Nature* 310: 677-679.

Rock B, Skole D, Choudhury B. 1993. Monitoring vegetation change using satellite data. *Vegetation Dynamics and Global Change*, edited by A. Solomon and H. Shugart, pp.153-167.

Rouse J, Haas R, Schell J, Deering D. 1974. Monitoring vegetation systems in the great pains with ERTS. *Third ERTS Symposium*, NASA SP-351,1,309-317.

Sader S, Stone T, Joyce A. 1990. Remote sensing of tropical forests: An overview of research and applications using non-photographic sensors. *Photogrammetric Engineering and Remote Sensing* 56: 1343-1351.

Schnetzler C, Bluth G, Krueger A, Walter L, Dciron S. 1992. A sulfur emission index (SEI) for explosive volcanic eruptions. *EOS Transactions*, American Geophysical Union, 73: 614.

Scholl M, Ingebritsen S. 1995. Total and non-seasalt sulfate and chloride measured in bulk precipitation samples from the Kilauea volcano area, Hawaii. *USGS Water-Resources Investigations Report 95-4001.*

Schroeder T. 1993. Climate Controls. In: M. Sanderson, editor. *Prevailing Trade Winds: Weather and Climate in Hawai`i.* Honolulu: University of Hawaii Press p.12-36.

Sigurdsson H. 1982. Volcanic pollution and climate: The 1783 Laki eruption. *EOS* 63: 601-602.

Song C, Woodstock C, Seto K, Lenney M, Macomber S. 2001. Classification and change detection using Landsat TM data: When and how to correct atmospheric effect? *Remote Sensing of Environment* 75:230-244.

SPOT Image Corp. 1999. SPOT Image: Technical Data. http://www.spot.com/home/system/introsat/seltec/seltec.htm#a. (13 March 2001).

Stone C, Pratt L. 1994. *Hawai`i's Plants and animals: Biological sketches of Hawai`i Volcanoes National Park.* Honolulu: University of Hawai'i Press. 339 p.

Sutton J, Elias T. 1993. Volcanic gases create air pollution on the Island of Hawai'i. *Earthquakes and Volcanoes* 24(4): 178-196.

Sutton J, Elias T, Navarrete R. 1994. Volcanic gas emissions and their impact on ambient air character at Kilauea volcano, Hawaii. USGS Open File Report 94-569.

Sutton J, Elias T, Hendley J, Stauffer P. 1997. Volcanic air pollution - a hazard in Hawai'i. USGS Fact Sheet 169-97.

Tivy J. 1993. *Biogeography: A study of plants in the ecosphere.* New York: John Wiley and Sons. 452 p.

Thordarson T, Self S. 1993. The Laki (Shaftár Fires) and Grímsvötn eruptions in 1783-1785. *Bulletin of Volcanology* 55: 233-263.

UCAR. 1995. Tip sheet on effects of clouds on global warming. http://www.ucar.edu/ (created June 1995)

Uehara G. 1983. Soils. In: Armstrong R, editor. *Atlas of Hawaii.* 2nd Edition. Honolulu: University of Hawaii Press. p 45-47.

Uehara G, Ikawa H, Hue N. Soils in Hawaii: Application of soil survey and classification. http://128.171.125.26/HIsoils/HIsoils.html (accessed 5 December 1997).

USGS 2000. Long-lasting rruption of Kilauea Volcano, Hawai`i leads to volcanic-air pollution. http://volcanoes.usgs.gov/Hazards/What/VolGas/VolGasPollution.html Accessed 7/2001.

Wallace J, Hobbs P. 1977. *Atmospheric science: an introductory survey.* New York: Academic Press. 467 p.

Watson R, Filho L, Sanhueza E, Janetos A. 1992. Greenhouse gases: Sources and sinks, Climate Change 1992: *The Supplementary Report to the IPCC Scientific Assessment.* Cambridge University Press, 200 p.

Wester L. 1983. Vegetation (Chapter 10). *Hawaii: A Geography*, edited by J. Morgan, Westview Press, Colorado, 293 p.

Wickland D. 1991. Mission to Planet Earth: The ecological perspective. *Ecology* 72: 1923-1933.

Winegardner D. 1996. *An introduction to soils for environmental professionals.* New York: Lewis Publishers. 270 p.

Winner W, Mooney H. 1980. Responses of Hawaiian plants to volcanic sulfur dioxide: stomatal behavior and foliar injury. *Science* 210: 789-791.

Winner W, Mooney H. 1985. Ecology of SO_2 resistance V. effects of volcanic SO_2 on native Hawaiian plants. *Oecologia* 66: 387-393.